

**Enzyme Immobilisation on Mesoporous Silica,  
Inspired by Chaperonins**

*Michele M. Lynch*

*Department of Chemical Engineering*

A thesis submitted for the degree of Doctor of Philosophy of UCL

September 2018

I, Michele M. Lynch, confirm that the work presented in this thesis is my own. Where information has been derived from other sources, I confirm that this has been indicated in the thesis.

## **Acknowledgments**

I would like to thank my supervisor, Prof. Marc-Olivier Coppens, for giving me the opportunity to continue my studies, and for giving me excellent support and guidance. I particularly appreciate the many opportunities I've been afforded to present my work to the wider research community. I would also like to thank my examiners, Prof. John Ward of UCL and Prof. Siddharth Patwardhan of the University of Sheffield, for their valuable critiques of my thesis.

I'd like to thank my research group, the NICE group, for giving me academic, technical, and emotional support for many years. I thank Lung-Ching Sang for his instructive thesis, and for the initial laboratory training he provided when I joined the NICE group. I thank Silo Meoto for her extensive laboratory assistance and support. I thank Michael Nigra for his valuable direction and laboratory assistance. I thank Gwyn Evans for his assistance with TEM images, and Toby Neville for his assistance with SEM images. I thank Justin Siefker, Haiyue Yu, and Silo for their assistance with gas physisorption. I thank Han Wu for her assistance with SAXS. I thank Jichuan Liu for his essential assistance with the activity assays of immobilised lysozyme. I thank Alexandra Young, Anna Lambert, and Gwyn for their valuable advice in the writing of this thesis.

On a more personal level, I would like to thank my family, particularly my parents, for their love and support. I'd like to thank my housemates at Brydon Walk for becoming like an adoptive family, and all my friends who have welcomed me to London and made it feel like home. Finally, I'd like to thank my partner, Harry, for supporting me through the end of my PhD and giving me hope for the future.

## **Abstract**

In nature, chaperonins stabilise enzymes and protect them from high temperature and unfavourable solution conditions. We are inspired by some of chaperonins' fundamental properties when investigating materials for enzyme immobilisation. In this project, mesoporous silica SBA-15 is used as a synthetic chaperonin analogue because of its controlled mesopore diameter and its negatively charged surface.

Mesoporous silica SBA-15 have been synthesised by an acidic sol-gel method. The morphologies and textural parameters of the SBA-15 have been characterised using electron microscopy, gas physisorption, and small-angle X-ray scattering.

The synthesised SBA-15 samples are used to immobilise several model proteins: myoglobin, lysozyme, trypsin, and pepsin. At equilibrium, protein immobilisation can be described by the Langmuir model of physical adsorption. The maximum amount of protein that can be adsorbed onto SBA-15 increases with increasing pore diameter. The kinetics of adsorption of the protein myoglobin is found to be affected by the pore size of the SBA-15, with the protein diffusing faster through a larger pore.

Immobilising enzymes to SBA-15 is shown to increase their biocatalytic activity under some solution conditions. For myoglobin and lysozyme, the protective effects were strongest in solutions where the enzyme is strongly electrostatically attracted to the silica surface. Immobilised myoglobin is also found to be protected from digestion by the protease pepsin. For trypsin, the relationship between electrostatic attraction and improved activity was inconclusive. SBA-15 pore size was shown to affect the activity of the smallest enzyme, lysozyme.

In summary, this thesis recommends the following prioritisations for enzyme immobilisation: strong electrostatic attraction between enzyme and material, followed by pore size just exceeding the diameter of the enzyme. By determining the relative importance of these parameters, this thesis increases the fundamental understanding of enzyme immobilisation by physical adsorption onto porous materials.

## Impact Statement

The knowledge and insight presented in this thesis can be put to beneficial use both within and outside of academia. Its primary practical application is to streamline the screening process of enzyme support systems, such as those used extensively in pharmaceutical and biopharmaceutical production processes. By making rational decisions with regards to the pore size and surface charge of available carriers, the effort required to find the optimal enzyme support material may be reduced.

This research has been carried out under the Centre for Nature Inspired Engineering (CNIE) at UCL. The CNIE draws lessons from nature to engineer innovative solutions to grand challenges in sustainability, resilience, and efficient utilisation of scarce resources. Rather than imitating nature out of context, research at CNIE takes a scientific approach to uncover fundamental mechanisms underlying desirable traits, and applies these mechanisms to the design and synthesis of artificial systems that borrow the traits of the natural model. These systems are endowed with the same desirable characteristic as their models in nature and exhibit extraordinary performance in scalability, robustness, or efficiency. While potentially useful in its industrial applications, this thesis is also valuable as a case study in the nature inspired engineering methodology. It has been included as such in the Nature Inspired Chemical Engineering module for MSc/MEng students in the Department of Chemical Engineering since its inception in 2015.

Many of the findings presented in this thesis have been disseminated to the wider research community. Results found in Chapters 2, 5, and 6 of this thesis have been published in *Langmuir*, in 2016, under the title “Chaperonin-Inspired pH Protection by Mesoporous Silica SBA-15 on Myoglobin and Lysozyme.” Presentations of the research expressed in this thesis have received awards at academic conferences both internal to UCL (Cross-Disciplinary Network on Soft Materials, 2017; Department of Chemical Engineering Industrial Advisory Board, 2017; CNIE Advisory Board, 2016) and at a national level (ChemEngDayUK, 2014-2017; IChemE Applied Catalysis and Reaction Engineering, 2014).

## Table of Contents

1. Introduction to chaperonin-inspired enzyme immobilisation .....	14
1.1 Need for enzyme stabilisation.....	14
1.1.1 Overview of industrial biocatalysis.....	14
1.1.2 Enzyme structure, specificity, and stability .....	15
1.2 Overview of enzyme immobilisation.....	18
1.2.1 Enzyme immobilisation methods.....	18
1.2.2 Enzyme immobilisation materials .....	21
1.2.3 Protein adsorption .....	25
1.3 Approach of this thesis.....	30
1.3.1 A chaperonin-inspired approach to enzyme immobilisation .....	30
1.3.2 Mesoporous silica SBA-15 .....	32
1.3.3 Model enzymes .....	36
1.3.4 Specific aims .....	39
2. Mesoporous silica SBA-15 synthesis and characterisation .....	41
2.4 Introduction .....	41
2.5 Materials and methods.....	42
2.5.1 Synthesis of mesoporous silica SBA-15.....	42
2.5.2 Electron microscopy .....	44
2.5.3 Nitrogen physisorption.....	45
2.5.4 Small-angle X-ray scattering .....	47
2.6 Results and discussion .....	49
2.6.1 Electron microscopy .....	49
2.6.2 Nitrogen gas physisorption.....	51
2.6.3 Small-angle X-ray scattering .....	53
2.7 Conclusion.....	55
3. Equilibrium protein adsorption on mesoporous silica SBA-15 .....	57

3.1	Introduction .....	57
3.2	Materials and methods.....	59
3.2.1	Protein adsorption isotherms on SBA-15 with varying pore sizes .	59
3.2.2	Determining protein concentration from the Beer-Lambert law .....	60
3.2.3	Langmuir adsorption model.....	60
3.3	Results and discussion .....	62
3.3.1	Myoglobin adsorption isotherms.....	62
3.3.2	Lysozyme adsorption isotherms .....	64
3.3.3	Trypsin adsorption isotherms .....	67
3.3.4	Enzyme adsorption isotherms across a single pore size of SBA-15 69	
3.4	Conclusion .....	72
4.	Kinetics of protein adsorption on mesoporous silica SBA-15 .....	74
4.1	Introduction .....	74
4.2	Materials and methods.....	75
4.2.1	Myoglobin adsorption on mesoporous silica SBA-15 over time.....	75
4.2.2	Diffusion-limited adsorption kinetics .....	76
4.3	Results and discussion .....	78
4.3.1	Myoglobin adsorption kinetics onto SBA-15 with different pore sizes 78	
4.3.2	Comparison of myoglobin and lysozyme adsorption kinetics .....	79
4.4	Conclusion .....	81
5.	Peroxidase activity of myoglobin immobilised on mesoporous silica SBA-15 83	
5.1	Introduction .....	83
5.2	Materials and methods.....	84
5.2.1	Myoglobin peroxidase assay .....	84
5.2.2	Myoglobin protection from the protease pepsin.....	86

5.2.3	Myoglobin pH protection.....	88
5.3	Results and discussion .....	89
5.3.1	Protease protection of immobilised myoglobin .....	89
5.3.2	pH protection of immobilised myoglobin.....	91
5.4	Conclusion.....	98
6.	Glycanase activity of lysozyme immobilised on mesoporous silica SBA-15 100	
6.1	Introduction.....	100
6.2	Materials and methods.....	101
6.2.1	Lysozyme glycanase assay.....	101
6.2.2	Lysozyme pH protection.....	103
6.3	Results and discussion .....	103
6.3.1	pH protection of immobilised lysozyme .....	103
6.4	Conclusion.....	109
7.	Hydrolase activity of trypsin immobilised on mesoporous silica SBA-15..	111
7.1	Introduction.....	111
7.2	Materials and methods.....	112
7.2.1	Trypsin hydrolase assay.....	112
7.2.2	Trypsin pH protection .....	113
7.3	Results and discussion .....	114
7.3.1	Hydrolase activity of immobilised trypsin on SBA-15.....	114
7.4	Conclusion.....	118
8.	Summary and recommendations.....	120
8.1	Summary .....	120
8.2	Further studies.....	122
8.2.1	Continuations of presented studies .....	122
8.2.2	Thermal stability of proteins immobilised to mesoporous silica SBA- 15	123

8.2.3	Co-immobilisation of enzymes to mesoporous silica SBA-15 for tandem reactions.....	124
8.2.4	Chaperonin-inspired refolding of denatured enzymes.....	125
	References.....	126

## List of Figures

Figure 1 – Schematic of molecular recognition by induced fit. <sup>19</sup> The enzyme's active site must have the correct shape to accept the substrate, and also be free to move.....	16
Figure 2 – Schematic of enzyme immobilisation methods, from left to right: external physical adsorption, covalent binding, encapsulation, and internal physical adsorption <sup>30</sup> .....	19
Figure 3 – Schematic of a protein with edges of different hydrostatic characters, indicating their variable interactions with surfaces with different hydrostatic characters. <sup>67</sup> .....	27
Figure 4 – Space filling model of GroEL/ES chaperonin complex. Colour-coded by subunit: the open-ended GroEL half, in green, is attached to a purple GroEL half, which is capped by a red GroES. <sup>89</sup> .....	31
Figure 5 – Space-filling models of myoglobin from horse heart, <sup>133</sup> pepsin from porcine gastric mucosa, <sup>134</sup> lysozyme from chicken egg white, <sup>135</sup> and trypsin from bovine pancreas. <sup>136</sup> .....	37
Figure 6 – Schematic of mesoporous silica SBA-15 synthesis procedure <sup>121</sup> ....	42
Figure 7 – Hexagonal lattice cell; Miller indices associated with <i>p6mm</i> 3D hexagonal space group.....	48
Figure 8 – Scanning electron micrographs of mesoporous silica SBA-15, hydrothermally aged at 40 °C (A) and 100 °C (B), and microwave-assisted SBA-15 aged at 220 °C (C). Micrographs are either at 5,000 times magnification (1) or at 50,000 times magnification (2).....	49
Figure 9 - Transmission electron micrographs of mesoporous silica SBA-15 hydrothermally aged at 75 °C (A) and 100 °C (B) .....	50
Figure 10- Nitrogen gas adsorption/desorption isotherms of mesoporous silica SBA-15, hydrothermally aged at 40 °C, 75 °C, and 100 °C, and of microwave-assisted mesoporous silica SBA-15, aged at 220 °C.....	51

Figure 11 – NLDFT pore size distributions of mesoporous silica SBA-15 synthesised at 40, 75, 100, and (MW) 220 °C .....	52
Figure 12 – Small-angle X-ray scattering patterns of SBA-15 synthesised at (A) 40 °C, (B) 75 °C, and (C) 100 °C .....	53
Figure 13 – Small-angle X-ray scattering spectra of SBA-15 aged at 40 °C and 100 °C (top) and SBA-15 aged at 75 °C (bottom). Graphs on the right are depict a smaller range of $q$ at lower intensity. ....	54
Figure 14 – Myoglobin adsorption isotherms onto mesoporous silica SBA-15 with different pore diameters (6.1, 6.6, and 8.1 nm) in phosphate buffer with pH 7.2 and 100 mM ionic strength. Error bars depict 95% confidence intervals. Solid lines represent the Langmuir adsorption model. ....	62
Figure 15 – Lysozyme adsorption isotherms on mesoporous silica SBA-15 with different pore diameters (6.1, 6.6, and 8.1 nm) in phosphate buffer with pH 7.2 and 100 mM ionic strength. Error bars depict 95% confidence intervals. Solid lines represent the Langmuir adsorption model. ....	64
Figure 16 - Trypsin adsorption isotherms on mesoporous silica SBA-15 with different pore diameters (6.6 and 8.1 nm) in phosphate buffer with pH 7.2 and 100 mM ionic strength. Error bars depict 95% confidence intervals. Solid lines represent the Langmuir adsorption model. ....	67
Figure 17 - Protein adsorption isotherms on mesoporous silica SBA-15 (8.1 nm) in phosphate buffer of pH 7.2 and 100 mM ionic strength, for lysozyme, myoglobin, trypsin, and pepsin. Error bars depict 95% confidence intervals. Solid lines represent the Langmuir adsorption model. ....	69
Figure 18 – Comparisons of Langmuir model parameters $q_m$ and $K_{eq}$ with proteins' pls and hydrodynamic diameters when adsorbed onto SBA-15, pore diameter of 8.1 nm, in phosphate buffer with pH 7.2 and 100 mM ionic strength .....	71

Figure 19 – Myoglobin adsorption to SBA-15 with pore diameters of 6.1 or 8.1 nm over time in 25 mM phosphate buffer pH 7.0. Error bars depict 95% confidence intervals. Solid lines depict the intraparticle diffusion-limited adsorption model. ....	78
Figure 20 – Lysozyme adsorption to SBA-15 samples with pore diameters of 5.9 or 7.3 nm over time in in 25 mM phosphate buffer pH 7.0. The solid lines depict the diffusion-limited model. ....	80
Figure 21 - Oxidation of 2,2'-Azino-bis(3-ethylbenzothiazoline-6-sulfonic acid) by hydrogen peroxide to a coloured cation, catalysed by myoglobin .....	85
Figure 22 – Peroxidase activity of free myoglobin and myoglobin immobilised on SBA-15 with a pore diameter of 5.9 nm that have been exposed to pepsin, in solutions with pH values of 3.6 to 6.3. Error bars depict 95% confidence interval. ....	89
Figure 23 – Peroxidase activities of free myoglobin and myoglobin immobilised to mesoporous silica SBA-15 (pore diameters of 6.1, 6.6, and 8.1 nm) in solution pH 3.6 to 7.6, 100 mM ionic strength. pH values to the left of the dashed line take place in acetate buffer while those on the left are in phosphate buffer. Inset is magnified x5. Error bars depict 95% confidence interval. ....	92
Figure 24 – Normalised peroxidase activities of free myoglobin and myoglobin immobilised to mesoporous silica SBA-15 (pore diameters of 6.1, 6.6, and 8.1 nm) from solution pH 3.6 to 7.6, 100 mM ionic strength. Error bars depict 95% confidence interval. ....	93
Figure 25 - Amount of initially-loaded myoglobin leached from mesoporous silica SBA-15 (pore diameters of 6.1, 6.6, and 8.1 nm) after 24 hours in solutions pH 3.6 to 7.6, 100 mM ionic strength. Error bars depict 95% confidence intervals. ....	94
Figure 26 – Schematic of electrostatic effects between silica and myoglobin...	96
Figure 27 - Hydrolysis of 4-MU- $\beta$ -(GlcNAc) <sub>3</sub> to a fluorescent product, catalysed by lysozyme .....	101

Figure 28 - Glycanase activities of free lysozyme and lysozyme immobilised to mesoporous silica SBA-15 (pore diameters of 6.1, 6.6, and 8.1 nm) in solutions of pH 3.6 to 7.6, 100 mM ionic strength. pH values to the left of the dashed line take place in acetate buffer while those on the left are in phosphate buffer. Error bars depict 95% confidence intervals.....	104
Figure 29 - Normalised glycanase activities of free lysozyme and lysozyme immobilised to mesoporous silica SBA-15 (pore diameters of 6.1, 6.6, and 8.1 nm) in solutions of pH 3.6 to 7.6, 100 mM ionic strength. Error bars depict 95% confidence intervals. ....	105
Figure 30 – Amount of initially-loaded lysozyme leached from mesoporous silica SBA-15 (pore diameters of 6.1, 6.6, and 8.1 nm) after 24 hours in solutions of pH 3.6 to 7.6, 100 mM ionic strength. Error bars depict 95% confidence intervals. ....	107
Figure 31 - Schematic of electrostatic effects between silica and lysozyme ...	108
Figure 32 – Hydrolysis of N <sub>α</sub> -Benzoyl-L-arginine ethyl ester, catalysed by trypsin .....	112
Figure 33 - Hydrolase activities of free trypsin and of trypsin immobilised to mesoporous silica SBA-15 (pore diameters of 6.6, 8.1, and 9.8 nm) in phosphate buffers, pH 5.6 to 7.6, 100 mM ionic strength. Error bars depict the 95% confidence intervals.....	115
Figure 34 - Normalised hydrolase activities of free trypsin and of trypsin immobilised to mesoporous silica SBA-15 (pore diameters of 6.6, 8.1, and 9.8 nm) in phosphate buffers, pH 5.6 to 7.6, ionic strength 100 mM. Error bars depict the 95% confidence intervals.....	116
Figure 35 - Amount of initially-loaded trypsin leached from mesoporous silica SBA-15 (pore diameters of 6.6, 8.1, and 9.8 nm) after 24 hours in phosphate buffers, pH 5.6 to 7.6, ionic strength 100 mM. Error bars depict the 95% confidence intervals. ....	117

# 1 Introduction to chaperonin-inspired enzyme immobilisation

## 1.1 Need for enzyme stabilisation

### 1.1.1 Overview of industrial biocatalysis

Making chemical reactions fast, specific, and efficient have always been top priorities for chemical engineers. Living organisms are able to do this intrinsically. Enzymes are nature's catalysts, and they ensure bioorganic reactions proceed quickly to the correct products. The ability to harness this natural efficiency is why biocatalysis is so central to modern industrial organic chemistry. The global enzyme market accounted for 8.2 billion USD in 2015 and is expected to reach 18.5 billion USD by 2024.<sup>1</sup> Enzymes are used extensively in the manufacturing of fine chemicals.<sup>2,3</sup> Enzymes are used to synthesise enantiomerically pure  $\alpha$ - and  $\beta$ -amino acids, alcohols, amides, amines, epoxides, organic acids, nitriles, and peptides.<sup>4</sup> They are also used to manufacture desired stereoisomers, and to modify complex target molecules.<sup>5</sup> Industrial enzymes, including those with applications in a wide range of sectors such as food and beverage, detergents, animal feed, textile, pulp, cosmetics, and wastewater treatments, accounted for 4.7 billion USD of the global enzyme market in 2015.<sup>1</sup>

Specialty enzymes, which address the market for lower volume, higher value products, accounted for 1.6 billion USD of the global enzyme market in 2015.<sup>1</sup> These enzymes have applications in diagnostics, biocatalysis and biotechnological research, and predominantly, pharmaceuticals. A crucial application of biocatalysis is in the synthesis of chiral pharmaceutical intermediates.<sup>6,7</sup> The most common classes of enzymes used in pharmaceutical production are hydrolases, reductases, transaminases, and oxidases.<sup>8</sup> Antianxiety, antidiabetic, antiviral, HIV protease inhibitor, anticancer, anticholesterol, anti-Alzheimer, anti-infective, antihypertensive, and Rhinovirus protease inhibitor drugs all utilise biocatalysis to produce their chiral intermediates.<sup>9-11</sup> In addition to the typical advantages of biocatalysis, which include high enantio- and stereoselectivity, the pharmaceutical industry also benefits from the mild reaction conditions involved in enzyme catalysis. Proceeding with reactions at ambient temperatures reduces the incidence of

epimerisation, isomerisation, racemisation, and rearrangement. Incorrect pharmaceutical enantiomers are often toxic.

Regardless of industry, biocatalysis is central to green chemistry. Also called sustainable chemistry, “green chemistry is the utilisation of a set of principles that reduces or eliminates the use or generation of hazardous substances in the design, manufacture and application of chemical products.”<sup>12</sup> This ideology aims to minimise the environmental impact of chemical manufacturing. Biocatalysis takes place between ambient and biological temperatures, reducing the energy needed for heating and cooling processes. Organic solvents are used less frequently, which reduces waste production. Biocatalysis also avoids the necessity of protective functional groups, which reduces the raw materials required and increases yield.<sup>13,14</sup> Increasing the utilisation of one-pot processes in pharmaceutical manufacturing is one way in which green chemistry goals can be reached. These multi-step processes couple two or more biocatalytic reactions in a single vessel, which reduces the number of process steps and overcomes thermodynamic barriers. These methods involve cascade, domino, or tandem reactions that form multiple bonds and avoid time-consuming recovery and purification steps.<sup>14–16</sup>

### **1.1.2 Enzyme structure, specificity, and stability**

Enzymes are proteins, long chains of amino acids that form three-dimensional structures. Like other catalysts, enzymes increase the rate of chemical reactions by lowering the free energy barrier separating the reactants and products. They achieve this by many different mechanisms that depend on the precise arrangement of functional groups in their active site, which is the part of an enzyme where substrate molecules bind and undergo a chemical reaction. Enzymes can increase rates of reaction by between  $10^6$  and  $10^{12}$  times the rate of the uncatalysed reaction.<sup>17</sup> Enzymes are also much more specific than ordinary chemical catalysts; enzymes will only bind to substrates that are both geometrically and electronically complementary to their active site. The high stereospecificity of enzymes means they distinguish reliably between enantiomers, molecules which are mirror images of one another. This high specificity is key to the industrial appeal of enzyme-based catalysis.

Proteins, including enzymes, have up to four layers of structural complexity. Their primary structure is their linear sequence of amino acids: polypeptides with various side chains. Secondary structure is the local structure of the peptide backbone of the protein. Two common types of secondary structure are alpha helices, which are clockwise spirals, and beta sheets, which have a pleated structure. Tertiary structure is the three-dimensional structure of the entire polypeptide subunit, including side chains. Quaternary structure is how different subunits fit together to form the entire protein. All levels of a protein's structure are said to be determined entirely by a protein's amino acid sequence; this is known as Anfinsen's dogma.<sup>17,18</sup>

During protein folding, hydrophobic amino acids come together in an effort to exclude water; this hydrophobic collapse has the greatest influence on a protein's three-dimensional shape.<sup>17</sup> Once the amino acid residues are closely packed due to this collapse, van der Waals forces and hydrogen bonds fine-tune the protein's tertiary structure. Proteins' structures are dynamic and flexible. Single side chains up to entire subunits can move angstroms while free in solution. This can be caused by small molecule binding or even just random intramolecular movements. This conformational flexibility is often integral to the protein's function.

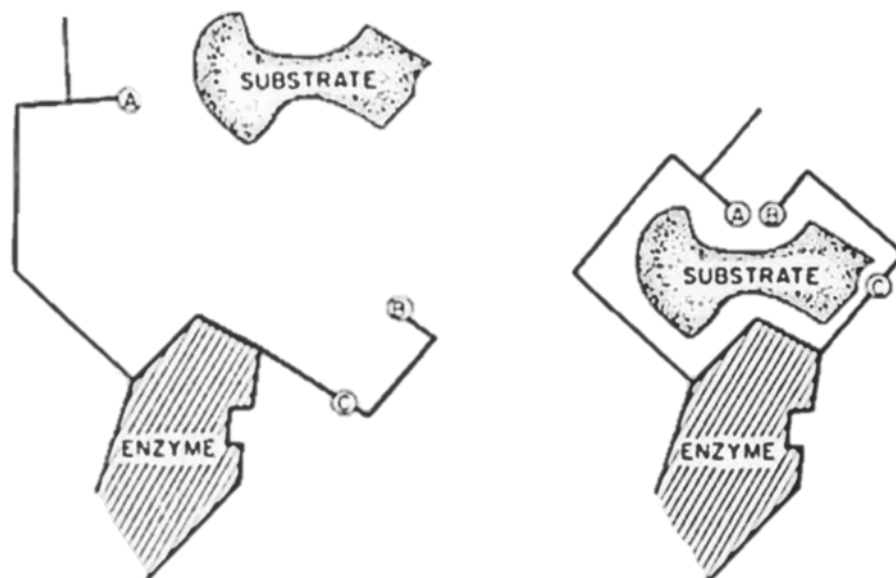


**Figure 1 – Schematic of molecular recognition by induced fit.<sup>19</sup> The enzyme's active site must have the correct shape to accept the substrate, and also be free to move.**

Maintaining an enzyme's correct structure is integral to its catalytic performance, and, more crucially, its specificity. In 1894, the "lock and key" mechanism for enzyme specificity was introduced by Emile Fisher.<sup>20</sup> In this analogy, the enzyme's active site is considered as a rigid lock in which a substrate key must enter before the catalysis can commence. Over the years, exceptions to this model arose, such as smaller substrates not reacting within in active that can accommodate larger substrates. Daniel Koshland modified the idea in 1958: "the substrate may cause an appreciable change in the three-dimensional relationship of the amino acids at the active site."<sup>21</sup> This amendment changed the analogy to resemble a hand going into a glove. In this induced fit mechanism, both the correct active site structure and specific degrees of freedom of movement are required for the high selectivity and activity of any enzyme.

While many enzymes can perform their catalytic function via the specific arrangement of amino acids within their active site, some enzymes require cofactors. Cofactors often consist of or contain metal ions to allow their enzymes to participate in reduction-oxidation reactions and some group transfer processes. Before a newly-synthesised protein has acquired a cofactor that is necessary to its function, it is known as an apoprotein.<sup>17</sup> If an enzyme makes use of cofactors, it often cannot renature if the cofactor has dissociated during its denaturation.

Native proteins are only marginally stable, even under physiological conditions. The covalent bonds of their primary structure, and of any disulphide crosslinks, are relatively strong, but the tertiary and quaternary structures are associated non-covalently via hydrophobic effects, electrostatic interactions, and hydrogen bonding. These forces rest in a delicate balance; it only requires 5-10 kcal of free energy per mole to denature a protein.<sup>22</sup> Several conditions lead to denaturation: temperature, pH, surfactants, and other chaotropic agents such as salts and alcohols. Salt ions differ by their ability to precipitate proteins from a solution; the Hofmeister series ranks salts' abilities to stabilise or destabilise protein structures.<sup>23</sup> When globular enzymes unfold, their hydrophobic residues, which are normally hidden within their core, are exposed. In high protein concentrations, these hydrophobic residues can stick between proteins, causing

them to aggregate, or cluster together.<sup>17</sup> If a protein's primary structure, its amino acid sequence, is maintained, proteins can, in some cases, renature once returned to physiological conditions.<sup>17</sup> If the protein's primary structure is lost, it cannot refold.

Enzymes have evolved to operate optimally within their host organisms: general, this means operating in a neutral, aqueous solution at moderate temperature. There are some microorganisms, known as extremophiles, which have developed unique means to cope with extreme temperatures, acidic and basic pH, and other unfavourable environmental conditions. Extremophile-derived enzymes can catalyse chemical reactions under these harsh, industrial conditions.<sup>24</sup> However, most enzymes cannot naturally endure industrial processes, which often involve high temperatures, acids and bases, and organic solvents. Unfortunately, exposure to these extreme conditions will result in the enzyme's denaturation and loss of function.

## **1.2 Overview of enzyme immobilisation**

### **1.2.1 Enzyme immobilisation methods**

Enzymes must be stabilised from unnatural temperature, organic solvents, and extreme pH to be used effectively in the industries of biological, pharmaceutical, agricultural, and dairy manufacturing. Enzyme immobilisation a widely-used solution to the problem of enzyme instability.<sup>25-29</sup> Attaching enzymes to an inert, insoluble material can increase their operational stability.<sup>25-29</sup> Immobilisation has the additional, significant benefit of allowing the enzyme to be easily removed and recycled.<sup>25-29</sup> There are many methods of enzyme immobilisation. Enzymes can be covalently bound to a supporting material, encapsulated within a host material, cross-linked to each other to form a matrix, or physically adsorbed onto a material.<sup>25-29</sup> Often, immobilisation leads to a negative alteration of an enzyme's activity, specificity, and selectivity, as will be discussed in Section 1.2.3. However, by choosing the best immobilisation method and material for the given application, this attenuation can be reduced or even reversed.<sup>25-29</sup>

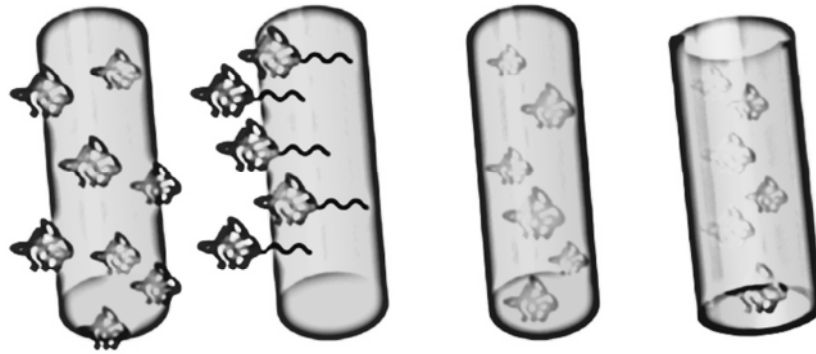


**Figure 2 – Schematic of enzyme immobilisation methods, from left to right: external physical adsorption, covalent binding, encapsulation, and internal physical adsorption<sup>30</sup>**

Binding enzymes to a support material has several subcategories: physical, ionic, and covalent binding. Physical adsorption, due to hydrophobicity, hydrogen bonds, and van der Waals forces, is often too weak to keep the enzyme fixed to the material.<sup>27,31,32</sup> Industrial conditions such as high stirring or continuous flow can strip the enzyme from its host. Covalent bonding is generally stronger, which has the advantage that the enzyme cannot be leached from the surface. The strength of ionic bonding rests between those of physical adsorption and covalent bonding.

Encapsulation, also known as entrapment, involves both the physical restraint of the enzyme within a polymer network, and sometimes an additional bonding attachment. In encapsulation, the enzyme is present as the entrapment material is assembled, as opposed to it being attached onto a prefabricated material. Many of the same materials are used in encapsulation as are used in support binding, as will be discussed in Section 1.2.2. By cross-linking enzyme aggregates using a bifunctional reagent, macroparticles that are not supported by materials can be prepared. This method avoids dilution of the enzyme by the support material. Cross-linked enzyme aggregates (CLEAs) generally enjoy high immobilised activity for relatively low optimisation of the immobilisation process.<sup>27,33</sup> They have even been shown to maintain their increased activity in the presence of organic solvent.<sup>30</sup>

Immobilised enzymes can be evaluated for industrial applications in several ways. An immobilised enzyme's effectiveness factor is determined by its observed reaction rate divided by the observed reaction rate of free enzyme,

under the same experimental conditions and the same substrate concentration.<sup>34</sup> However, this method is limited by the substrate concentration via enzyme kinetics.<sup>29</sup> The immobilised enzyme's turnover number is another way of determining its effectiveness. Turnover number, as with traditional non-biological catalysis, is expressed by amount of product produced per amount of catalyst used, taking stoichiometry into account. This measure is independent of the substrate concentration.<sup>29</sup> Turnover number should be as high as possible, though the turnover numbers of even fully optimised biocatalysts are often several orders of magnitude lower than that of non-biocatalysts for their corresponding inorganic transformations.

Many categories of knowledge must be consulted to optimise an immobilised enzyme system: biochemistry to protect the enzyme's activity against unfavourable conditions; chemistry to ensure its attachment to the surface of the material; and chemical engineering to ensure that the system's transport phenomena are sufficient for good product yield.<sup>34</sup> Traditional chemical engineering is involved in biocatalytic systems in many ways: choosing process conditions such as temperature, pressure, and pH; determining the best reaction medium, whether aqueous, organic, or two-phase; and selecting from reactor configurations like continuous stirred tank, plug flow, fluidised bed, and batch reactors.<sup>35</sup> Additional technologies can be applied to optimise the enzyme's catalytic components: activity, selectivity, and stability, and the immobilisation method's non-catalytic components: recyclability and process control. Particularly useful is the ability to control the microenvironment around the immobilised enzyme with excipients; small molecule quenching agents and hydrophilic macromolecules have been shown to increase the stability of immobilised enzymes by increasing the hydration layer around the enzymes and thereby preventing their aggregation.

In the past decade, protein engineering has increasingly been used as a complementary tool to enzyme immobilisation.<sup>36</sup> Enzymes have been developed to have improved stabilities against temperature and unfavourable solvent, and improved lifespans. Immobilising such an enzyme can further augment its stability, or allow it to remain stable in an environment that would otherwise not be ideal. Enzymes have also been engineered to have increased

conformational stabilities by altering the lengths of secondary structure motifs around the enzyme's active site, or binding regions. Binding functionalities have also been altered through genetic engineering. Directed evolution, in particular has proven an effective methodology for improving enzyme performance and stability.<sup>37-39</sup>

### **1.2.2 Enzyme immobilisation materials**

There are a wide variety of materials that can be used as enzyme immobilisation supports; this section will review them in brief. Synthetic resins, biopolymers, and inorganic polymers can all be used as supports for enzyme immobilisation via physical adsorption.<sup>27,33</sup> Modification of the material's surface can be used to increase the stability and reactivity of immobilised enzymes. Silica materials are particularly suitable for post-synthetic modification because of the easily functionalised silanol groups on the materials' surfaces. Alkyl, amine, carboxylate, and phenyl groups are commonly used to serve as anchor points for covalent binding of enzymes on silica.<sup>30</sup>

Synthetic organic polymers are used as support materials for enzyme immobilisation. Macroporous acrylic resins have been used to immobilise enzymes by physical adsorption.<sup>40</sup> Acrylic resins can be surface-functionalised to allow to covalent attachment, which avoids enzyme leaching. A common acrylic polymer used via covalent attachment is Eupergit C, which is highly hydrophilic and stable over an extremely wide pH range. The high density of surface functional groups means that enzymes are immobilised at multiple points, leading to their high operational stability.<sup>27,41,42</sup> A recent improvement to enzyme immobilisation involves the use of "smart polymers". These synthetic polymers experience significant conformational changes in response to small changes in environmental factors such as temperature, pH, and ionic strength.<sup>43</sup> Poly-N-isopropylacrylamide (NIPAM) is an example of a thermo-responsive polymer; at 32 °C, it dissolves in water, but above this temperature it is insoluble. Use of this "smart" support materials helps overcome challenges of immobilisation such as diffusion limitations, while still allowing the enzyme to be recycled.<sup>44</sup>

Biopolymers are similarly used to immobilise enzymes. These naturally-occurring materials can be sustainably sourced as by-products of existing agricultural industries, which is in line with green chemistry ideology. Some examples of natural polymers are agarose, cellulose, and chitin, which are all water-insoluble polysaccharides.<sup>45-47</sup> Prevalent commercial gel-filtration matrices such as Sephadex and Sepharose consist of biopolymers which are synthetically crosslinked to different degrees.<sup>27</sup> Protein-based biopolymers, such as gelatin, have also been used to immobilise enzymes. In the case of gelatin, both physical entrapment and covalent crosslinking are involved in the immobilisation process; this has been hypothesised to inactivate several enzymes due to “steric hindrance, restricted conformational changes or because their active site is compromised in the binding to gelatin,” as evidenced by decreases in activity.<sup>48</sup>

A variety of inorganic supports are used for the immobilisation of enzymes. Zeolites are naturally occurring, microporous, aluminosilicate materials. They can also be industrially produced, and are also known as molecular sieves because of their ability to selectively sort molecules by size exclusion. Zeolites have heterogeneous surfaces with variable adsorption sites; this is hypothesised to explain their usefulness for enzyme immobilisation, as they can modulate the interactions between the enzyme and the surface.<sup>49-51</sup> Many other inorganic support materials have been investigated for enzyme immobilisation, including ceramics, diatomaceous earth, and carbon nanotubes.<sup>52-54</sup>

Perhaps the most ubiquitous inorganic supports used for enzyme immobilisation are silicates, particularly mesoporous silica which contains pores that are between 2 and 50 nm in diameter.<sup>55</sup> Mesoporous silicas are frequently used as enzyme supports because of their uniform pore diameters, very high surface areas and pore volumes, inert nature and thermal stability.<sup>27</sup> Besides mesoporous silica SBA-15, which will be discussed in Section 1.3.2, another morphology of mesoporous silica commonly used for enzyme immobilisation is MCM-41.<sup>56</sup> Another advantage of using silicates for enzyme immobilisation is how easily such materials can be functionalised. When immobilised to functionalised silica nanoparticles or pores, covalently-bonded enzymes can

experience enhanced thermal stability and a high retention of activity over a wider pH range.<sup>57,58</sup>

Regardless of the additional technologies used to augment the system, enzyme immobilisation onto porous supports has particular advantages over external surface immobilisation. Enzymes on an interior surface will avoid interaction with interfaces, such as gas bubbles, which will disrupt the hydrophobic core of enzymes, leading to their denaturation. This additionally helps to stabilise the enzyme in reactors which call for high stirring. Porous supports can protect enzymes from organic solvent in bulk solution, again by preventing the interface of the solvent from interacting with the immobilised enzyme.<sup>59</sup> A crucial advantage of immobilisation onto porous materials is that it can lead to “rigidification” of the enzyme. By attaching at multiple points a surface with negative curvature, an enzyme’s structure is highly stabilised against conformational changes. Rigidification is especially potent with multimeric enzymes, which need all of their subunits to be associated in their proper formations to function.<sup>60</sup>

A major design factor for immobilised enzyme systems is the mass transport limitations involved, particularly in microporous materials.<sup>34</sup> Access to immobilised enzymes within the capillaries of porous networks by reactants can be limited by diffusion, drastically lowering the system’s catalytic efficiency. Reactants must pass through the stagnant film boundary layer around the material, diffuse through the pores to the enzymes’ active sites, and then return back to the bulk. Mass transport in the stagnant film can be increased by increasing the stir rate in a batch or semi-batch reactor, or the flow rate in a continuous reactor. However, this also increases the mechanical stress on the particles and can lead to fragmentation. The mechanical stability of the immobilisation material is critical to the system’s success, as disintegrated particles can neither protect their enzymes nor be easily removed in downstream processing. This quality is negatively affected by increased porosity, so this must be balanced with the benefits of using porous materials.<sup>29</sup>

Whether on organic polymers or inorganic supports, material’s surface can be covered with functional groups to alter their interactions with adsorbing proteins.

By coating the immobilisation surface with alkyl functional groups, enzymes can be immobilised to the surface via a mixture of van der Waals and hydrophobic interactions; this is particularly useful for enzymes that are natively membrane-bound, or enzymes that have large hydrophobic patches, like lipase.<sup>61,62</sup> To encourage covalent bonding on the material's surface, amino or diol functional groups are commonly used, which bind to primary amines such as those found on lysine side chains.<sup>61,62</sup> Alternatively, epoxy functional groups can be used to covalently bind to an enzyme's nucleophilic amide and thiol groups.<sup>61,62</sup> To change the electrostatic properties of silica's negatively-charged surface, one can functionalise the surface with trialkyl ammine or tetra alkyl ammonium groups. Carboxylate function groups, on the other hand, will create negatively charged areas of the material surface.<sup>61,62</sup>

Choice of immobilisation material for a given enzyme is influenced by several factors. The ease of recyclability will depend on the reaction medium and its viscosity. Smaller particles are more difficult to separate from reaction media, but larger particles have a lower ratio of surface area to mass, which means less of the material is able to effectively support an enzyme.<sup>34</sup> This dilemma can be mitigated by using porous materials, which have a much greater surface area to mass ratio even at larger particles sizes. Porous or not, small particle sizes can lead to greater pressure drops in fixed bed reactors.<sup>29</sup> Immobilisation materials must be evaluated for their immobilisation yield as well, which is how much of the enzyme can be loaded onto the material. This is often expressed in terms of weight or moles of enzyme per weight of material. Alternatively, it can be expressed as enzyme per surface area of material, which can give more insight about how close neighbouring enzyme molecules are to each other, or if attachment is single- or multi-layered.

Enzyme loading onto its immobilisation material can be determined by comparing the activity of the stock solution, immobilised enzyme, and supernatant, in conjunction with mass balance. However, if immobilisation confers an increase or decrease of enzyme specific activity, this method cannot give accurate estimations of the enzyme loading.<sup>29</sup> When possible, through either large amounts of available enzyme or high-resolution detection techniques, this can be avoided by measuring enzyme concentration in the

supernatant directly. For several types of immobilisation, the immobilisation yield is highly dependent on both the enzyme's and the material's surface potentials in aqueous suspension. Surface charge is generated by ionised surface groups or the adsorption of ions from solution, and will lead to a different local electrostatic environment than is found in the bulk solution. Measuring zeta potential of both the enzyme to be immobilised and the support material under the desired reactor's solution conditions can help determine how strongly they will be attracted to one another.<sup>29</sup> If the material and enzyme have opposite charges, they will likely have a higher loading capacity and exhibit less leaching over time. However, this method is limited: zeta potential measurements show the charge layer as it interacts with the bulk solution, not necessarily how it truly exists on the material surface, which is particularly irrelevant for porous materials.<sup>29</sup>

### **1.2.3 Protein adsorption**

The study of enzyme immobilisation by physical adsorption benefits from the comprehensive experimental works on general protein adsorption. This field has been researched extensively since the 1970s due to its broad applicability in topics such as biosensors, biomedical devices, biological processes, and protein chromatography.<sup>63</sup> Proteins do not behave like rigid small molecules, which have fixed probabilities of attachment and detachment from a solid support; proteins' structural complexities lead to behaviour that is more difficult to predict.<sup>63</sup> Both the kinetics of adsorption and the equilibrium states are valuable for describing a protein's relationship with its solid support under a given set of conditions.

Factors that influence protein adsorption arise from the attributes of the three "actors" in the system: the protein, the surface, and their environment. Concerning the experimental environment, the most pertinent parameters are temperature and the buffer's pH, ionic strength, and composition. Higher temperature leads to increased diffusion to the surface, resulting in increased adsorption rates.<sup>63</sup> Further, high temperature tends to increase the amount of proteins adsorbed to the surface.<sup>63</sup> The pH of the system governs the electrostatic states of the proteins and the adsorbate. This can be predicted by the protein's isoelectric point (pI), which is the pH at which the protein has zero

net charge. Proteins with more basic amino acid residues than acidic will have higher pI values, while for acidic proteins the pI will be lower. Protein adsorption is generally observed to have maximal mass loading at equilibrium when pH is near the protein's pI, as protein-protein repulsion is minimised.<sup>64,65</sup> The protein's electrostatic condition has also been seen to affect the kinetics of adsorption: proteins of the net opposite charge to that of the material may have quicker adsorption due to its attraction.<sup>64</sup>

Higher concentrations of dissolved ions act to dampen the range of electrostatic effects between charges. This can serve to weaken either electrostatic repulsion or attraction between protein and surface. High ionic strength can also weaken repulsion between protein molecules, causing them to pack more closely. Very high salt concentrations promote the precipitation of proteins, which is known 'salting out' due to the water absorption by salt ions.<sup>63</sup> Different salt ions differ by their ability to precipitate proteins from a solution, and are ranked by this ability in the Hofmeister series.<sup>23</sup> Ions that promote protein precipitation are called kosmotropes because they are hypothesised to stabilise the native conformation of proteins. Ions that slow protein precipitation are called chaotropes, due to their destabilising effects. However, the Hofmeister series has not been shown to be useful in predicting protein adsorption.<sup>66</sup>

The complexity of proteins' structures mean that each has unique adsorption behaviour and a distinctive molecular "personality".<sup>67</sup> This makes overly-simplistic predictions concerning protein adsorption from single parameters, such as pI, difficult. Smaller proteins, such as lysozyme, tend to inherently have less flexibility and are less susceptible to structural rearrangements upon adsorption.<sup>68</sup> Larger proteins, such as myoglobin, have enough surface area to have multiple domains with different adsorption tendencies based on the surface and environment.<sup>67,68</sup> This can lead to multiple orientations of the protein on the surface and changes in conformation.

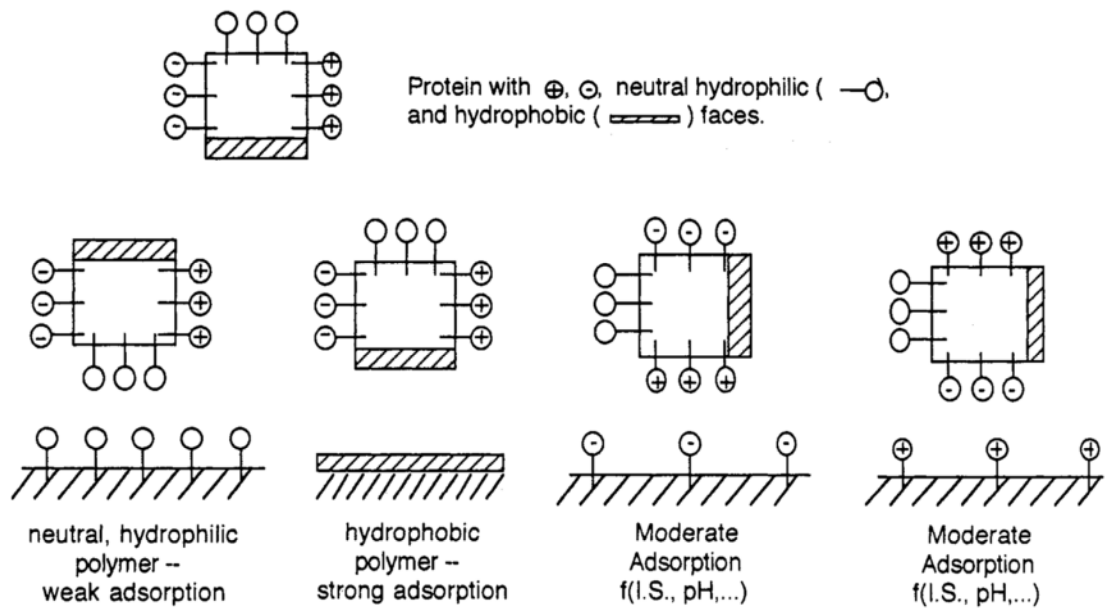


**Figure 3 – Schematic of a protein with edges of different hydrostatic characters, indicating their variable interactions with surfaces with different hydrostatic characters.**<sup>67</sup>

The hydrostatic characters of a protein and of the material it is adsorbing onto affect the preferred orientation of the protein on the surface, as seen in Figure 3. Relatively weak adsorption is observed between neutral hydrophilic surfaces, and strong adsorption is observed between hydrophobic surfaces. Intermediate adsorption is seen between oppositely-charged surfaces, which are modulated by ionic strength and pH. The schematic in Figure 3 demonstrates the effect the material surface can have on a protein's adsorbed orientation.

When a protein's function is localised to a particular section of its surface, such as in enzymes, receptors, and antibodies, its orientation on the surface is important to consider. Proteins are only very rarely spherical, more often having elliptical or more complex shapes, and their preferred surface for adsorption will depend on the free energy minimum from attractive Coulomb and van der Waals interactions, hydrogen bonds, and the entropy gain of solvent or ion release.<sup>63</sup> Hydrophobic patches will adsorb to hydrophobic surfaces, positively charged patches will adsorb to negatively charged surfaces, etc. Under this explanation, it can be understood why proteins have been observed adsorbing to surfaces of the same overall electrostatic charge.<sup>69,70</sup>

Proteins change their conformation upon adsorption to a solid surface; small alterations in their structure can allow more surface regions that prefer adsorption to the material to interact with the material and lower the proteins' free energy.<sup>71,72</sup> How much a protein's structure can change is dependent on its flexibility, which is related to its size and also its modifications, such as cofactors or disulphide bonds. This relaxation process is not immediate and it involves many rotations within a molecule. As with changes in orientation, this slow restructuring can be seen in the kinetics of protein adsorption, and also seen through infrared (IR) and circular dichroism (CD) spectroscopy.<sup>71,73</sup> These conformational changes have been linked to changes in an adsorbed protein's biological function, by altering specificity and reaction rate, but such effects are not always seen.<sup>74</sup>

When adsorbing onto materials with positive curvature, such as spherical nanoparticles, globular proteins have been observed to experience greater conformational changes when adsorbed onto larger particles.<sup>75,76</sup> As the particle size increases and the surface curvature approaches that of a flat surface, proteins attach at more points onto the surface and stretch out of their native conformation. In contrast, on very small particles with high positive curvature, proteins attach to the material's surface at fewer points and experience less conformational change.<sup>75,76</sup> For surfaces with negative curvature, such as porous materials, this relationship is partially inversed; adsorbed proteins can attach at more points to a surface with greater curvature, as discussed in the previous section. However, as the size of the pore approaches that of the protein, the protein's tendency to stretch out will decrease.<sup>77</sup>

The protein layer on the surface can be sparsely or densely packed, depending on the repulsions between proteins, or lack thereof, due to their electrostatic state.<sup>64,65,78</sup> Low repulsion is also required to form multilayers on the surface, and can sometimes lead to aggregation of the protein molecules.<sup>64</sup> The density of the protein layer on the surface is also dependent on the concentration of protein in the bulk; it is hypothesised that high bulk protein concentrations lead to more rapid adsorption onto the surface, which limits the amount of structural rearrangement the protein can experience.<sup>79</sup>

The Langmuir adsorption model describes adsorption of molecules to a surface in terms of empty and occupied adsorption sites and assuming that the adsorbate acts like an ideal gas at isothermal conditions.<sup>80</sup> It is commonly used for describing protein adsorption, and is discussed in more detail in Section 3.2.3. An improvement upon using the Langmuir model for protein adsorption is to describe it using random sequential adsorption (RSA) theory.<sup>81,82</sup> In this theory, protein molecules adsorb randomly onto a surface over time, but are rejected and sent back into the bulk if they attempt to adsorb at a site that is partially blocked by an existing adsorbed protein. This model has explained experimental adsorption kinetic data better than the Langmuir model, but fails to incorporate conformational and orientation changes, protein desorption, and multilayer formation.

The adsorption of various specific proteins onto various inert solid surfaces have been investigated, including those enzymes which are used throughout this thesis and are discussed further in Section 1.3.3. Adsorption of trypsin to nanoparticles indicated that it has an adsorptive preference for hydrophobic polystyrene surfaces over hydrophilic silica surfaces. Different conformational changes were observed, by CD and IR, of the immobilised trypsin on either material. The trypsin immobilised onto silica particles had reversible adsorption and attenuated activity, but the trypsin immobilised onto polystyrene had irreversible adsorption and no activity at all.<sup>83</sup> Trypsin, a globular enzyme, likely had its structure so altered by adsorption onto the hydrophobic polystyrene surface that its activity was completely lost. Myoglobin has shown adsorptive affinity to titania and zirconia nanoparticles over silica nanoparticles. This affinity was found, by CD, to correlate with larger conformational changes once myoglobin adsorbed to the particles. Higher irreversibility was also displayed in adsorption and refolding of the myoglobin to zirconia and titania particles than seen with silica particles.<sup>84</sup>

Carbonic anhydrase adsorbed to silica nanoparticles of three distinct sizes, was found by CD and nuclear magnetic resonance (NMR) to have greater perturbation of its secondary structure. It is hypothesised that the greater curvature of the smaller particles means that less of the protein interacts with the particle surface and is less disturbed.<sup>85</sup> Similar results were seen with

lysozyme adsorbed to silica nanoparticle, where adsorption to larger particles lead to greater changed in  $\alpha$ -helicity and a correlated drop in lysozyme's catalytic activity.<sup>75</sup> In this and another article, lysozyme adsorption to very small silica nanoparticles can cause a "bridging aggregation" of the particles. Lysozyme aggregates, depending on their electrostatic state via pH, can act as a bridge, or glue, between small silica particles.<sup>86</sup>

### **1.3 Approach of this thesis**

#### **1.3.1 A chaperonin-inspired approach to enzyme immobilisation**

Evolution over millennia has impelled biological systems to create clever solutions to challenges involving efficiency and resilience. Drawing inspiration from nature and understanding systems' fundamental concepts allows for the innovative design of chemical engineering systems. In a nature-inspired approach, it is important to not imitate natural systems out of context or succumb to superficial analogies. By scientifically identifying the fundamental mechanisms underlying desirable traits and applying these mechanisms to the design and synthesis of artificial systems, one can efficiently borrow the qualities of the natural model.

Proteins, including enzymes, are synthesised in vivo as strings of amino acids and must fold into their proper three dimensional shapes. An unfolded polypeptide chain has a very large number of degrees of freedom, so the molecule has an astronomical number of possible conformations. This observation leads to what is known as Levinthal's paradox: if a protein were to reach its correctly folded configuration by sequentially sampling each of its possible conformations, even if conformations are sampled at a picosecond rate, it would require a time longer than the age of the universe to arrive at its correct native conformation.<sup>17,87</sup> The paradox is that most proteins fold spontaneously within milliseconds. Levinthal suggested that this paradox is overcome by the existence of thermodynamically favourable folding pathways and stable, partially-folded transition states for proteins. In addition, there are molecular chaperonins, which are proteins that bind unfolded polypeptide chains to help them fold correctly. Chaperonins are essential, as they prevent polypeptide aggregation and precipitation by preventing the improper

association of exposed hydrophobic segments. Chaperonins are also known as heat shock proteins, specifically of the subclass HSP60, because more are synthesised in vivo upon exposure to high temperature.<sup>88</sup>

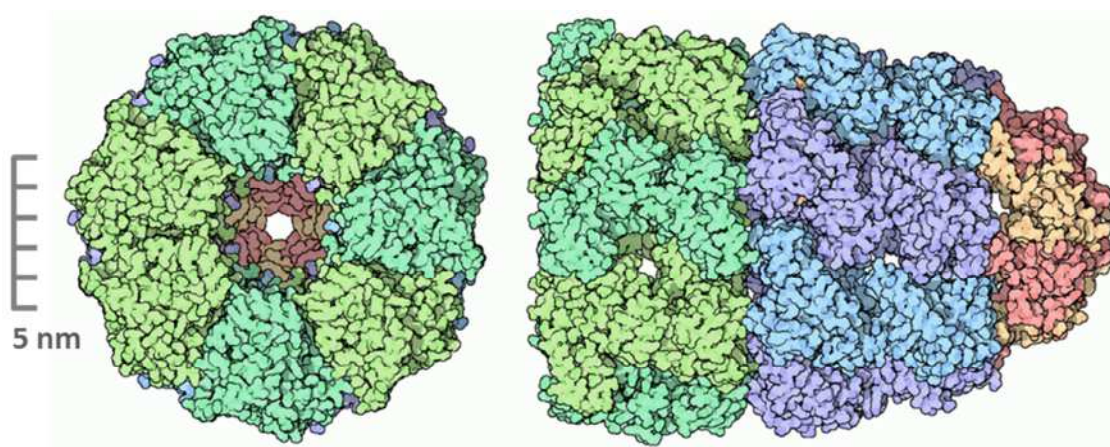


**Figure 4 – Space filling model of GroEL/ES chaperonin complex. Colour-coded by subunit: the open-ended GroEL half, in green, is attached to a purple GroEL half, which is capped by a red GroES.<sup>89</sup>**

In the bacteria *Escherichia coli*, chaperonins are formed of two subunits known as GroEL and GroES, as seen in Figure 4. GroEL resembles a cylinder, consisting of two stacked rings of seven identical subunits each. The internal diameter of this cylinder is approximately 4.5 nm. GroES has a dome-like structure of seven subunits which caps one end of the open GroEL cylinder.<sup>88,89</sup> GroEL/ES requires energy to help fold its substrate protein, which it acquires by hydrolysis of adenosine triphosphate (ATP). First, the unfolded substrate protein enters the GroEL cavity. The exposed hydrophobic residues of the unfolded protein associate with hydrophobic patches on GroEL's interior. At the same time, seven molecules of ATP bind to GroEL. Next, the GroES caps one end of the GroEL cylinder, preventing the substrate protein's escape. As GroEL/ES hydrolyses the ATP, it widens and elongates its cavity, nearly doubling its volume.<sup>90,91</sup> This conformational change also buries GroEL's inner hydrophobic patches and exposes hydrophilic patches. This shift in the local steric and polar environment helps the substrate protein to bury its own hydrophobic residues in an isolated microenvironment where it cannot aggregate with other proteins.<sup>92-96</sup> The release of the substrate protein is triggered allosterically by the ATP-binding on the other end of the GroEL cylinder, as that end chaperones the

folding of a separate substrate protein. The allosteric effects are the twisting of the subunit ring, the burying of the ring's hydrophilic patches, and the release of the GroES cap. After these shifts, the substrate protein is released. It will either have been assisted in following along the folding path determined by its amino acid sequence, or, if it has not, its exposed hydrophobic patches will cause it to be attracted to the open end of a GroEL for additional cycles.<sup>97,98</sup>

GroEL/ES's effectiveness is due to three of its attributes: a narrow, cylindrical pore just large enough to fit a single protein; a local electrostatic environment that encourages rapid protein adsorption; and, when activated, a hydrophilic core that encourages the correct folding of newly synthesised proteins. This thesis investigates a synthetic immobilisation material that is similar to chaperonins in these three fundamental ways.

### **1.3.2 Mesoporous silica SBA-15**

The immobilisation material used in this thesis is mesoporous silica SBA-15. This material is made of amorphous, non-crystalline, silicon dioxide. "Mesoporous" silica contains pores that are between 2 and 50 nm in diameter.<sup>99</sup> "SBA-15" refers to a particular morphology of mesoporous silica, named "Santa Barbara amorphous" after the location of its invention in 1998.<sup>100</sup> SBA-15 can be synthesised as a rod-like particle approximately one micrometre long. Its pores are block co-polymer templated; they are cylindrical and arrayed hexagonally such that they stretch axially down the silica rod. SBA-15's pore diameter is monodisperse and can be controlled within nanometres upon synthesis. This precise control of pore diameter is particularly useful in our chaperonin-inspired approach, as it allows for the rational design of SBA-15 for a target enzyme size. Further, mesoporous silica is hydrophilic and negatively charged in most solutions.<sup>101</sup>

Enzyme immobilisation on mesoporous silicates have extensively studied over the past two decades, and several informative review articles have been published on the topic.<sup>26,28,31,102-106</sup> The most common mesoporous silicates investigated in these studies are the mesoporous silicas MCM-41 and SBA-15, although other morphologies are investigated, as are materials that incorporate other compounds such as titania and alumina. Frequent topics of investigation

for mesoporous silicates are the effects of pore size, pH, ionic strength, and surface functionalisation on the adsorption of proteins. Mesoporous silicates' pore size affects protein adsorption, as has been seen in several studies utilising cytochrome c, trypsin, and other proteins.<sup>107–111</sup> In these studies, greater amounts of protein are found to adsorb to materials with larger pores. Previous work has indicated that maximum protein adsorption on SBA-15 is influenced more by pore volume than surface area; that is, for sufficiently large pores, enzymes will pack within pores rather than just adsorbing onto the interior surface.<sup>112,113</sup> This packing can be predicted by a simple geometric model, which considers the morphology and dimensions of both the material particles and the protein, to investigate the packing behaviour within a cross-section of a pore.<sup>114</sup> The effects of mesoporous silicates' pore size on the kinetics of proteins adsorption have also been investigated for proteins such as cytochrome c, lysozyme, and myoglobin.<sup>115–118</sup> These studies generally indicate that protein adsorption goes more quickly in wider, shorter pores. The electrostatic character of the material and of protein-protein interactions are also hypothesised to contribute to the kinetics of protein adsorption.<sup>116,117</sup>

The solution's pH also has been shown to affect the equilibrium adsorption of several proteins to mesoporous silicates, including cytochrome c, lysozyme, and myoglobin.<sup>77,117–121</sup> These studies did not show maximal protein adsorption amounts at equilibrium to generally increase or decrease with pH; rather, the effects of pH on the system were interpreted with respect to the electrostatic characters of the different proteins and their dependent attraction or repulsion to the mesoporous silicate materials and each other. At a protein's isoelectric point, the protein has no net electrical charge and can pack more closely on the material's surface to achieve the highest maximum loading. At pH values higher than both the protein's isoelectric point and the silicate's point of zero charge (pzc), both the protein and the silicate surface are negatively charged, and are only attracted by their hydrophilic surfaces. Similar effects are seen at pH values below both the protein's pI and the material's pzc, when both are positively charged. At pH values between the protein's pI and the material's pzc, the protein is strongly attracted to the material's surface, but repels other protein molecules with like charge, so not as much protein is loaded on the material.

The ionic strength of a solution also affects protein adsorption, in conjunction with pH.<sup>115,116,118,122</sup> In these studies, which again used proteins such as cytochrome c, lysozyme, and myoglobin, the buffered solution's ionic strength was shown to moderate the pH effects previously discussed. High ionic strength weakens the electrostatic repulsion or attraction between protein and surface, and can also weaken repulsion between protein molecules.

Modification of mesoporous silicates' surface with functional groups, either during or post-synthesis, has also been shown to affect protein adsorption.<sup>123</sup> A brief review of commonly-used functional groups and their effects on protein adsorption is discussed in Section 1.2.2. It has been seen that the hydrophilicity of mesoporous silica's surface is crucial to protein loading for hydrophilic proteins. SBA-15 functionalised with propyl groups has lower maximum loadings of lysozyme and myoglobin than un-functionalised silica of similar pore volume.<sup>77</sup>

The same general parameters have also been examined for their effects on the catalytic activities of enzymes immobilised to mesoporous silicates. The effects of pore size on the activity of cytochrome c on MCM-41 in early studies were unclear; it seemed that even the relatively small enzyme was mostly adsorbing to the external surface of the materials and were therefore displaying comparable activities.<sup>107,108</sup> Later studies on trypsin also showed that the enzyme couldn't fit into the small pores of MCM-41, but did within those of SBA-15 and showed higher activity therein.<sup>110,111</sup> Experiments on myoglobin and lysozyme adsorbed to SBA-15 with different pore sizes indicated that their respective catalytic activities increased as the pore diameter approached that of the immobilised enzymes.<sup>77</sup> The effect of adsorption onto SBA-15 on these enzymes' secondary structure was also investigated using Fourier transform infrared (FTIR) spectroscopy. The secondary structures lysozyme and myoglobin experienced greater departures from their native structures with increasing mesoporous silica pore diameter. In other words, more tightly confining the proteins resulted in better structural maintenance.<sup>77</sup> It is hypothesised that this effect of confinement gives rise to the increased activities observed.

The effects of solution pH on immobilised enzymes' activities have also been studied with enzymes such as cytochrome c, trypsin, myoglobin, and the tandem of chloroperoxidase and glucose oxidase. For some of these studies, only the pH at which the enzyme was immobilised was tested; in these cases no clear effect on activity was seen, except that samples with higher loadings due to favourable adsorption conditions had correspondingly higher activities.<sup>116,124</sup> Other studies investigated the pH values at which the immobilised enzymes reacted with their substrates, to apparently mixed effects. For myoglobin, immobilising to mesoporous silica has been observed to shift the range of pH values at which it is most effective as a peroxidase to be more basic.<sup>118</sup> For the chloroperoxidase and glucose oxidase tandem, immobilising to mesoporous silica shifts their optimal pH range to more acidic values.<sup>125,126</sup> These results can be cohesively interpreted by considering the relative electrostatics of each system: in both cases, the optimal pH for immobilised enzyme activity is shifted towards pH values intermediate to the pIs and pzc's of the respective enzymes and materials.

Functionalisation of mesoporous silicates has been seen to affect subsequently-immobilised enzymes' catalytic activities. Trypsin has been seen to perform best when immobilised to silica covered in thiol or carboxyl functionalisation.<sup>127</sup> Lysozyme and myoglobin immobilise to propyl-functionalised SBA-15 were found to have decreased specific activities.<sup>77</sup> This is hypothesised to be because the hydrophobic character of the propyl-functionalised surface partially unfolds the immobilised enzymes, rendering it significantly less active. Other enzymes such as lipase and a tandem of chloroperoxidase and glucose oxidase have also been investigated with regards to surface functionalisation's effects on their activity after immobilisation.<sup>128,129</sup>

Besides investigating and optimising the various parameters of pore size, pH, ionic strength, and surface functionalisation for enzymes immobilised on mesoporous silicates, these systems have also been tested against some common problems in industrial biocatalysis: heat, organic solvents, and recycle. Cytochrome c and horseradish peroxidase have been shown to have increased thermal stability when immobilised to SBA-15.<sup>116,130</sup> Mesoporous silicate-immobilised myoglobin and trypsin have demonstrated catalytic activity even in

organic media, which is normally beyond their capabilities.<sup>124,131</sup> The reusability of chloroperoxidase and myoglobin immobilised on mesoporous silicates have also been explored, with favourable results.<sup>118,132</sup>

These works have contributed greatly to our understanding of the process of enzyme immobilisation by physical adsorption, and to the development of stabilised enzymes for biocatalytic applications. Several of these studies suffer from systematic flaws, which leave room for improvement in the field. In several experiments, different morphologies of mesoporous silicates, created via different synthesis methods, were compared.<sup>107,110,111,115,118,124,129</sup> This approach is valid, but can make it difficult to determine what aspects of the material's shape and surface are responsible for changes in protein adsorption or activity. Many experiments fail to hold ionic strength constant when pH changes; this is a known problem as ionic strength can greatly affect proteins' structures.<sup>116,118–120</sup> Similarly, the choice of buffer salt is not generally taken into account in these experiments, and their effects on adsorption and activity remain uncertain. Crucially, some of these reported experiments lack replicates, which makes it difficult to compare data points across systems.<sup>107,108,116,118–120,124,130</sup>

The dozens of recent studies on the topic of enzyme immobilisation to mesoporous silicates demonstrates its need and relevance. There is also much room for a more thorough and systematic investigation of the two parameters we have identified from chaperonin complexes, steric confinement and electrostatic attraction, in experiments where all other parameters are held as constant as possible.

### **1.3.3 Model enzymes**

In the systematic study of materials and methods for enzyme immobilisation, researchers often choose to begin experiments with model enzymes. These enzymes may not be useful for chemical manufacturing, but they are often more easily procured in bulk, have well-characterised three-dimensional structures, and have simple assays for quantifying activity. In this thesis, three enzymes are immobilised and investigated: myoglobin, lysozyme, and trypsin. A fourth enzyme, pepsin, is also used in this thesis, though it is not immobilised.

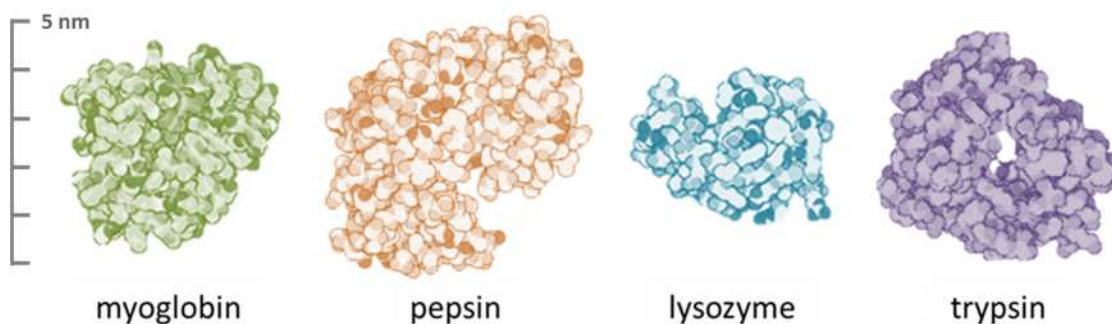


**Figure 5 – Space-filling models of myoglobin from horse heart,<sup>133</sup> pepsin from porcine gastric mucosa,<sup>134</sup> lysozyme from chicken egg white,<sup>135</sup> and trypsin from bovine pancreas.<sup>136</sup>**

Myoglobin (Mb) is a protein found in mammalian muscles and, like haemoglobin, is responsible for transporting molecular oxygen. Myoglobin uses a cofactor prosthetic group, haem, to bind and transport oxygen. The haem group consists of an Fe(II) atom surrounded by a porphyrin derivative. Two hydrophobic side chains, valine and phenylalanine, hold the haem in place, and their flexibility is important to proper oxygen uptake and release.<sup>17</sup> While its native function is not catalysis, myoglobin can act as a peroxidase in vitro.<sup>137</sup> Myoglobin is a monomer made of 153 residues shaped into eight  $\alpha$  helices, with a molecular weight of 17.6 kDa. Myoglobin's crystal structure has the unit cell dimensions of 4.4 x 4.4 x 2.5 nm.<sup>133</sup> It is a globular protein with an approximate hydrodynamic diameter of 4.1 nm.<sup>138</sup> Myoglobin's isoelectric point is 7.2, so it has a no net charge in neutral solutions.

Pepsin (Pp) is an aspartic protease that aids in digestion in the stomach. It is optimally active in gastric acid, and cleaves the peptide bonds of proteins, preferentially after aromatic residues. In high concentrations, pepsin will even cleave itself, so new pepsin must be synthesised as zymogens, which are in an inactive form that is later activated by acid. Pepsin consists of 327 residues, has a molecular weight of 34.6 kDa, and has an approximate hydrodynamic diameter of 5.1 nm.<sup>138</sup> It crystal structure has the dimensions of 5.5 x 3.6 x 7.4 nm.<sup>134</sup> Pepsin's isoelectric point is 3.2, so it has a net negative charge in most solutions.

Lysozyme (Lz) is an antibacterial enzyme that has evolved to damage bacterial and fungal cell walls. It hydrolyses the 1,4-beta-glycosidic linkages found

between N-acetylmuramic acid and N-acetyl-D-glucosamine residues in peptidoglycan.<sup>139</sup> Lysozyme uses the negatively charged aspartic and glutamic acid residues in its active site cleft to catalyse this hydrolysis. It is crucial that these residues are located within a cleft: in addition to aiding specific substrate binding, the cleft protects the acid residues from losing their protons. Lysozyme is a monomer consisting of 129 residues cross-linked by four internal disulphide bonds. Lysozyme's crystal structure has the dimensions of 3.0 x 3.0 x 4.5 nm.<sup>135</sup> It is also a globular protein, with a molecular weight of 14.3 kDa and an approximate hydrodynamic diameter of 3.9 nm.<sup>138</sup> Lysozyme's isoelectric point is 11.3, so it has a net positive charge in most solutions.

Trypsin (Tp) is a serine protease which cleaves amino acid chains, preferentially after negatively charged residues. It contains a catalytic triad of histidine, aspartate, and serine. A nearby glycine forms an oxyanion hole, which stabilises transitional negative charges in the substrate molecule.<sup>140</sup> These residues' positions within the active site cleft are crucial to its proper function. Like pepsin, trypsin is found in the digestive tract of many animals. Trypsin consists of 223 amino acids and has a molecular weight of 23.8 kDa. Its crystal structure has the dimensions 5.4 x 5.8 x 6.6 nm,<sup>136</sup> and its approximate hydrodynamic diameter is 4.6 nm.<sup>138</sup> Its isoelectric point is around 10.3, so it is positively charged in most solutions.<sup>141</sup>

**Table 1 – Selected properties of proteins investigated in this thesis**

<b>Protein</b>	<b>Molecular weight (kDa)</b>	<b>Hydrodynamic diameter<sup>138</sup> (nm)</b>	<b>Isoelectric point (pH)</b>
Myoglobin (equine)	17.6	4.1	7.2
Pepsin (porcine)	34.6	5.1	3.2
Lysozyme (galline)	14.3	3.9	11.3
Trypsin (bovine)	23.8	4.6	10.3

The proteins used in this thesis vary in somewhat in size and widely in net electrostatic charge. A summary of these parameters can be found in Table 1. They also have different enzymatic functions and mechanisms. By using proteins with a wide range of characteristics, the relative importance of steric confinement and electrostatic attraction to protein adsorption to and enzyme activity when immobilised on mesoporous silica can be determined.

#### **1.3.4 Specific aims**

The specific aim of this thesis is to investigate the influence of chaperonin-inspired parameters in developing mesoporous silica SBA-15 as an enzyme immobilisation material. This is accomplished by investigating the influence of SBA-15's similarities to chaperonins on its ability protect cargo proteins from denaturation. In Chapter 2, methods for synthesising and characterising mesoporous silica SBA-15 are described. The morphological attributes of the synthesised SBA-15 are discussed, including the materials' particle morphologies, pore size distributions, surface areas, and porosities. This chapter is necessary to support the original contributions to research in the subsequent chapters, because it demonstrates the high control that is possible over SBA-15's morphology, which is required for investigating the chaperonin-inspired properties.

The first contribution to research in this thesis is the determination of the relevant importance of electrostatic attraction and steric confinement on the equilibrium adsorption of myoglobin, lysozyme, trypsin, and pepsin onto SBA-15. In Chapter 3, we look at the adsorption of the proteins to SBA-15 with different pore sizes under a single solution condition, as described by the Langmuir adsorption model. These experiments aim to investigate maximum adsorption and adsorption affinity with respect to the two chaperonin parameters studied in this thesis. The second contribution to research is the determination of the relevant importance of electrostatic attraction and steric confinement on the kinetics of myoglobin and lysozyme adsorption onto SBA-15. In Chapter 4, the adsorption kinetics of myoglobin onto SBA-15 with different pore diameters are compared to those reported for lysozyme under the same conditions. These experiments investigate if protein adsorption within the SBA-15 pores is diffusion-limited, and the lack of electrostatic attraction

between myoglobin and silica helps clarify the role of electrostatic attraction on protein adsorption within silica pores.

The last contributions to research in this thesis are the determination of the relevant importance of electrostatic attraction and steric confinement on the catalytic activity of myoglobin, lysozyme, and trypsin. In Chapters 5, 6, and 7, these enzymes are immobilised to SBA-15 with varying average pore diameters, exposed to a range of pH conditions, and their relative activities are compared. Each enzymes investigated is different in size, charge, and catalytic mechanism, which is meant to help clarify the roles of electrostatic attraction and steric hindrance in their confinement and activity. These chapters report on the relative importance of the two chaperonin-inspired parameters of this thesis to the enzymes' activity, and enquire if more general trends about enzyme immobilisation could be inferred for application to a wide range of industrial enzymes. By probing the effects of pore diameter and surface charge of the SBA-15 materials on the adsorption and activity of these enzymes, we can achieve a better understanding of the fundamentals behind enzyme immobilisation in general, and make future efforts in this field more straightforward.

## 2 Mesoporous silica SBA-15 synthesis and characterisation

### 2.4 Introduction

As introduced in Section 1.3.1, chaperonin complexes serve as a source of inspiration for the rational design of enzyme immobilisation materials. Their narrow, cylindrical centres are just large enough to host and protect one substrate protein, conferring steric support. The centre's hydrophilic surface ensures that the protein inside reaches its native, globular shape. Chaperonins also utilise electrostatically charged patches to control their interaction with the substrate protein. To investigate the importance of these aspects to the immobilised enzyme's stability and activity, a material with tuneable pore diameter is needed which also has a surface that is easily chemically controlled.

Mesoporous silica SBA-15 is an ideal candidate material for investigating chaperonin-like properties. As mentioned in Section 1.3.2, the pore diameters of SBA-15 can be altered upon synthesis by changing the temperature at which the hydrothermal condensation step occurs. The resulting pores have a very narrow, unimodal pore size distribution, which demonstrates a high degree of control over the material's nanostructure. This attribute allows us to draw conclusions about the effect of pore size with great accuracy. Further, the range of pore diameters of which SBA-15 can be synthesised (5-30 nm)<sup>100</sup> includes the size of chaperonins when fully dilated (7-8 nm).<sup>91</sup> The surface of SBA-15, most of which is found internally, along its pores, is amorphous silica and thus has a pzc near pH 2.<sup>101,142</sup> In aqueous solutions with pH values higher than 2, SBA-15 is negatively charged. This property is hardly unique to SBA-15, or to silica generally, but having a uniform charge distribution on the immobilisation material's surface is useful for understanding the relationship between the electrostatic attraction between protein and material, and the adsorbed enzyme's activity and stability.

In this chapter, the methods for synthesising and characterising the SBA-15 used in the subsequent chapters of the thesis are described. The morphological attributes of the synthesised SBA-15 are discussed, including the material's particle morphology, pore size distribution, surface area, and pore wall thickness. This chapter demonstrates the high control over SBA-15's

morphology, which aids the investigation of chaperonin-inspired properties. Particularly, the SBA-15 synthesised in this chapter was used as the supporting material in subsequent chapters, which investigate both the equilibrium and kinetic adsorption of protein molecules to SBA-15, and the activity and stability of enzymes immobilised in the pores of SBA-15.

## 2.5 Materials and methods

### 2.5.1 Synthesis of mesoporous silica SBA-15

Tetraethyl orthosilicate (TEOS) (reagent grade, 98%), tri-block copolymer poly(ethylene glycol)-block-poly(propylene glycol)-block-poly(ethylene glycol) (Pluronic P123, molecular weight 5,800 g/mol,  $\text{EO}_{20}\text{PO}_{70}\text{EO}_{20}$ ), and hydrochloric acid (ACS reagent, 37%) were purchased from Sigma Aldrich.

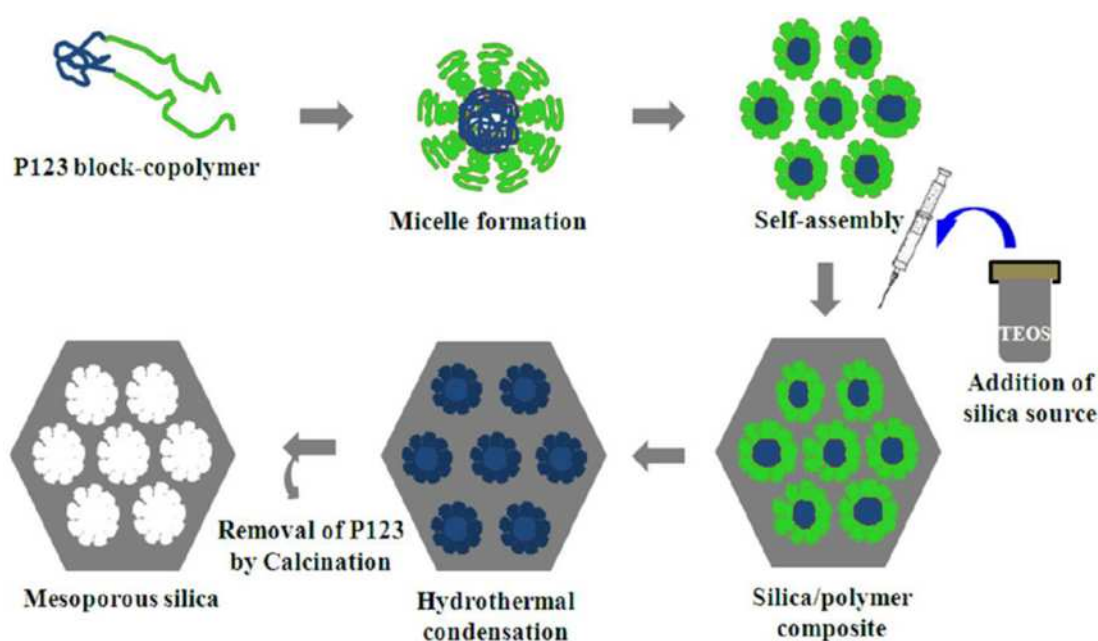


Figure 6 – Schematic of mesoporous silica SBA-15 synthesis procedure<sup>121</sup>

Rod-like SBA-15 was synthesised using amphiphilic triblock-copolymer Pluronic P123 as a structure-directing agent, as shown in Figure 6. P123 serves as a surfactant template by giving the subsequent silica a mesostructure around which to form. For a typical batch, 8 g of P123 was dissolved into 60 g of deionised water in a polypropylene bottle, stirring until a clear solution is obtained. 240 g of 2 M HCl solution was added and the solution was stirred for 2 hours at 40 °C. 18 g of TEOS, the silica source, was added drop-wise to the centre of the stirred solution, which was stirred at 500 rpm. The resultant

concentration of TEOS is 0.3 M. The solution was then stirred for precisely 10 min as the silica formed around the polymer.

P123 was chosen as a template because of its mesostructural ordering properties and amphiphilic character, but other EO:PO ratios have been shown as suitable alternatives.<sup>100</sup> The middle block of the tri-block copolymer is hydrophobic and buries itself when dissolved in water. Above a critical concentration, P123 forms micelles, which are initially spherical. This critical concentration is reported as 0.03% w/v in water at 25 °C.<sup>143</sup> Cryo-TEM has indicated that the micelles become long, straight threads when a silica source is added under suitable conditions.<sup>144</sup> The solution must be acidic, lower than silica's pzc at pH 2, in order for the silica to form a composite gel with the template.<sup>100,101</sup>

After stirring the solution, the resulting homogeneous mixture was kept in static conditions for 72 hours. Hydrothermal condensation occurs as the silica/polymer composite is aged. The material's tuneable pore diameter is controlled by altering the temperature at which the composite is aged. For this thesis, SBA-15 batches were prepared with their hydrothermal aging steps at 40 °C, 75 °C, and 100 °C, and SBA-15 samples are referred to by these temperatures for the remainder of this chapter. Higher temperatures resulted in larger pore sizes; the temperature-dependent hydrophilicity of the copolymer's PEO block causes the micelles to swell under the acidic synthesis conditions.<sup>145</sup> The sample was then filtered immediately, while hot, using a Büchner funnel filtration setup. The filtered material was subsequently washed with deionised water, filtered and washed three more times, and dried in an oven overnight at around 80 °C. The material was then calcined in a furnace for 24 hours at 540 °C, which removes the surfactant template and leaves a hexagonally-ordered array of pores. Using this procedure, and by changing the hydrothermal condensation temperatures, SBA-15 with a controllable, narrow, unimodal pore size distribution and rod-like morphology was obtained.<sup>100,120,121,146</sup>

To obtain rod-like SBA-15 with larger pores, the following microwave-assisted synthesis method was used. After adding TEOS, dropwise, to P123 dissolved in HCl solution, the reaction mixture was immediately transferred to Teflon-lined

autoclaves for further reaction in a power-controlled and temperature-programmed microwave system. In this thesis, the microwave used was the Ethos EZ Microwave Digestion System. These microwave batches were only half the size of those made conventionally, because the autoclaves are small. The mixture reacted at 40 °C for 2 hours, and was subsequently heated for another 2 hours at the desired temperature. For this thesis, a microwave-assisted (MW) SBA-15 batch was prepared with its hydrothermal aging step taking place at 220 °C. After, as in the conventional method, the solid product was filtered and washed several times with distilled water, and dried overnight at around 80 °C. Removal of P123 templates from MWSBA-15 composites was similarly accomplished by calcination at 540 °C.<sup>121</sup>

In addition to yielding SBA-15 with larger average pore diameters, the microwave synthesis method allowed for a shorter total synthesis time of 5 hours, compared to the conventional method, which required 4 days. Both methods required an additional 3-day calcination step, which brings the total preparation times to 4 and 7 days, respectively. One drawback to the microwave-assisted method is that the batch size was limited by the autoclave volume capacity and was therefore smaller.

### **2.5.2 Electron microscopy**

Electron microscopy is an important analytical technique in the chemical, physical, and biological sciences. Focused beams of electrons are used to probe samples, and are collected by detectors, resulting in images with much finer detail than those of visible light microscopes. This is due to the small de Broglie wavelength of electrons, so that images can have resolutions of less than one nanometre.

Scanning electron microscopes (SEM) use the electron beam to scan over the surface of a sample, line by line. As the electron beam traces over the sample, it interacts with its surface and dislodges secondary electrons. A secondary electron detector attracts the scattered electrons and registers different levels of brightness. Additional sensors detect backscattered electrons, which are those from the initial beam that reflect off the sample's surface. The instrument uses these signals to create a topological image of the sample. In this thesis, SBA-15

particle morphologies were observed on a JEOL JSM-6480LV SEM, run in high vacuum mode, typically operating at 7 kV. Samples were first spray coated in gold, as they are otherwise non-conducting, and mounted with carbon tape onto aluminium stubs. Working distance was typically 6 mm. Particle sizes were judged via visual inspection, not by image processing software.

Transmission electron microscopes (TEM) transmit a beam of electrons through a sample, rather than scanning over it. The detector in this case is underneath the sample, and gathers the scatter of electrons through an objective lens to create an image of the internal structure of the sample on a fluorescent screen. In this thesis, SBA-15 pore orientations were observed with a JEOL 2100 TEM operating at 200 keV. For TEM, samples were dispersed in methanol and 2 drops of the suspension were added to holey carbon-coated copper TEM grids.

### **2.5.3 Nitrogen physisorption**

Gas molecules have a tendency to adsorb onto solid surfaces; this adsorption can tell us more about the ensemble properties of a porous material than microscopy alone can. Physisorption instruments hold samples at a constant, very low temperature under vacuum and slowly release an inert gas to the sample chamber. The low temperature and non-reactive nature of the gas are necessary to ensure that the gas adsorption to the material surface is purely physical. By measuring the change in volume over time, the quantity of gas molecules adsorbed to the surface can be determined.

The Brunauer-Emmett-Teller (BET) theory is widely used for interpreting physisorption of inert gases, typically nitrogen or argon, onto mesoporous silicas.<sup>55,104,147,148</sup> The theory describes the random adsorption of gas molecules onto the surface of an adsorbent material in multiple layers. BET theory is an extension of the Langmuir theory of adsorption, which is discussed further in Section 3.2.3. In BET theory, gas molecules are assumed to adsorb non-preferentially onto the material surface and existing gas molecules, at random.<sup>149</sup> By using a smaller gas molecule, like nitrogen, a surface area that accounts for more of the smaller details of the irregular surface is obtained than if a larger molecule were used.

The International Union of Pure and Applied Chemistry (IUPAC) defines micropores as those below 2 nm in diameter, and mesopores as those between 2 and 50 nm in diameter.<sup>55</sup> Gas adsorption into micro- and mesopores is more complex, because it cannot reasonably be assumed that molecules are only interacting with one surface in small capillaries. In mesopores, nitrogen gas can undergo capillary condensation; it passes from vapour to liquid phase well below its saturation pressure, due to increased van der Waal forces with the pore walls. The relative pressure required for gas molecules to enter small capillaries is therefore greater than the pressure required to exit them, leading to hystereses in mesoporous isotherms.

In much of the cited literature, the Barrett-Joyner-Halenda (BJH) computational method has been used to determine pore size distributions of mesoporous silicates.<sup>150</sup> These calculated pore diameters do not always match those shown with microscopy.<sup>151</sup> The non-local density functional theory (NLDFT) is the current state-of-the-art for calculating mesopore size,<sup>152–154</sup> and is recommended by IUPAC guidelines for use when possible.<sup>99</sup> Commercial software provided by some instrument manufacturers include NLDFT kernels for certain adsorbate-adsorbent systems that have pores of a particular shape. These kernels are sets of isotherms representing adsorption in pores of different sizes at a given temperature, and are used to solve the general adsorption isotherm equation for that system. If kernels do not exist for the system being measured, NLDFT cannot be accurately applied and classical methods such as BJH must be returned to.<sup>155</sup>

Nitrogen adsorption and desorption isotherms of SBA-15 samples were measured in this thesis using a Quantachrome Autosorb iQ<sub>2</sub> automated gas sorption analyser. Samples were outgassed at 380 °C for 8 hours before analysis to remove surface contaminants. Samples were cooled using liquid nitrogen (77 K). The samples' specific surface areas were estimated using standard BET theory, and the samples' pore size distributions were calculated using NLDFT using kernels for nitrogen sorption on cylindrical silica pores. Pore volume is calculated from the ideal gas law. All calculations are performed by the instrument software.

## 2.5.4 Small-angle X-ray scattering

X-ray scattering encompasses a range of techniques for the bulk, microstructural investigation of partially ordered materials. X-ray diffraction (XRD) is commonly used to determine the order of mesoporous materials, such as SBA-15, but small-angle X-ray scattering (SAXS), when available, can pick up order at even longer ranges.<sup>147,153,156</sup>

Both XRD and SAXS involve a narrow X-ray beam illuminating a sample, and the elastic scatter of the diffracted electrons being collected off a plate behind the sample. If the sample contains atoms arranged in a crystal lattice, then their scattering interferes in such a way that patterns are formed on the detector plate, which can be interpreted from a database of known crystal structures. Even amorphous materials, such as the amorphous silica that makes up SBA-15, can show crystal patterns from ordered pores. The distance between crystal planes is inversely proportional to the angle at which diffraction peaks occur; therefore small-angle X-rays can see a broader field of the sample's order than wide-angle X-rays. In this thesis, SAXS patterns are obtained with a Ganesha SAXSLAB machine, using a capillary PXRD analysis.

### Equation 1 - Bragg's law

$$n\lambda = 2d\sin\theta$$

SAXS data were interpreted using the Bragg model of diffraction. In this model, a given reflection is associated with a set of evenly spaced sheets running through the crystal. Incoming X-rays are scattered from each plane. From that assumption, X-rays scattered from adjacent planes will combine constructively when the angle  $\theta$  between the plane and the X-ray results in a path-length difference that is an integer multiple  $n$  of the X-ray wavelength  $\lambda$ , as shown in Equation 1.

### Equation 2 - Definition of scattering vector

$$q = \frac{4\pi}{\lambda} \sin\theta$$

Powder diffraction operates on the assumption that every possible crystalline orientation is represented equally in a powdered sample. Averaging these

orientations results in the three-dimensional space seen in single crystal diffraction being projected in a single dimension. Mesoporous silica is amorphous, not crystalline. Therefore, its scattering peaks are relatively broad. As shown in Equation 2, the scattering vector  $q$  can be plotted against X-ray signal intensity to quantitatively define the reflections. Again,  $\theta$  is the scattering angle between the X-ray and the crystal plane, and  $\lambda$  is the wavelength of the X-ray. The Ganesha SAXSLAB instrument used in this thesis allows for scattering angle of up to  $31^\circ$ , which corresponds to a  $q$  vector of  $4.2 \text{ \AA}^{-1}$ .

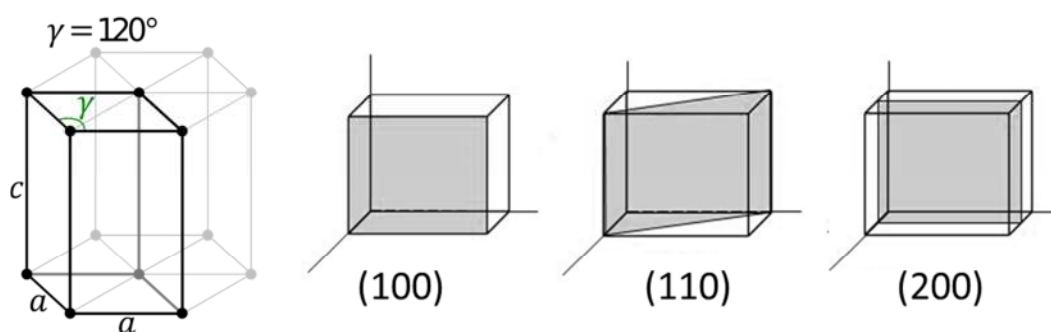


**Figure 7 – Hexagonal lattice cell; Miller indices associated with  $p6mm$  3D hexagonal space group**

The orientation of a particular set of sheets is identified by its three Miller indices. A reflection is said to be indexed when its reciprocal lattice vector components have been identified from the known wavelength and the scattering angle  $2\theta$ . Such indexing gives the unit-cell parameters, the lengths and angles of the unit-cell, as well as its space group. SBA-15 is known to have three-dimensional hexagonal order, specifically having a  $p6mm$  space group (two-dimensional hexagonal periodicity of the one-dimensional pore array), shown in Figure 7. The Miller indices of the three peaks found in SBA-15 SAXS spectra are then (100), (110), and (200).<sup>17</sup>

**Equation 3 – Unit cell size for hexagonal symmetry**

$$a_0 = \frac{2d(100)}{\sqrt{3}}$$

SAXS data can be used to calculate the samples' pore wall thicknesses, in conjunction with pore size distribution data from nitrogen physisorption, by finding the unit cell dimension  $a_0$ . The  $d$ -spacing is determined from the

scattering vector,  $q$ , with the greatest intensity, as shown in Equation 3. The difference between the relative intensities of the peaks can also be used in porous samples to indicate pore wall thicknesses.<sup>157</sup>

## 2.6 Results and discussion

### 2.6.1 Electron microscopy

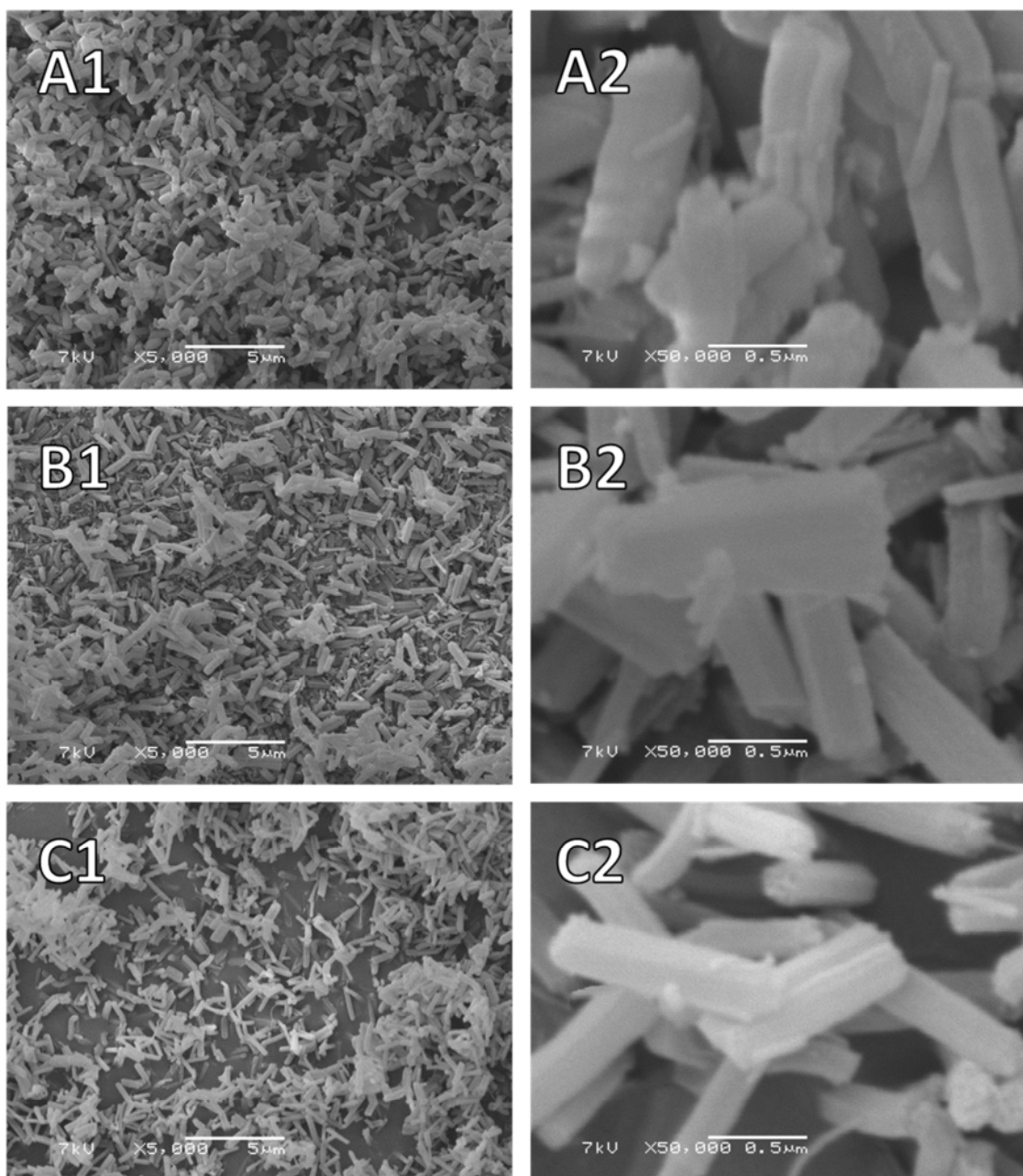


**Figure 8 – Scanning electron micrographs of mesoporous silica SBA-15, hydrothermally aged at 40 °C (A) and 100 °C (B), and microwave-assisted SBA-15 aged at 220 °C (C). Micrographs are either at 5,000 times magnification (1) or at 50,000 times magnification**

**(2)**

The SEM images in Figure 8 show that all SBA-15 particles have a rod-like morphology and that their particle size distributions have low polydispersity. A single SBA-15 particle is approximately 1  $\mu\text{m}$  in length. From these micrographs, it appears that the use of a microwave during synthesis affects the particles' thicknesses: convention SBA-15 particles synthesised at 40 or 100  $^{\circ}\text{C}$  have slightly variable diameters around 350 nm. Microwaved-synthesised SBA-15 particles, made at 220  $^{\circ}\text{C}$ , have approximate diameters closer to 200 nm. The micelle swelling that takes place during the hydrothermal ageing step of the SBA-15 synthesis takes place more quickly and under constant pressure in the microwave-assisted method, why may be why smaller, more uniform SBA-15 particles are observed.

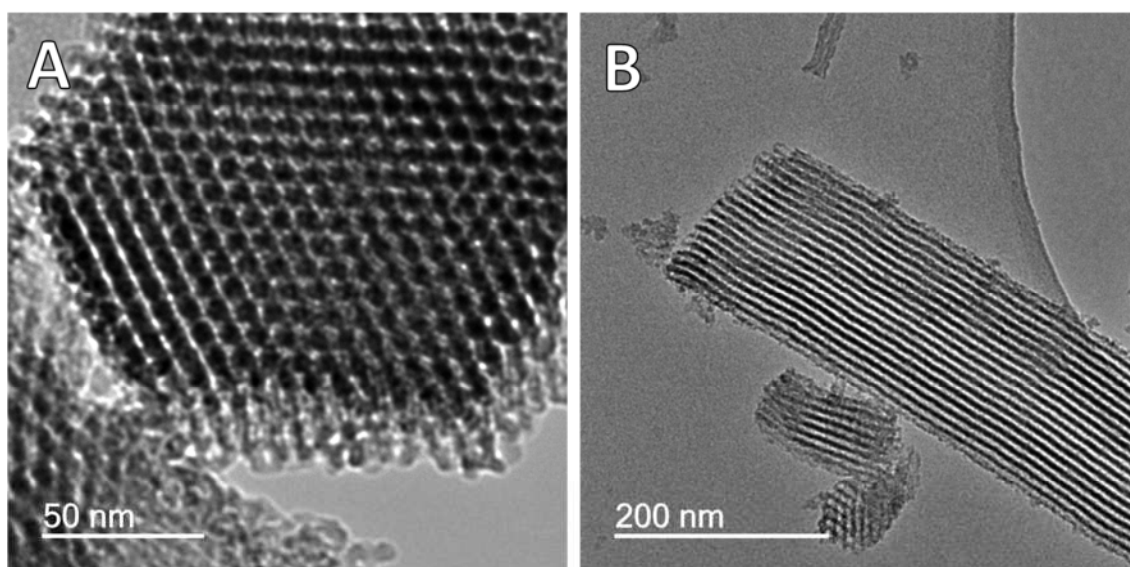


**Figure 9 - Transmission electron micrographs of mesoporous silica SBA-15 hydrothermally aged at 75  $^{\circ}\text{C}$  (A) and 100  $^{\circ}\text{C}$  (B)**

TEM images shown in Figure 9 show the orientation and shape of the pores within the SBA-15 particles. Looking at an SBA-15 rod end-on, the hexagonal packing of its pores is very clear. The uniformity of pore size and spacing is also evident. These SBA-15 pores are found to be oriented down the length of the rod-like particles, and very low tortuosity of the cylindrical pores is observed. These micrographs agree with literature initially reporting synthesis methods for rod-like SBA-15.<sup>109,146</sup>

## 2.6.2 Nitrogen gas physisorption

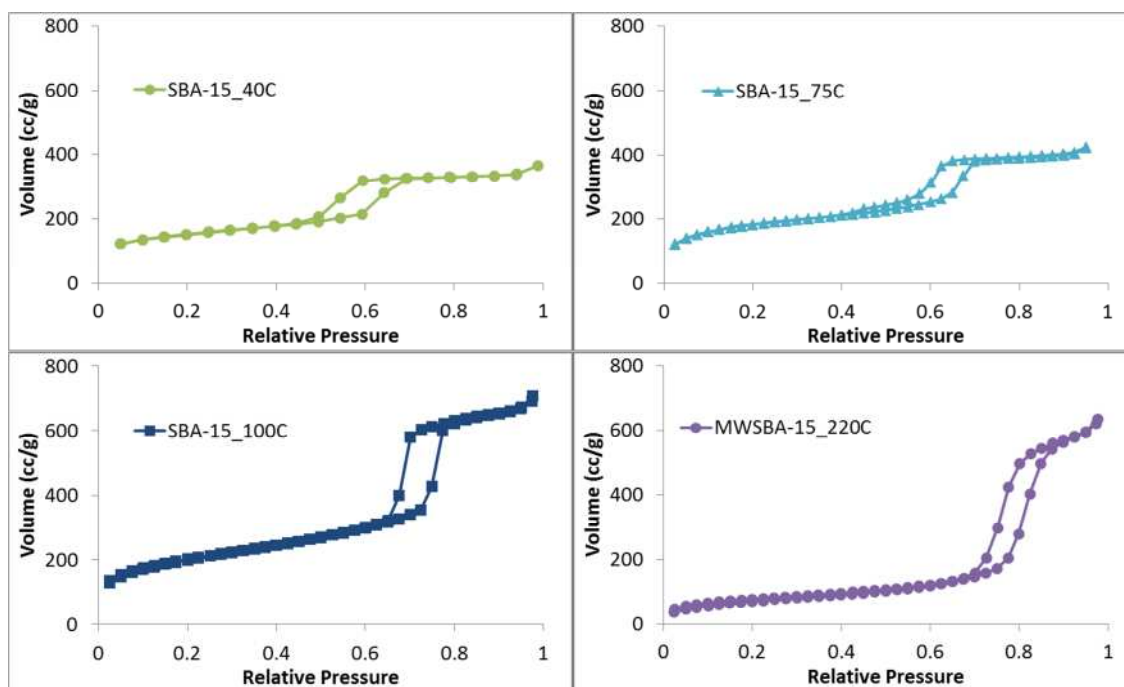


**Figure 10- Nitrogen gas adsorption/desorption isotherms of mesoporous silica SBA-15, hydrothermally aged at 40 °C, 75 °C, and 100 °C, and of microwave-assisted mesoporous silica SBA-15, aged at 220 °C**

Nitrogen adsorption and desorption isotherms of all SBA-15 samples contain hysteresis loops defined as type H1 by the IUPAC classification, which is associated with well-defined cylindrical pore channels.<sup>99</sup> The SBA-15 sample aged at 40 °C experiences a capillary condensation step when relative pressure is around 0.6. The pressure at which capillary condensation occurs increases with increasing ageing temperature of the SBA-15 batch; takes place at a relative pressure of 0.8 for the microwave-synthesised SBA-15, which has an ageing temperature of 220 °C. This finding suggests that the mean pore size is larger when the ageing temperature of the batch is higher. The steep nitrogen adsorption branch during capillary condensation in the mesopores seen for the conventionally synthesised samples shows how rapidly the gas is adsorbed over a small pressure range; this is indicative of a narrow pore size distribution. This steep adsorption isotherm due to capillary condensation is also seen for the microwave-assisted sample, but to a lesser extent.

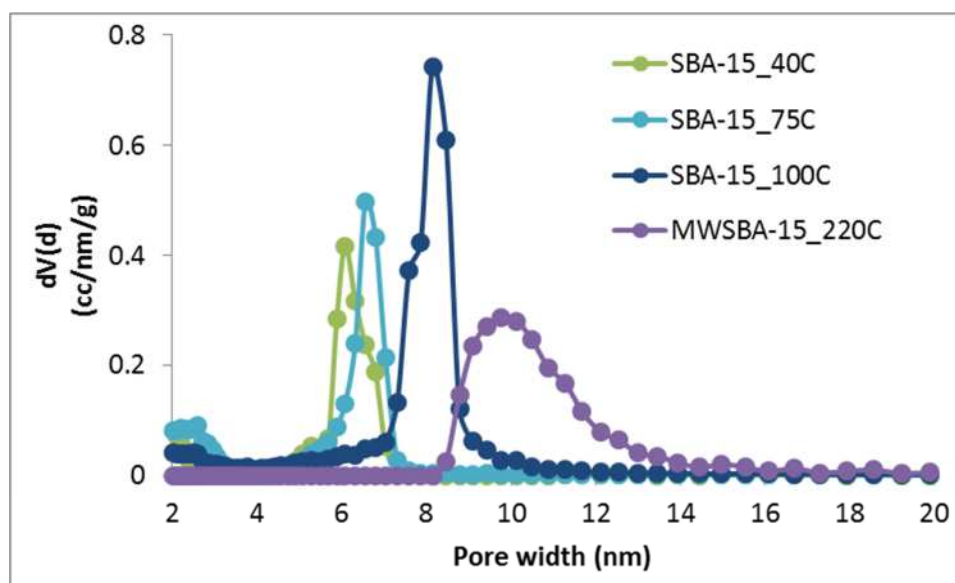


**Figure 11 – NLDFT pore size distributions of mesoporous silica SBA-15 synthesised at 40, 75, 100, and (MW) 220 °C**

The narrow pore size distributions shown in Figure 11, calculated by the NLDFT method, indicate good control of the SBA-15's mesopore diameter. As expected, pore size increases at higher hydrothermal ageing temperatures. The pore size distributions are also broader, i.e., less controlled, for syntheses carried out at higher temperatures.

**Table 2 – Morphological parameters of mesoporous silica SBA-15 derived from N<sub>2</sub> physisorption**

<b>Synthesis temperature (°C)</b>	<b>NLDFT pore diameter (nm)</b>	<b>BET surface area (m<sup>2</sup>/g)</b>	<b>Mesopore volume (cm<sup>3</sup>/g)</b>
40	6.1	505	0.467
75	6.6	602	0.656
100	8.1	685	1.093
220 (MW)	9.8	268	0.983

Table 2 shows the morphological parameters, derived from nitrogen physisorption, of all SBA-15 samples. Total surface area, calculated by the BET method, increases with increasing synthesis temperature for all conventionally-synthesised SBA-15 batches. However, the microwave-assisted SBA-15 has a

significantly lower surface area despite its larger pores. The pore volume associated with pores smaller than 50 nm also increases with increasing synthesis temperature for all conventionally-synthesised SBA-15 samples. No appreciable interparticle macropore volume is observed for any sample. It has been reported that SBA-15 synthesised at high temperatures, including those synthesised via microwave, experience increased merging of primary pore channels due to having thinner pore walls.<sup>158,159</sup> This may explain why, in addition to having a wider pore size distribution trailing to larger pore size distribution, the microwave-synthesised SBA-15 batch has a significantly smaller surface area while retaining a high pore volume.

### 2.6.3 Small-angle X-ray scattering

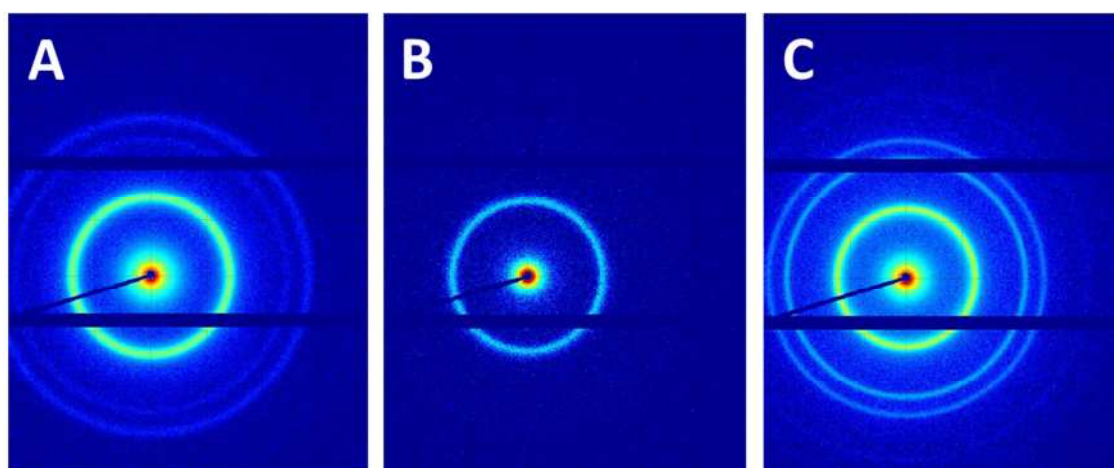


**Figure 12 – Small-angle X-ray scattering patterns of SBA-15 synthesised at (A) 40 °C, (B) 75 °C, and (C) 100 °C**

SAXS patterns of the three conventionally synthesised SBA-15 are shown in Figure 12. These patterns show that all three samples have ordered porous structures. The SBA-15 synthesised at 75 °C is shown to have the shortest range of order, while the 40 and 100 °C batches of SBA-15 have long-range order. This is determined by the number of clearly-visible overtones in the scattering patterns. The SBA-15 synthesised with a microwave at 220 °C was not investigated via SAXS.

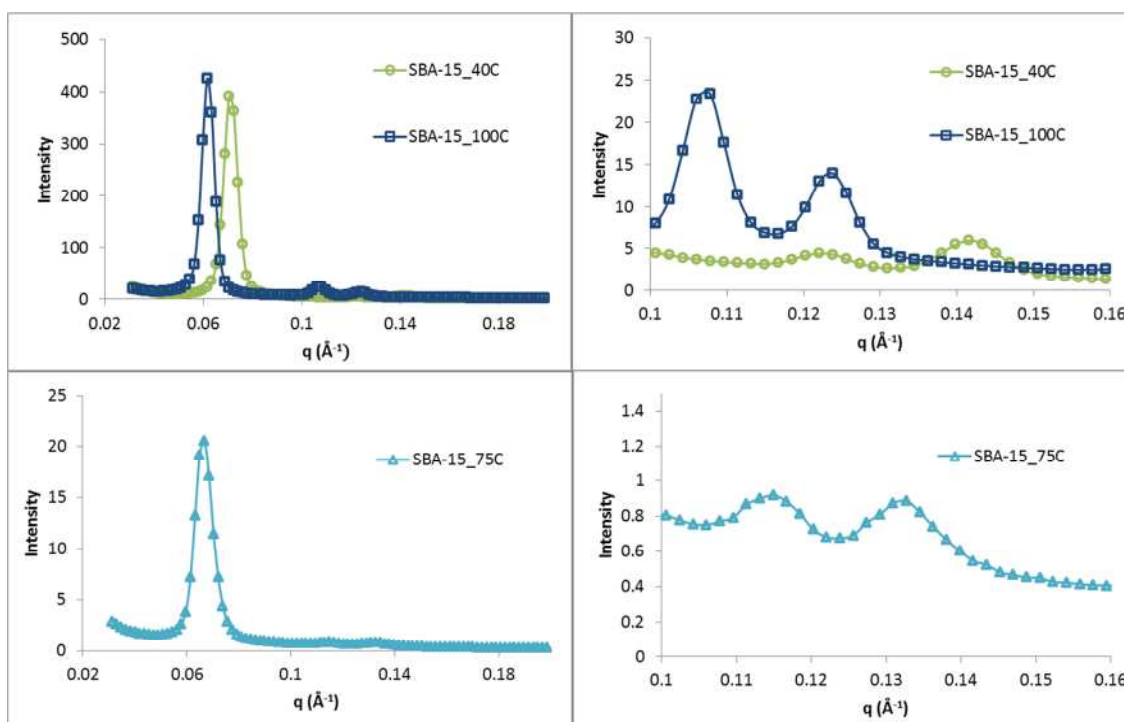


**Figure 13 – Small-angle X-ray scattering spectra of SBA-15 aged at 40 °C and 100 °C (top) and SBA-15 aged at 75 °C (bottom). Graphs on the right are depict a smaller range of  $q$  at lower intensity.**

The SAXS spectra for the SBA-15 synthesised at 40 °C and at 100 °C show three Bragg reflections peaks. The left-shift of the peaks at a higher synthesis temperature indicates that the samples have a different unit cell dimensions. The difference between the relative intensities of the peaks suggests that the two samples have different pore wall thicknesses. The SAXS spectrum of the SBA-15 synthesised at 75 °C has lower intensity Bragg reflections peaks than the 40 °C and 100 °C SBA-15 samples, so they are here shown with different intensity axes. The lower intensity may be from inadequate exposure of the sample during measurement, or may indicate that there are larger amorphous regions of silica. However, the positioning of the peaks, compared to the two other samples, indicates that the 75 °C SBA-15 sample has an intermediate unit cell size between those of the 40 °C and 100 °C SBA-15 samples. Additionally, the relative intensity of the peaks show a different pore wall thickness for this sample, compared to those of the other two syntheses.

**Table 3 – Morphological parameters of mesoporous silica SBA-15 derived from small-angle X-ray scattering**

<b>Synthesis temperature (°C)</b>	<b>Unit cell dimension (nm)</b>	<b>Pore wall thickness (nm)</b>
40	10.3	4.2
75	11.2	4.6
100	11.8	3.7

The unit cell dimension corresponds to the distance between the centres of the pores; therefore, each sample's pore wall thickness is calculated by subtracting the NLDFT-calculated pore diameter from the unit cell dimension. The pore wall thicknesses for all conventionally-synthesised SBA-15 are very similar and do not appear to trend with synthesis temperature.

From these three characterisation methods in conjunction, we can calculate approximations of the external and internal surface area of the SBA-15 materials. Assuming that the cylindrical pores of a given diameter are arranged hexagonally with a given unit cell dimension, we can calculate the porosity of the material by subtracting the cross-sectional area of the pore from a hexagonal silica unit. Using this method, we estimate the porosity of the 40 °C SBA-15 batch at 0.318, the 75 °C batch as 0.315, and the 100 °C batch as 0.427. We also know from SEM micrographs, very approximately, the external dimensions of an SBA-15 particle: a cylinder 1 µm in length and 350 nm in diameter. Knowing also the density of silica to be 2.65 g/cm<sup>3</sup> and the calculated porosities, i.e. lost mass, of these particles, we can determine the external surface area of these SBA-15 particles to be 7 m<sup>2</sup>/g for both the 40 °C and 75 °C batches, and 9 m<sup>2</sup>/g for the 100 °C batch. Comparing these values, even as rough estimates, to the BET surface areas in Table 2 puts the external surface area of the SBA-15 particles at approximately 1% that of the surface area within the particle's pores.

## **2.7 Conclusion**

In this chapter, batches of mesoporous silica SBA-15 have been synthesised and characterised in such a way that confirms their suitability for future

experiments. Altering the temperature at which SBA-15's hydrothermal condensation step takes place changes the material's pore diameter, thereby altering the material's surface area and pore volume. Gas physisorption indicates that the median pore diameter of the SBA-15 batches increases with increasing synthesis temperature in accordance with literature. Gas physisorption also shows that the SBA-15's pore size distributions are narrow, which is further confirmed with TEM. SAXS spectra indicate that the pore wall thickness is not significantly altered by the swelling of micelles. These characterisation techniques show the control that is achievable over the pore morphology of SBA-15; their mean, narrowly-distributed diameter can be changed without substantially altering pore tortuosity or external particle morphology. These materials can be used to examine the effects of steric confinement on adsorbed proteins without other morphological changes obscuring the results.

From this chapter, it is clear that SBA-15 is not a sophisticated synthetic analogue for chaperonin complexes; there are no moving parts or switching of charges. SBA-15 is simple in comparison, and this thesis will show how it is effective in examining two parameters that make chaperonins efficient: steric confinement and electrostatic attraction. In Chapters 3 and 4, protein adsorption onto these materials will be investigated, to better understand the physical effects between the surface of the materials' long, narrow pores and flexible, globular proteins. Then, in Chapters 5, 6, and 7, the protective properties that adsorption to these materials confers to enzymes will be tested. These experiments investigate the catalytic activities of enzymes immobilised onto SBA-15 of different pore sizes and exposed to different attenuating conditions, and help clarify the relative importance of the chaperonin-inspired parameters.

### **3 Equilibrium protein adsorption on mesoporous silica SBA-15**

#### **3.1 Introduction**

There have been many investigations on how proteins interact with the interior cavity of GroEL/ES chaperonins, as discussed in Section 1.3.1 of this thesis. Those interactions are complex and multi-staged: a combination of electrostatic attraction, hydrophobic residue-induced water exclusion, and ATP-induced compression. In contrast, SBA-15's interactions with proteins are more straightforward. Efforts have already been made to describe these interactions with simple models, treating proteins as spheroids with fixed electrical charges, as discussed in Section 1.3.2. In this way, we can interpret the adsorption of proteins to the surface of SBA-15 in the contexts of the steric confinement of the protein within a narrow, cylindrical channel, and of the net electrostatic attraction, or repulsion, of the protein to the negatively charged walls of the silica pore.

The first step for experimentally investigating these interactions is to observe the adsorption of protein molecules onto the surface of SBA-15 once equilibrium between protein molecules and available adsorption sites on the material has been reached. The proteins attach, primarily by a combination of van der Waals forces, hydrophobic interactions, and hydrogen bonds, within the pores of the material, as discussed in Section 1.2.1. Proteins also attach to the external surface of the SBA-15 particles, but, as discussed in Section 2.6.3, approximately 99% of the SBA-15's surface area is within the pores. These equilibrium points are strongly affected by the temperature of the system, so to meaningfully compare how the equilibrium shifts across different systems, we need to collect these data isothermally. We expect, initially, that protein adsorption is directly proportional to protein concentration in the bulk solution when there are many adsorption sites available. This region of the isotherm, at low protein concentration, is sometimes referred to as the Henry's law region for following this relation.<sup>160</sup> As sites become more fully occupied, the excess protein is left free in solution. This means there is a maximum amount of protein that can be adsorbed onto the surface of the material. This type of adsorption is

described by the Langmuir adsorption model, which is detailed further in the methods section of this chapter.

Previous studies of proteins adsorbed to SBA-15 have found that maximum loadings of protein increase with increasing pore size, which is attributed to more efficient packing of the proteins within the pores of the material.<sup>112–114</sup> These experiments also indicated that proteins pack within the pores in multiple layers when adsorption occurs at a protein's isoelectric point, where the protein has a net neutral charge. This is demonstrated by the observation that pore volume is a more accurate prediction of maximum protein loading than surface area. This interpretation was also obtained with the help of a simple geometric model of protein packing within the pores. It has also been reported that maximum protein loading onto SBA-15 changed with pH such that it was maximal at the protein's isoelectric point. This is interpreted as being due to more complete packing of proteins within the pores being achievable when the proteins have net neutral charges and are, therefore, not experiencing intermolecular repulsion.<sup>121</sup>

In the following experiments, the protein adsorption isotherms are not collected at each protein's isoelectric point, but rather at a fixed pH of 7.2. This is to investigate the effect of the protein's charge on its equilibrium adsorption. Furthermore, performing these isotherm experiments at a neutral pH, where their native structure is not perturbed, is necessary for supporting the experiments concerning enzyme activity in Chapters 5, 6, and 7; in those experiments, we want to work in the Henry's law region of protein adsorption where the enzymes are maximally on the silica surface and minimally free in solution. Additionally, in these experiments, we look at the affinity for adsorption of the proteins to the SBA-15, in the form of the Langmuir adsorption constant. These experiments aim to investigate maximum protein adsorption and adsorption affinity with respect to steric confinement and electrostatic attraction, the two chaperonin parameters studied in this thesis.

## 3.2 Materials and methods

### 3.2.1 Protein adsorption isotherms on SBA-15 with varying pore sizes

Sodium phosphate monobasic (BioXtra,  $\geq 99\%$ ), sodium phosphate dibasic (BioXtra,  $\geq 99\%$ ), lysozyme from chicken egg white (lyophilized powder, protein content  $\geq 90\%$ ,  $\geq 40,000$  units/mg protein), myoglobin from equine heart ( $\geq 90\%$ , essentially salt-free, lyophilized powder), trypsin from bovine pancreas (Type XI, lyophilized powder,  $\geq 6,000$  BAEE units/mg protein), and pepsin from porcine gastric mucosa (powder,  $\geq 400$  units/mg protein) were all purchased from Sigma-Aldrich and used without further purification. Mesoporous silica SBA-15 was prepared and characterised as discussed in Chapter 2. In this chapter, SBA-15 samples are referred to by their NLDFT-calculated pore diameters, rather than by the temperatures used during the hydrothermal condensation step of their syntheses. Ultraviolet-visible spectrophotometry (UV-Vis) was carried out using a BioTek Synergy H1 Multi-Detection Reader.

To study the thermodynamics of protein adsorption onto mesoporous silica SBA-15 samples with different pore diameters, adsorption isotherms of several proteins were prepared. Phosphate buffer with a pH of 7.2 and an ionic strength of 100 mM was prepared by mixing a 100 mM solution of sodium phosphate monobasic and a 33.3 mM solution of sodium phosphate dibasic. SBA-15 was suspended in this phosphate buffer at a concentration of 4 g/L. The suspension was sonicated and visually checked for adequate dispersion. Protein solutions were prepared in the same buffer at varying concentrations between 0.1 g/L and 3.0 g/L. The SBA-15 solutions were then mixed with equal volumes of protein solutions, resulting in final SBA-15 concentrations of 2 g/L and varying final concentrations of protein. Each combination of protein, SBA-15 sample, and protein concentration were prepared and measured in triplicate. These composite solutions were agitated overnight at room temperature to ensure equilibrium; evidence that protein adsorption onto SBA-15 reaches equilibrium. Protein adsorption onto SBA-15 reaches equilibrium over several hours, as can be seen in Chapter 4 of this thesis.

To determine the loading of protein on the SBA-15 sample, the composite solutions were centrifuged at 12,000 rpm for 5 minutes. The concentrations of

protein in the supernatants were measured via UV-Vis at a characteristic absorbance wavelength of 280 nm (and also 409 nm for myoglobin). These measurements were compared to a calibration curve, and the protein concentrations were determined by the Beer-Lambert law. The amounts of protein adsorbed to the SBA-15 were calculated using mass balance.<sup>114</sup> Adsorption isotherms were prepared for myoglobin and lysozyme on SBA-15 samples with pore diameters of 6.1, 6.6, and 8.1 nm. Isotherms for trypsin were prepared with 6.6 and 8.1 nm SBA-15, and an isotherm for pepsin was prepared on just 8.1 nm SBA-15.

### **3.2.2 Determining protein concentration from the Beer-Lambert law**

The Beer-Lambert law, shown in Equation 4, describes the relationship between the absorbance of light and a concentration of light-absorbing species within a sample. It is used in this and future chapters to correlate the UV-Vis absorbance of a sample with its concentration of a specific protein.

#### **Equation 4 – Beer-Lambert law for a single attenuating species**

$$A = l\varepsilon c$$

where absorbance  $A$  is directly proportional to  $l$ , the path length of light through the sample,  $\varepsilon$ , the extinction coefficient of the species, and  $c$ , the concentration of the species. This correlation is limited to low concentrations of a species, as the absorbance reaches a maximum value at high concentrations. This relationship allows the preparation of calibration curves, where protein solutions of known concentrations are linearly correlated with absorbance for a particular path length on a particular spectrophotometer. Samples with unknown concentrations can then have their absorbance values compared to this calibration curve to determine their protein concentration.

### **3.2.3 Langmuir adsorption model**

A protein adsorption isotherm discerns the relationship between unbound protein concentration and protein loaded onto the adsorbent material at the system's equilibrium. Adsorption isotherms are important for determining the maximum amount of protein that can load on the material and the adsorption affinity between the protein and the material.

### Equation 5 – Langmuir adsorption model

$$\frac{q}{q_m} = \frac{K_{eq}C}{1 + K_{eq}C}$$

The Langmuir adsorption model, shown in Equation 5, describes adsorption of molecules to a surface in terms of empty and occupied adsorption sites, and assuming that the adsorbate acts like an ideal gas at isothermal conditions.<sup>80</sup> Here,  $q$  and  $q_m$  are loading (mg protein/g SBA-15) of the adsorbent at equilibrium and its maximum value, respectively.  $K_{eq}$  (L/g) is the Langmuir equilibrium constant, which can also be expressed as the ratio of the adsorption rate constant to the desorption rate constant.  $C$  is the concentration of protein in the solution, which acts similar to pressure in an ideal gas system.

However, many of the assumptions of the Langmuir model are not met by the physical system described in this chapter. The adsorbing surface of SBA-15 is not perfectly flat: it is both curved and slightly rough, due to the presence of microporosity between the cylindrical pores. It is unlikely that proteins adsorb into completely immobile states, because proteins have flexible structures. Protein adsorption onto the silica surface is likely affected by electrostatic attraction, so adsorption can change as local environments fluctuate. At high concentrations, proteins can compete for adsorption sites and repel other proteins via electrostatic repulsion. Lastly, this model assumes that only monolayer coverage is possible, whereas there may be limited multilayer adsorption, or pore filling, within the SBA-15 pores. The Langmuir adsorption model is fitted to the experimental protein adsorption isotherms reported in this chapter via a sum of least squares method in order to determine these parameters.

Other models are available for describing adsorption of molecules onto surfaces at equilibrium. A precursor to the Langmuir model is the Freundlich model, which also describes the relationship between the concentration of a solute on the surface of an adsorbent and the concentration of the solute in the liquid with which it is in contact.<sup>161</sup> This relationship is entirely empirical, however, and does not incorporate monolayer loading onto the material, which is why the Langmuir model is chosen for this chapter. When compared, protein adsorption

onto mesoporous silica has been seen to follow Langmuir model better than the Freundlich model for these reasons.<sup>57,162</sup> Another adsorption model that may be considered for this work is the Dubinin-Radushkevich model, which was originally developed for vapour adsorption within microporous carbons.<sup>163</sup> The Dubinin-Radushkevich model assumes that there is a change in the potential energy of a gas as it adsorbs, and that a given solid has a characteristic energy.<sup>164</sup> Protein adsorption onto mesoporous silica has not been seen to follow the Dubinin-Radushkevich model as well as the Langmuir model, particularly at lower protein concentrations where the Dubinin-Radushkevich model does not transition into the Henry's law region.<sup>165,166</sup>

### 3.3 Results and discussion

#### 3.3.1 Myoglobin adsorption isotherms

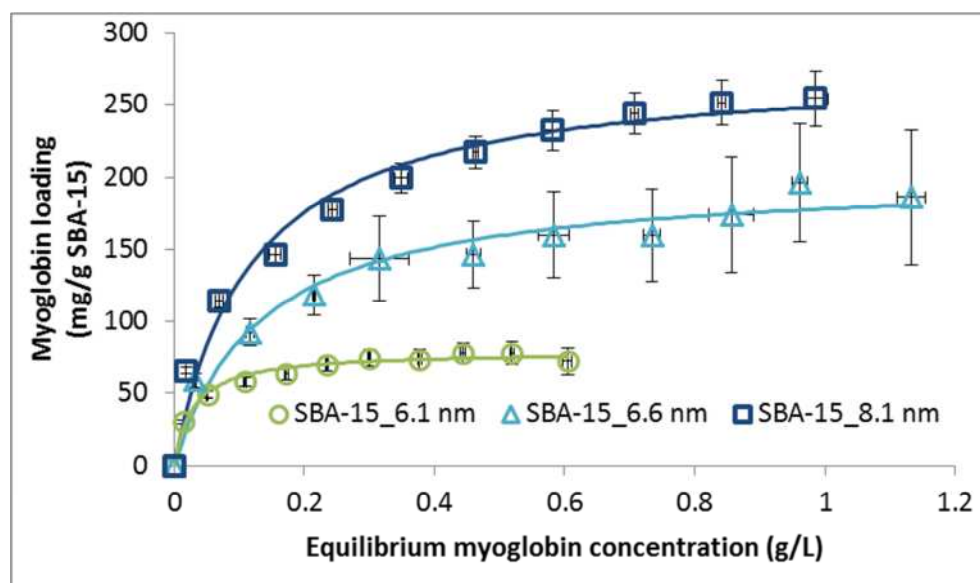


**Figure 14 – Myoglobin adsorption isotherms onto mesoporous silica SBA-15 with different pore diameters (6.1, 6.6, and 8.1 nm) in phosphate buffer with pH 7.2 and 100 mM ionic strength. Error bars depict 95% confidence intervals. Solid lines represent the Langmuir adsorption model.**

The adsorption isotherms of myoglobin onto SBA-15 of different pore diameters in phosphate buffer with pH 7.2 and 100 mM ionic strength are shown in Figure 14 with error bars depicting 95% confidence intervals. The solid lines depict the Langmuir model fitted to these data sets. The Langmuir model parameters extracted from these least-squares fittings for each SBA-15 sample are displayed in Table 4.

**Table 4 – Langmuir model parameters for isothermal myoglobin adsorption to SBA-15 with different pore diameters (6.1, 6.6, and 8.1 nm) in phosphate buffer with pH 7.2 and 100 mM ionic strength**

<b>SBA-15 pore diameter (nm)</b>	<b><math>q_m</math> (mg Mb/ g SBA-15)</b>	<b><math>K_{eq}</math> (L/g Mb)</b>
6.1	78.8	35.0
6.6	201	7.57
8.1	278	8.62

For all experimental data sets, the Langmuir model fits well. As expected, larger pore diameter SBA-15 has a higher maximum loading of myoglobin,  $q_m$ . It should be noted that the experimental values of myoglobin adsorption do not reach the predicted  $q_m$  for the two larger pore sizes of SBA-15; therefore, these values are extrapolated.

As discussed in Section 2.6.3, nearly all of these SBA-15's surface areas are within the pores. Some of the SBA-15 surface area reported by nitrogen physisorption is not directly available for protein adsorption, however; though an individual protein can theoretically access the mesopore surface, adsorption sites may be blocked by other adsorbed proteins within the curved, narrow pores. Still, we hypothesise the majority of myoglobin adsorption to be internal to the SBA-15. The estimated external SBA-15 surface areas range from 7 to 9 m<sup>2</sup>/g. The packing area of myoglobin, from its diameter of 4.1 nm, is approximately 13.2 nm<sup>2</sup>. The SBA-15 particles could therefore not support more than approximately 15 to 18 mg myoglobin per g SBA-15 on their external surfaces, and myoglobin would likely prefer to adsorb to the internal silica surface over multilayer external adsorption. However, these possible external loadings are not insignificant, and may account for up to 6 to 7% of the loading seen on the 6.6 nm and 8.1 nm SBA-15, and up to 19% of that seen on the 6.1 nm SBA-15.

As seen in Table 2, the surface area of these three SBA-15 batches increases with increasing pore diameter. Maximum myoglobin loading still increases with

increasing SBA-15 surface area, although to a more moderated extent. Interestingly, because each SBA-15 sample has much greater pore volume with increasing pore diameter, maximum myoglobin loading does not trend with pore volume. Similar results have been seen where protein loading within SBA-15 pores can be well-described by pore-filling models.<sup>113,114</sup> Also interesting is that, from these experiments, the equilibrium constant  $K_{eq}$  is not found to have a clear relationship with pore diameter; adsorption onto SBA-15 with the 6.6 nm and the 8.1 nm pores have very similar  $K_{eq}$ , while that of the 6.1 nm SBA-15 has a  $K_{eq}$  that is an order of magnitude higher.

### 3.3.2 Lysozyme adsorption isotherms

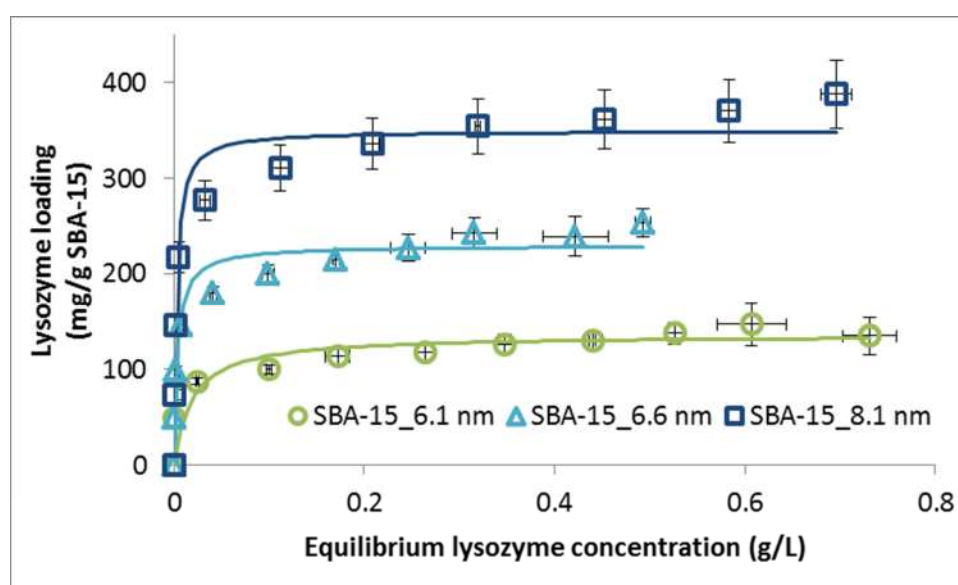


**Figure 15 – Lysozyme adsorption isotherms on mesoporous silica SBA-15 with different pore diameters (6.1, 6.6, and 8.1 nm) in phosphate buffer with pH 7.2 and 100 mM ionic strength. Error bars depict 95% confidence intervals. Solid lines represent the Langmuir adsorption model.**

The adsorption isotherms of lysozyme onto SBA-15 of different pore diameters in phosphate buffer with pH 7.2 and 100 mM ionic strength are shown in Figure 15 with error bars depicting the 95% confidence intervals. The solid lines depict the Langmuir model fitted to these data sets. The Langmuir model parameters extracted from these least-squares fittings for each SBA-15 sample are displayed in Table 5.

**Table 5 - Langmuir model parameters for isothermal lysozyme adsorption to SBA-15 with different pore diameters (6.1, 6.6, and 8.1 nm) in phosphate buffer with pH 7.2 and 100 mM ionic strength**

<b>SBA-15 pore diameter (nm)</b>	<b><math>q_m</math> (mg Mb/ g SBA-15)</b>	<b><math>K_{eq}</math> (L/g Lz)</b>
6.1	136	53.1
6.6	229	265
8.1	350	387

In Figure 15, it can be seen that the Langmuir model does not fit the lysozyme adsorption data as well, with the model exceeding the data's error bars at some points. For the two larger pore sizes, the Langmuir model underestimates lysozyme adsorption at lower concentrations, and the model also does not account for the continued increase in adsorbed lysozyme at high concentrations. This may be also attributed to the experiment taking place away from lysozyme's isoelectric point: while lysozyme molecules are charged, they will interact more strongly by repelling each other and attracting more strongly to the silica surface. These attractive interactions may cause more complete lysozyme adsorption at low protein concentrations, and also the self-repulsive effects may be why higher protein concentrations are required to reach maximum lysozyme packing onto the silica surface.

As expected, larger pore diameters of SBA-15 have higher maximum loading of lysozyme,  $q_m$ . Unlike in the myoglobin isotherms of the previous section, the experimental values of lysozyme adsorption do reach the predicted  $q_m$ . These maximum loadings are higher than the respective maximum myoglobin loadings. Lysozyme is a smaller protein; therefore more lysozyme molecules can fit into the cross-sectional area of a pore than myoglobin molecules. The estimated external SBA-15 surface areas, from Section 2.6.3, could not support more than approximately 13 to 16 mg lysozyme per g SBA-15. We hypothesise the majority of lysozyme adsorption to be within the SBA-15 pores; the positively-charged lysozyme would prefer multilayer external adsorption even less than myoglobin. These external loadings could only account for up to 5 to

6% of the lysozyme loading seen on the 6.6 and 8.1 nm SBA-15, and up to 10% of that seen on the 6.1 nm SBA-15. As seen in the previous section with myoglobin, maximum lysozyme loading increases with increasing SBA-15 surface area, although to a lesser extent. Again, not all surface area represents available adsorption sites, as other lysozyme may block the surface within the narrow, curved pores. Maximum lysozyme loading does not trend with pore volume, supporting the hypothesis that pore volume is the limiting factor of maximum protein adsorption to SBA-15.

The Langmuir equilibrium constant,  $K_{eq}$ , increases significantly with increasing pore diameter, meaning that lysozyme has greater adsorption affinity for the silica surface of the larger pores. There is a particularly large increase between the 6.1 nm SBA-15 and the 6.6 nm SBA-15, which was also seen with the myoglobin isotherms. The values for  $K_{eq}$  for lysozyme on all pore diameters of SBA-15 are higher than those for myoglobin. This may be because these adsorption isotherm experiments are carried out at pH 7.2, which is myoglobin's isoelectric point. While myoglobin has a net neutral charge, it is not strongly attracted to the negatively charged surface of the silica. In comparison, lysozyme's isoelectric point of 11.3 means it will have a positive charge in a buffer with pH 7.2. This electrostatic attraction may account for its stronger affinity for the material. The increased  $K_{eq}$  could also be attributed to the smaller size of lysozyme, which means it has more available sites on the silica surface to adsorb onto.

### 3.3.3 Trypsin adsorption isotherms

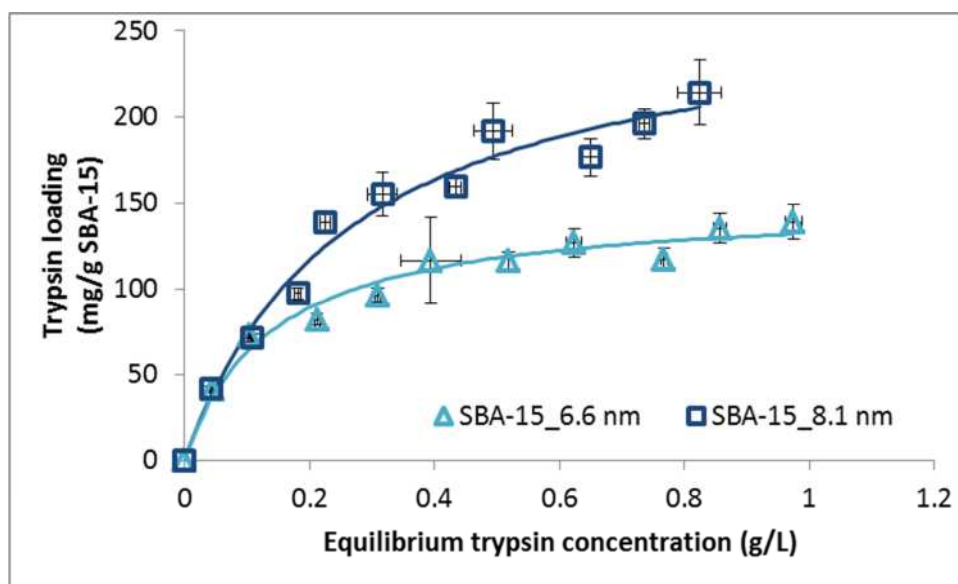


Figure 16 - Trypsin adsorption isotherms on mesoporous silica SBA-15 with different pore diameters (6.6 and 8.1 nm) in phosphate buffer with pH 7.2 and 100 mM ionic strength. Error bars depict 95% confidence intervals. Solid lines represent the Langmuir adsorption model.

The adsorption isotherms of trypsin onto SBA-15 of different pore diameters in phosphate buffer with pH 7.2 and 100 mM ionic strength are shown in Figure 16 with error bars depicting the 95% confidence intervals. The solid lines depict the Langmuir model fitted to these data sets. The parameters extracted from least-squares fittings of the Langmuir model are shown in Table 6.

Table 6 - Langmuir model parameters for isothermal trypsin adsorption to SBA-15 with different pore diameters (6.6 and 8.1 nm) in phosphate buffer with pH 7.2 and 100 mM ionic strength

SBA-15 pore diameter (nm)	$q_m$ (mg Mb/ g SBA-15)	$K_{eq}$ (L/g Tp)
6.6	150	7.32
8.1	271	3.81

Both adsorption isotherms of trypsin onto SBA-15 are described by the Langmuir model well. The larger pore diameter SBA-15 has a higher maximum

loading of trypsin,  $q_m$ . As with the myoglobin isotherms, the experimental values of trypsin adsorption do not reach the predicted  $q_m$ ; therefore, these values are extrapolated. These maximum loadings are lower than both the respective myoglobin and lysozyme loadings. This is to be expected, as trypsin is larger than both myoglobin and lysozyme, so fewer trypsin molecules can fit within the same sized pores. The estimated external SBA-15 surface areas, from Section 2.6.3, could support approximately 16 to 19 mg trypsin per g SBA-15; these external loadings could account for up to 11% of the 6.6 nm SBA-15 trypsin loading and 7% of the 8.1 nm SBA-15 loading.

The equilibrium constant,  $K_{eq}$ , for trypsin on both pore diameters of SBA-15 lower than those found for both myoglobin and lysozyme. This was unexpected, because trypsin, with an isoelectric point of pH 10.3, is positively charged at pH 7.2 while the silica surface is negatively charged. One would expect  $K_{eq}$  values intermediate to those of myoglobin and lysozyme, which have isoelectric points of 7.2 and 11.3 respectively, if  $K_{eq}$  were based primarily on this electrostatic attraction. Perhaps trypsin's  $K_{eq}$  values onto SBA-15 are instead lower because it is a larger protein than both myoglobin and lysozyme, therefore there are fewer available sites for it to adsorb onto.

### 3.3.4 Enzyme adsorption isotherms across a single pore size of SBA-15

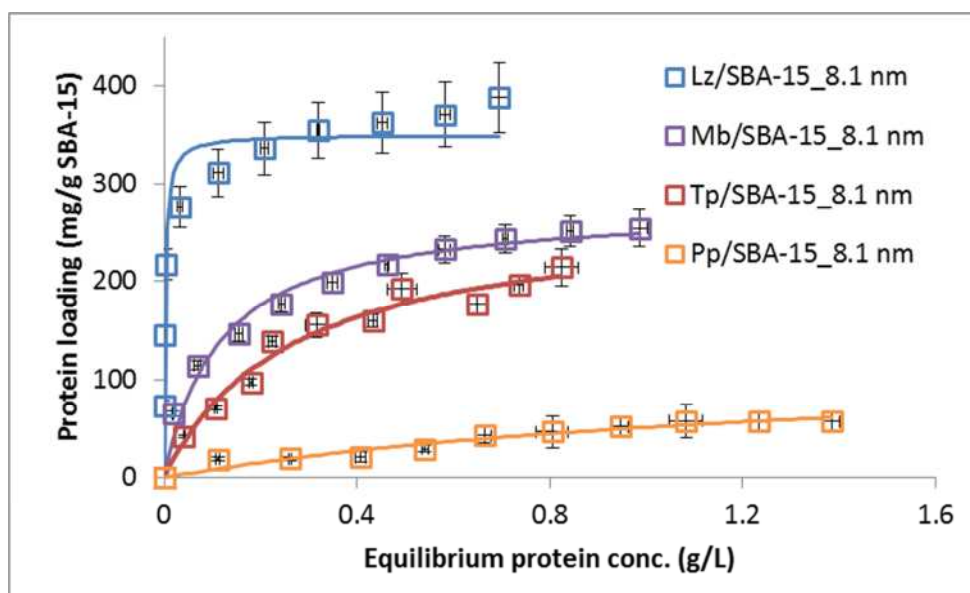


Figure 17 - Protein adsorption isotherms on mesoporous silica SBA-15 (8.1 nm) in phosphate buffer of pH 7.2 and 100 mM ionic strength, for lysozyme, myoglobin, trypsin, and pepsin. Error bars depict 95% confidence intervals. Solid lines represent the Langmuir adsorption model.

The adsorption isotherms of lysozyme, myoglobin, trypsin, and pepsin onto SBA-15 with a pore diameter of 8.1 nm in phosphate buffer with pH 7.2 and 100 mM ionic strength are shown in Figure 17 with error bars depicting the 95% confidence intervals. Data for the lysozyme, myoglobin, and trypsin isotherms onto this pore size of SBA-15 are also shown in previous figures, but are combined here for comparison at one pore size. The solid lines again depict the Langmuir model fitted to these data sets. The parameters extracted from least-squares fittings of the Langmuir model are shown in Table 7.

**Table 7 - Langmuir model parameters for isothermal protein adsorption to SBA-15, pore diameter of 8.1 nm, in phosphate buffer with pH 7.2 and 100 mM ionic strength**

<b>Protein</b>	<b><math>q_m</math> (mg/g SBA-15)</b>	<b><math>K_{eq}</math> (L/g)</b>
Lysozyme	350	387
Myoglobin	278	8.62
Trypsin	271	3.81
Pepsin	122	0.731

Comparing the Langmuir model parameters  $q_m$  and  $K_{eq}$  across several proteins, but on SBA-15 of a fixed pore diameter of 8.1 nm, allow us to draw conclusions about whether a protein's size or net surface charge has more of an effect on its maximum loadings and adsorption affinities onto porous silica. Lysozyme is both the smallest protein and the most positively charged, while pepsin is both the largest and most positively charged. The different effects of size and charge must therefore be seen from the isotherms of myoglobin and trypsin: myoglobin is second smallest but has no net charge, while trypsin is second largest and is positively charged.

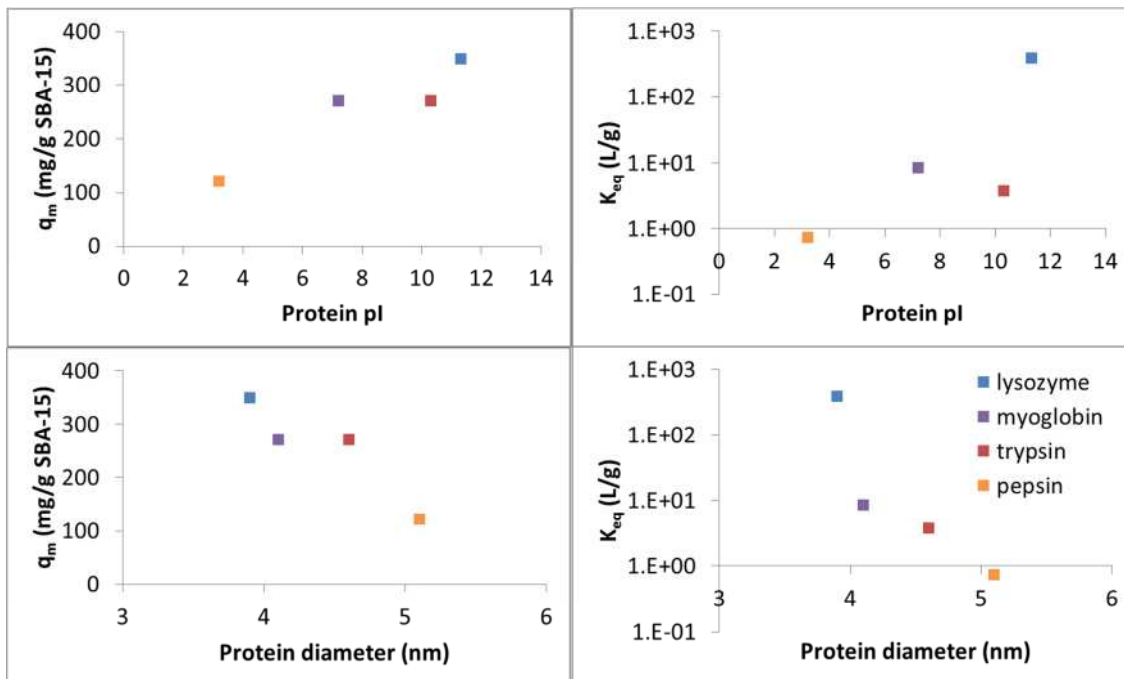


**Figure 18 – Comparisons of Langmuir model parameters  $q_m$  and  $K_{eq}$  with proteins' pIs and hydrodynamic diameters when adsorbed onto SBA-15, pore diameter of 8.1 nm, in phosphate buffer with pH 7.2 and 100 mM ionic strength**

Figure 18 contains four plots of the data in Table 7. They display the maximum protein loadings and Langmuir adsorption constants as a function of the four proteins' pIs and diameters.  $q_m$ , the maximum protein loading to the pores of SBA-15, appears to increase with increasing pI. Considering that SBA-15 has a pzc of 2 and is negatively charged under the conditions of this isotherm, it is possible that the greater electrostatic attraction that more positively-charged proteins, such as lysozyme, experience to the silica lead to greater maximum loadings.  $q_m$  also increases with decreasing size of the protein. This is reciprocal to the effect seen with increasing SBA-15 pore diameter across the isotherms for any one protein. From these data alone, it is not possible to determine which of these protein characteristics, size or electrostatic charge, has a greater effect on maximum loadings of protein onto the surface of SBA-15. The Langmuir adsorption constant,  $K_{eq}$ , which represents adsorption affinity, is not more clearly affected by protein size than by net electrostatic charge. We might have expected the electrostatic attraction between the proteins and SBA-15 to have a clearer effect on the adsorption affinity, perhaps with a stronger affinity being shown for more positively charged proteins, but this is not shown to be the case from these experiments.

### 3.4 Conclusion

In this chapter, the adsorption isotherms of several proteins to several pore sizes of SBA-15 under one solution condition and at room temperature are reported. These isotherms are fit to the Langmuir model of adsorption, and the parameters from this model are compared across the different proteins and pore sizes. For each protein, maximum protein loading,  $q_m$ , is found to increase with increasing pore size. The Langmuir equilibrium constant  $K_{eq}$  does not consistently trend with pore size for the different proteins investigated, but for lysozyme it increases with increasing pore size. For several proteins adsorbed on SBA-15 of the same pore size, we find that maximum protein loading, by mass, increases with decreasing protein size and increasing protein pI.  $K_{eq}$  was not found to clearly trend with either protein size or pI from these experiments.

The clear trends of  $q_m$  with pore and protein size are consistent with previous findings, and indicate that more proteins can fit within the larger pores. The findings also support the hypothesis that the proteins can pack within the pores.  $K_{eq}$  does not trend clearly with either the proteins' steric confinement within the pores or their electrostatic attraction to the silica surface across the systems tested. This may mean that  $K_{eq}$  is affected by other features of the proteins entirely, or that the range of these parameters was not wide enough to generate conclusions. The effect of electrostatic attraction on equilibrium adsorption has been shown in previous literature by altering the pH of the adsorption experiments;<sup>113,121</sup> such an extension to the existing experiments would clarify the effects for these proteins as well, and should be considered as future work. The isotherms reported in this chapter have been prepared at a neutral pH in order to inform the experiments involving enzyme activity in Chapters 5, 6, and 7, so that those experiments can take place in the Henry regime, where most of the enzymes are adsorbed, rather than free in solution.

These experiments support the method of interpreting the equilibrium adsorption of proteins to SBA-15 through the lens of steric confinement and describing the process as spheroid proteins packing within cylindrical pores. The effects of electrostatic attraction between protein molecule and silica surface, which is the other chaperonin-inspired parameter this thesis investigates, on protein adsorption is also demonstrated. The next chapter will

investigate the kinetics of protein adsorption onto SBA-15, again in the context of the two chaperonin-inspired parameters, to see if electrostatic attraction has an effect on the rate of adsorption and if steric confinement continues to play an important role.

## **4 Kinetics of protein adsorption on mesoporous silica SBA-15**

### **4.1 Introduction**

To understand the dynamics between proteins and the interior surfaces of mesoporous silica SBA-15, protein adsorption is observed both at thermodynamic equilibrium and before equilibrium is reached, during the adsorption process. In both types of experiments, the steric confinement of the proteins within the pores and the electrostatics experienced by the proteins are considered while interpreting the results. As previously discussed, chaperonins have complex interactions with their substrate proteins. However, we are primarily interested in these two simplified parameters, inspired by our understanding of chaperonins.

In the previous chapter, protein adsorption on SBA-15 at thermodynamic equilibrium was found to be strongly influenced by the relationship between the protein's size and the pore's size; more protein could be adsorbed onto SBA-15 with larger pores. The electrostatic attraction or repulsion of the protein to the silica surface was also shown to influence equilibrium loading in the experiments presented. This chapter investigates similar questions for the kinetics of protein adsorption onto SBA-15, particularly concerning how protein size and charge affect its diffusivity within a pore.

The experiments in this chapter are derived primarily from the work of Lung-Ching Sang, as described in Chapter 3 of his thesis.<sup>121</sup> In his work, Sang performed experiments to investigate the adsorption kinetics of the protein lysozyme. In Sang's experiments, the solutions used for adsorption have a pH of 7.0, in which lysozyme is positively charged. He also created a theoretical model to describe lysozyme's adsorption to SBA-15, taking into account both the geometry and electrostatics of the system. Sang observed that lysozyme adsorbed faster to the surface of SBA-15 with larger pores. From this, he determined that the adsorption process is diffusion-limited. In this chapter, we perform similar adsorption kinetic experiments on the protein myoglobin. Myoglobin, as discussed in Section 1.3.2, is a larger protein than lysozyme. More importantly, myoglobin has a net neutral charge at pH 7.0. These experiments should strengthen Sang's conclusion of protein adsorption being

diffusion-limited at this length scale, and the lack of electrostatic attraction between myoglobin and the silica surface should help investigate the broader applicability of his kinetic adsorption model. More practically, these experiments also show how quickly we can expect proteins to fully physically adsorb onto the surface of SBA-15 for our work on enzyme immobilisation in future chapters.

## **4.2 Materials and methods**

### **4.2.1 Myoglobin adsorption on mesoporous silica SBA-15 over time**

Sodium phosphate monobasic (BioXtra,  $\geq 99\%$ ), sodium phosphate dibasic (BioXtra,  $\geq 99\%$ ), and myoglobin from equine heart ( $\geq 90\%$ , essentially salt-free, lyophilized powder) were purchased from Sigma-Aldrich and used without further purification. Mesoporous silica SBA-15 was prepared and characterised as discussed in Chapter 2. In this chapter, SBA-15 samples are referred to by their pore diameters. UV-Vis was carried out using a BioTek Synergy H1 Multi-Detection Reader.

To study the kinetics of protein adsorption onto SBA-15 with different pore diameters, myoglobin was adsorbed onto SBA-15 batches and the adsorptions were monitored over time. These experiments were performed with SBA-15 with 6.1 or 8.1 nm pore diameter; the 6.6 nm SBA-15 sample was not included. 4 g/L of SBA-15 was prepared in 25 mM sodium phosphate buffer, pH 7.0. This buffer had an ionic strength of approximately 51 mM, which is weaker than those used Chapters 3, 5, 6, and 7. This discrepancy is so that the experimental results can be compared with data taken from Sang's thesis.<sup>121</sup> This dispersion was sonicated for 10 minutes in order to obtain a well-dispersed SBA-15 mixture. 2 g/L myoglobin was also prepared in 25 mM sodium phosphate buffer, pH 7.0. Equal volumes of well-dispersed SBA-15 and myoglobin solutions were mixed, for initial concentrations of 2 g/L SBA-15 and 1 g/L myoglobin. As soon as these two solutions were mixed, myoglobin rapidly began to adsorb onto the silica surface.

In the adsorption kinetics experiments, the mixtures were continuously shaken at room temperature. Myoglobin adsorption over time was monitored by taking an aliquot from the adsorption mixture into a microcentrifuge tube every 10 minutes for the first two hours, and every 20 to 30 minutes thereafter. A final

equilibrium measurement was also taken after 24 hours. These samples were centrifuged at 12,000 rpm for 5 minutes to separate solid myoglobin/SBA-15 composites from the myoglobin solution. The supernatant concentrations of myoglobin were measured by UV-Vis at 280 nm, and compared to a myoglobin calibration curve calculated using the Beer-Lambert law, as described in Section 3.2.2. The amount of myoglobin adsorbed on SBA-15 was then calculated from a mass balance. Each adsorption experiment was performed in triplicate.

#### 4.2.2 Diffusion-limited adsorption kinetics

Protein adsorption onto mesoporous silica is hypothesised to be a complex, multi-step process. As with other porous sorption processes, the four consecutive kinetic steps are considered to be: transport in the bulk solution; diffusion across the film surrounding the sorbent particles; diffusion in the pores of the sorbent; and sorption and desorption on the solid surface.<sup>167</sup> We hypothesise that protein diffusion within the SBA-15 pores would be the slowest, due to the steric confinement of the protein down the very long pores. While some protein will likely adsorb onto the exterior surface of the SBA-15 particles, the majority of the silica surface is within the pores of the SBA-15, as discussed in Section 2.6.3. Therefore, the intraparticle diffusion is assumed to be the rate-limiting step. The intraparticle diffusion-limited adsorption kinetics model used to describe protein adsorption onto SBA-15 in this chapter is seen in Equation 6.<sup>167,168</sup>

**Equation 6 – Intraparticle diffusion-limited adsorption kinetics model**

$$\frac{q_t}{q_e} = 1 - \frac{6}{\pi^2} \exp\left(\frac{-Dt\pi^2}{r^2}\right)$$

where  $q_t$  (mg/g) is the amount of adsorbed protein at any given time,  $t$  (s) and  $q_e$  (mg/g) is the amount of protein adsorbed at equilibrium.  $D$  (m<sup>2</sup>/s) is the diffusivity within the pore, and  $r$  (m) is the half-length of the pore. For all SBA-15 samples, the particles were approximately 1 μm in length, so  $r$  is taken as  $5 \times 10^{-7}$  m. This model is also known as the homogenous solid diffusion model (HSDM), and describes mass transfer in an amorphous and homogeneous sphere.<sup>167,168</sup> Clearly, the geometry of the SBA-15 system is different, but this

model should give us an indication of the diffusivities the proteins experience within the restricted pore of the material. Equation 6 is considered valid at long times, i.e. when  $q_t/q_e$  is greater than 0.3.<sup>167,168</sup> At short times, the HSDM reduces to a form where  $q_t$  is proportional to the square-root of  $t$ , which is a more common feature of diffusion-limited kinetics.

Diffusion coefficients of proteins including BSA and cytochrome c, free in solution, have been experimentally determined to be on the order of  $10^{-11}$   $m^2/s$ .<sup>169</sup> Diffusivities of proteins such as BSA onto Spheredex pores, calculated with an intraparticle diffusivity model, were found to be on the order of  $10^{-19}$   $m^2/s$ .<sup>170,171</sup> We would therefore expect the diffusivities extracted from the intraparticle diffusion model to fall somewhere between these orders of magnitude, likely closer to that of proteins diffusing within pores. Typically, diffusivity of a solute within a solvent is dependent on things such as temperature, the particle size, and the solution's viscosity. Holding these parameters constant, we would expect to see decreased protein diffusivity within smaller pores of SBA-15. Furthermore, comparing the diffusivities of myoglobin to those of lysozyme adsorbed under the same temperature and solution conditions may indicate if a protein with a net positive charge diffuses faster through a negatively-charged silica pore than a neutral protein does.

### 4.3 Results and discussion

#### 4.3.1 Myoglobin adsorption kinetics onto SBA-15 with different pore sizes

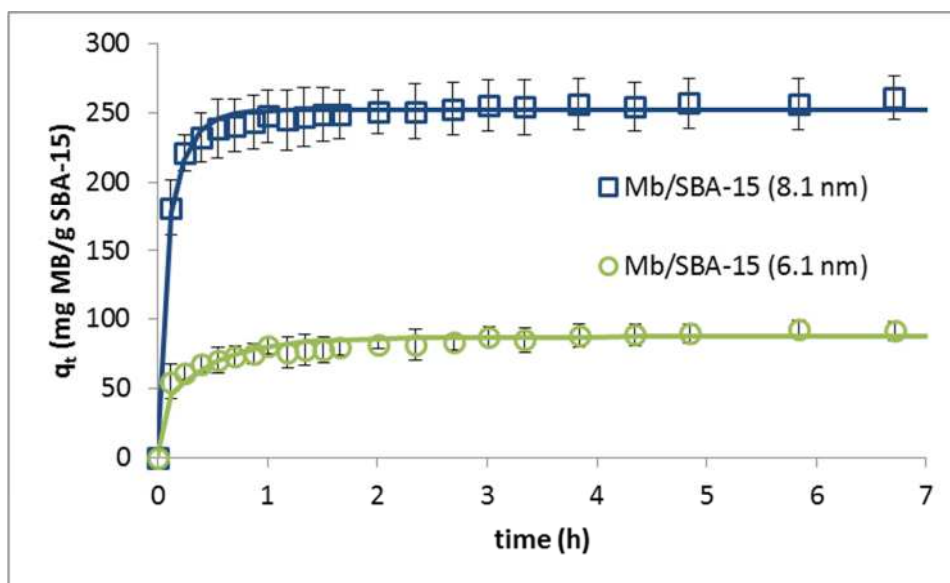


Figure 19 – Myoglobin adsorption to SBA-15 with pore diameters of 6.1 or 8.1 nm over time in 25 mM phosphate buffer pH 7.0. Error bars depict 95% confidence intervals. Solid lines depict the intraparticle diffusion-limited adsorption model.

In 25 mM phosphate buffer, pH 7.0, myoglobin adsorbs to the surface of the SBA-15 samples over the period of several hours. The mass of myoglobin adsorbed over time onto SBA-15 with pore diameters of 6.1 or 8.1 nm are shown in Figure 19. Not shown in this figure are the adsorption data points taken after 24 hours; the equilibrium myoglobin loading onto SBA-15 with a 6.1 nm pore diameter after 24 hours is found to be 98.7 mg myoglobin per g SBA-15, and onto SBA-15 with 8.1 nm pore is 263 mg myoglobin per g SBA-15. More than twice as much myoglobin can adsorb to the larger pores of the 8.1 nm SBA-15 sample than did to the 6.1 nm sample. This result is corroborated by the discrepancies in maximum myoglobin loadings at equilibrium for different pore sizes of SBA-15 as discussed Section 3.3.1. Those experiments, however, were undertaken in solutions of a different pH and ionic strength, and therefore those maximum myoglobin loadings cannot be directly compared with these experiments. The solid lines in Figure 19 show the intraparticle diffusion-limited adsorption model, fit to the data via sum of least squares. It can be seen that

the model fits within the 95% confidence intervals of the adsorption data. The parameters extracted from these fittings are found in Table 8.

**Table 8 – Intraparticle diffusion-limited kinetics parameters for myoglobin adsorbed onto SBA-15 samples with pore diameters of 6.1 or 8.1 nm, in 25 mM phosphate buffer pH 7.0**

<b>SBA-15 pore diameter (nm)</b>	<b><math>q_e</math> (g Mb/g SBA-15)</b>	<b><math>D</math> (m<sup>2</sup>/s)</b>
6.1	87.1	$1.40 \times 10^{-17}$
8.1	252	$4.19 \times 10^{-17}$

The  $q_e$  values extracted from the intraparticle diffusion-limited kinetics model are close to the experimental equilibrium adsorption quantities found after 24 hours, but this model underestimates these values. Myoglobin's unconstrained diffusivity in aqueous solution, calculated from the Stokes-Einstein equation is  $1.20 \times 10^{-10} \text{ m}^2/\text{s}$ .<sup>172</sup> As stated in Section 4.2.2, experimental diffusion coefficients for proteins in pores are much smaller; the diffusivities reported in Table 8 are of a reasonable order of magnitude when compared to this literature. The intraparticle diffusivity,  $D$ , is found to be larger for myoglobin adsorbing onto the larger pore size of SBA-15. This indicates that myoglobin can diffuse about three times more quickly within a slightly larger pore. Since temperature, solution viscosity, and protein size remain constant between these two experiments, the decreased diffusivity seen in the smaller pores of SBA-15 is likely due to steric hindrance within the pore.

#### **4.3.2 Comparison of myoglobin and lysozyme adsorption kinetics**

Comparing the kinetics of adsorption of proteins with net-positive and net-neutral electrostatic charge onto the negatively-charged porous surfaces of SBA-15 may indicate if electrostatics has a significant effect on adsorption rates. To this end, data reported by Sang concerning the adsorption of lysozyme onto SBA-15 of different pore diameters is examined here. These SBA-15 batches were prepared using the same method described in Section 2.5.1; the batches had hydrothermal ageing steps at 40 °C and 75 °C, and had NLDFT-calculated average pore diameters of 5.9 nm and 7.3 nm

respectively.<sup>121</sup> The diffusion-limited kinetics model has been fit to these data via a least-squares method to support this thesis.

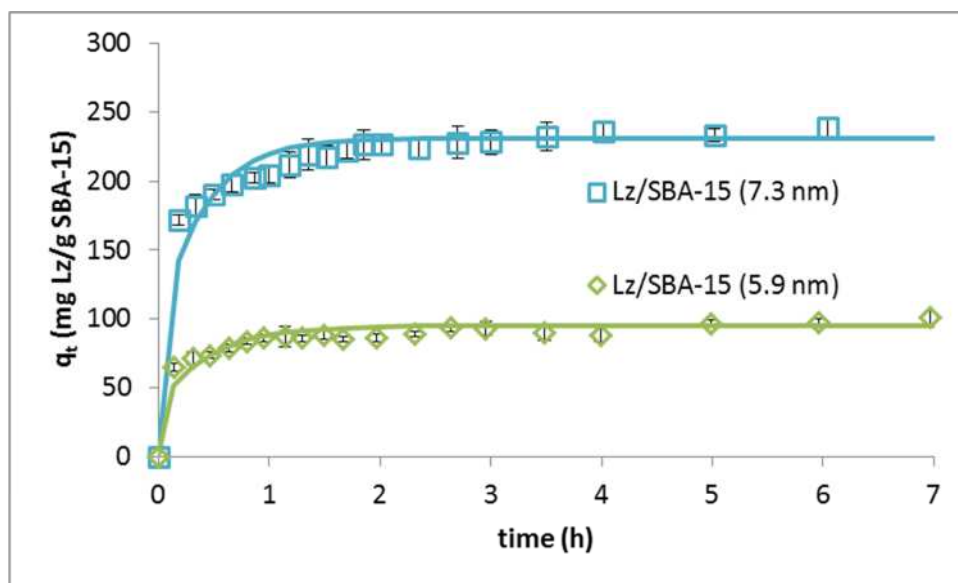


**Figure 20 – Lysozyme adsorption to SBA-15 samples with pore diameters of 5.9 or 7.3 nm over time in in 25 mM phosphate buffer pH 7.0. The solid lines depict the diffusion-limited model.**

The mass of lysozyme adsorbed over time to SBA-15 with pore diameters of 5.9 or 7.3 nm, as reported by Sang, is shown in Figure 20. The method for determining the error bars for these data sets was not stated in his thesis. Data were not collected at 24 hours, so the equilibrium lysozyme adsorption cannot be confirmed in this way as it was in the myoglobin experiments. Lysozyme adsorption to SBA-15 with a 5.9 nm pore diameter was found to be 101 mg lysozyme per g SBA-15 after 17 hours. Lysozyme adsorption to SBA-15 with a 7.3 nm pore diameter was found to be 243 mg lysozyme per g SBA-15 after 14 hours. The data collected between 7 hours and the final data collection for both SBA-15 samples are omitted from Figure 20 for clarity, but are included for model fitting. More than twice as much lysozyme adsorbed to the surface of the 7.3 nm SBA-15 sample than did to the 5.9 nm sample at their final time points. This result is qualitatively comparable to the adsorption isotherms reported in Section 3.3.2. The solid lines in Figure 20 show the intraparticle diffusion-limited adsorption model, fit to the data via sum of least squares. The model appears to underestimate the initial lysozyme adsorption, overestimate adsorption in an

intermediary period, and then underestimate the equilibrium lysozyme adsorption. The parameters extracted from this fitting are found in Table 9.

**Table 9 - Intraparticle diffusion-limited kinetics parameters for lysozyme adsorbed onto SBA-15 samples with pore diameters of 5.9 or 7.3 nm in 25 mM phosphate buffer pH 7.0**

<b>SBA-15 pore diameter (nm)</b>	<b><math>q_e</math> (g Lz/g SBA-15)</b>	<b><math>D</math> (m<sup>2</sup>/s)</b>
5.9	95.0	$1.50 \times 10^{-17}$
7.3	231	$1.78 \times 10^{-17}$

The  $q_e$  values extracted from the intraparticle diffusion-limited kinetics model, are close to the experimental equilibrium adsorption quantities, but this model underestimates these values. Lysozyme's unconstrained diffusivity in aqueous solution, calculated from the Stokes-Einstein equation is  $1.26 \times 10^{-10}$  m<sup>2</sup>/s.<sup>172</sup> This is very slightly smaller than that of myoglobin, due to lysozyme's smaller diameter. The intraparticle diffusivities,  $D$ , reported in Table 9 for lysozyme, are not smaller than those reported for myoglobin in Table 8, but this small difference may be obscured by the greater effects the different pore diameters have on the proteins' diffusivities.  $D$  is found to be slightly larger for lysozyme adsorbing onto the larger pore size of SBA-15. This is a smaller increase than was seen with myoglobin diffusing within different sized pores, even taking into account the smaller pore size discrepancy in the lysozyme experiments.

As previously mentioned, myoglobin has an isoelectric point of pH 7.2 and has net neutral charge in these experiments. Lysozyme's isoelectric point is pH 11.3, so it has a net positive charge under these experimental conditions. We do not see a significant difference in diffusivities within the pore of the SBA-15 between these proteins under the solution conditions tested. In these limited cases, electrostatic attraction does not appear to affect the diffusivity of proteins within the pores of SBA-15.

#### **4.4 Conclusion**

In this chapter, experiments investigating the rate at which myoglobin adsorbs onto SBA-15 of two different pore sizes has been reported. Myoglobin is found

to adsorb significantly faster onto SBA-15 with a larger pore size, supporting the hypothesis that protein adsorption is diffusion-limited. A model representing intraparticle diffusion-limited adsorption kinetics has been fitted to this data, and has also been fit to literature data of lysozyme adsorbed to SBA-15 of similar pore diameters under the same solution conditions. Myoglobin's intraparticle diffusivities were comparable to those of lysozyme, despite myoglobin having a net neutral charge at this pH while lysozyme has a net positive charge. This observation appears to indicate that electrostatic attraction between protein and silica pore does not affect a protein's intraparticle diffusivity. A conclusion that electrostatics would have no effect on a protein's diffusivity in mesopores cannot be drawn, due to how few systems the hypothesis has been tested on. By performing similar adsorption kinetics experiments on myoglobin and lysozyme under different solution conditions, varying pH and ionic strength, this hypothesis could be better tested. Other proteins could also be investigated by the same methodology to generalise these relationships.

This chapter and the previous one have indicated that protein adsorption to the pores of SBA-15 can be described by and predicted with simple geometric models. Both kinetically and at equilibrium, steric confinement of proteins within the pores has a significant effect on protein adsorption, while electrostatics is not found to have demonstrable effects from the experiments with myoglobin at neutral pH. These are surprising findings, considering the importance of electrostatics in the chaperonins we take as a source of inspiration, and the experiments with positively-charged lysozyme. However, the pores of SBA-15 are orders of magnitude longer than the central cavity of chaperonins, which might be why steric effects play a more important role. In Chapters 5, 6, and 7, the enzymatic activity of proteins adsorbed to the pores of SBA-15 will be investigated, again in the context of steric confinement and electrostatic interactions, in order to extract fundamental, applicable understanding about how nature stabilises proteins from unfriendly environments via chaperonin complexes.

## **5 Peroxidase activity of myoglobin immobilised on mesoporous silica SBA-15**

### **5.1 Introduction**

In the previous two chapters, this thesis investigates the process by which proteins physically adsorb to mesoporous silica SBA-15. In keeping with previous studies on the protein lysozyme, it has been demonstrated that the protein myoglobin diffuses more quickly through larger pores of SBA-15. It has also been shown that, across several proteins, more protein can be adsorbed to SBA-15 with larger pore volumes. We also see that more of a smaller protein can be loaded onto SBA-15 of a given pore size than of a larger protein. These experiments have confirmed our understanding of protein adsorbed to SBA-15 using current geometric models, and have given us practical information about the loading times and concentrations necessary for designing future experiments.

The overarching aim of this thesis is to better understand how enzymes interact with silica mesopores comprehensively, including the monitoring of the enzymes' structures and functions. This aim is guided by what we know about chaperonin complexes: that their charged, narrow pores stabilise proteins from unfolding due to unfavourable conditions. To this end, the next few chapters investigate the activity of enzymes immobilised to SBA-15 under a range of solution conditions. In chaperonins, the proteins that are stabilised within the complex are not involved in biocatalysis whilst inside the pores. However, this line of investigation will both tell us more about the condition of the proteins attached to the pore walls of SBA-15, and further our application goal of improving enzyme immobilisation for biochemical manufacturing processes. In the kinetic and equilibrium adsorption experiments of the previous chapters, we have seen that the geometric models can accurately explain, and therefore predict, protein adsorption to SBA-15. This and future chapters will investigate if the effects of immobilisation on an enzyme's activity can be predicted with similarly straightforward geometric models, or if other factors, such as electrostatic attraction, become more influential in this context.

In this chapter, the enzyme immobilised to SBA-15 is myoglobin. As previously discussed in Section 1.3.2, myoglobin is a well-characterised and easily

obtainable model enzyme that has a hydrodynamic diameter of approximately 4.1 nm and an isoelectric point of pH 7.2. In vivo, myoglobin is not classified as an enzyme; it functions as an oxygen transport protein. However, myoglobin can act as a peroxidase in vitro, and its peroxidase activity can easily be quantified via a colorimetric assay. Myoglobin has a net neutral charge in many solutions in which it is stable and active, due to its neutral isoelectric point, which means that the contributions of steric and electrostatic effects can be more easily separated in the following experiments.

The activity of free or immobilised myoglobin, as determined by activity assay, is used as a proxy for understanding the condition of the protein: its maintained structure and requisite flexibility, or even where these conditions have been improved. It is a useful method for quantifying the protein's condition because the ultimate application of this thesis is to improve the catalytic activities of immobilised enzymes for industrial manufacturing processes. However, the insights that activity assays can truly provide concerning immobilised myoglobin's structure and freedom are limited by complicating factors. Chief among these is the concern that enzyme may adsorb to the silica in such a way that its active site is blocked and inaccessible by substrate molecules.<sup>77,173</sup>

## **5.2 Materials and methods**

### **5.2.1 Myoglobin peroxidase assay**

Hydrogen peroxide solution (ACS reagent, 30 wt%), 2,2'-Azino-bis(3-ethylbenzothiazoline-6-sulfonic acid) diammonium salt ( $\geq 98\%$  (HPLC)) (ABTS), sodium phosphate monobasic (BioXtra,  $\geq 99\%$ ), sodium phosphate dibasic (BioXtra,  $\geq 99\%$ ), glacial acetic acid (ACS reagent,  $\geq 99.7\%$ ), and sodium acetate ( $\geq 99\%$ , anhydrous) were purchased from Sigma Aldrich. UV-Vis was carried out using the absorbance mode of a BioTek Synergy H1 Multi-Detection Reader.

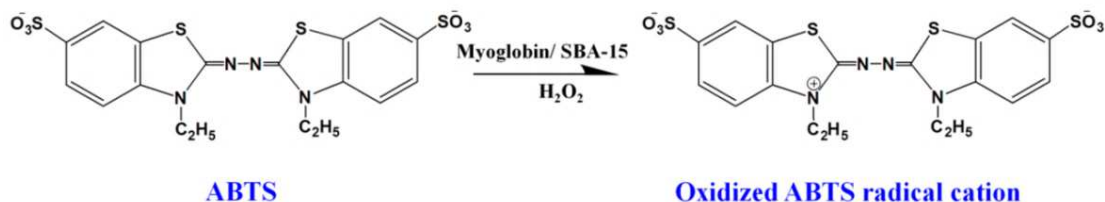


**Figure 21 - Oxidation of 2,2'-Azino-bis(3-ethylbenzothiazoline-6-sulfonic acid) by hydrogen peroxide to a coloured cation, catalysed by myoglobin**

The peroxidase activity of myoglobin was quantified via colorimetric assay; the oxidation of ABTS is catalysed with myoglobin as a peroxidase.<sup>137,174</sup> As in most spectrophotometric enzyme assays, the initial, linear rate of reaction was monitored. This corresponds to the maximal catalysed reaction rate, before enough substrate is consumed to slow the rate of reaction.

The ABTS salt was dissolved in deionised water to produce a 50 mM solution, which is kept away from light when not in use. Dilute ABTS is clear to slightly yellow in solution, but oxidises to a metastable radical cation which has a dark green-blue colour and several characteristic peaks of absorbance. Though oxidised ABTS's maximal absorbance peak is at 414 nm, this peak's proximity to myoglobin's characteristic peak of 409 nm necessitates the use of an alternative peak, at 725 nm, for this assay. The hydrogen peroxidase solution was diluted to 1 wt% with deionised water.

The reaction components were mixed in the wells of 96-well microplates: for a 300  $\mu$ L reaction mixture, 10  $\mu$ L of 50 mM ABTS solution, 30  $\mu$ L of 1 wt% hydrogen peroxide solution, and 30  $\mu$ L of myoglobin-containing sample were mixed in 230  $\mu$ L of buffer. For the pH protection experiments, outlined in a subsequent section, the reaction buffers were the same buffers used to produce unfavourable pH conditions. The reaction mixture was observed at 725 nm for two minutes. Activity was then normalised by enzyme loading onto the composite material. Thus activity was quantified in units of absorbance per second per g/L myoglobin.

It is worth considering if the ABTS substrate experiences significant mass diffusion limitations within the pores of the SBA-15 that may affect the utility of this colorimetric assay, which takes place on the order of minutes. Small

molecules have been shown to experience restricted diffusivity within mesopores. A wide variety of molecules with diameters on the order of 1 nm were found to diffuse through silica-alumina pores, with average pore diameters of different samples ranging from 4 to 15 nm, with diffusivities on the order of  $10^{-9}$  to  $10^{-11}$  m<sup>2</sup>/s.<sup>175,176</sup> With diffusivities of this order of magnitude, one could expect small molecules, including substrates such as ABTS, to diffuse within the 1 µm long pores of SBA-15 within milliseconds. It is possible that substrate diffusion may be further impacted by adsorbed myoglobin partially blocking the pores and making them even narrower. However, the myoglobin loading onto SBA-15 is very low, as will be discussed in the results section. Further, the substrate is likely to be oxidised when it encounters an adsorbed myoglobin within a pore, rather than trying to pass by it.

As mentioned in the introduction, this activity assay does not give direct insight into immobilised myoglobin's conformation, as low activity may mean its active site is blocked by the pore wall. An additional complicating factor with the use of myoglobin as a model enzyme is the presence of its prosthetic haem group. Myoglobin's peroxidase activity relies on access to the haem, but even a haem group that has dissociated from myoglobin can give rise to peroxidase activity.<sup>17</sup> High activity can therefore not be directly correlated to myoglobin retaining its native conformation.

### **5.2.2 Myoglobin protection from the protease pepsin**

Sodium phosphate monobasic (BioXtra, ≥99%), sodium phosphate dibasic (BioXtra, ≥99%), glacial acetic acid (ACS reagent, ≥99.7%), sodium acetate (≥99%, anhydrous), myoglobin from equine heart (≥90%, essentially salt-free, lyophilized powder), and pepsin from porcine gastric mucosa (powder, ≥400 units/mg protein) were purchased from Sigma-Aldrich and used without further purification. A different batch of SBA-15 is used in these experiments than those described in Chapter 2; this batch is also prepared with the same conventional method described, and a hydrothermal ageing step at 40 °C. It has an NLDFT pore diameter of 5.9 nm. We assume similar particle dimensions, surface area, and porosity for this batch, but these characteristics are unavailable.

To test the protective effects of SBA-15 on immobilised enzyme, myoglobin/SBA-15 composites were prepared and exposed to the protease pepsin at a range of pH conditions. These experiments were originally designed with the view of developing SBA-15 in its capacity as a drug delivery material, which is an application that has been given considerable attention.<sup>177,178</sup> Pepsin, and also trypsin, are present in the human digestive tract, as are low pH conditions. Investigating SBA-15's ability to protect a cargo protein from these conditions was desirable. Although the direction of this research has since changed, these experiments are included in this thesis because they demonstrate changes in myoglobin stability upon immobilisation onto SBA-15.

Myoglobin/SBA-15 composites were initially prepared with a target loading of 50 mg myoglobin per g SBA-15 in 25 mM phosphate buffer pH 7.2 via the physical adsorption method described in Section 3.2.1. After myoglobin adsorbed to the SBA-15 over 24 hours, the solutions were centrifuged at 12,000 rpm for 5 minutes, and the supernatants and pellets were separated. The supernatants were saved and later measured with UV-Vis to determine enzyme loading. The pellets were re-suspended to 2 g/L in 25 mM acetate buffers with pH values of 3.6, 4.1, 4.6, or 5.1, or 25 mM phosphate buffer pH 6.3. In these experiments, the buffers were adjusted to their final pH with sodium hydroxide and hydrochloric acid. This means the ionic strengths of the different buffers were not identical. After the myoglobin/SBA-15 composites were agitated for 24 hours at room temperature, they were centrifuged again. The supernatants were saved and measured with UV-Vis to determine enzyme leaching. The pellets were re-suspended in the same buffers and their enzymatic activities were measured via peroxidase assay, described in the previous section. Each sample was prepared and measured in triplicate.

These experimental conditions were replicated for 0.1 g/L solutions of free myoglobin in the same series of buffers, as controls. In these experiments, lyophilised myoglobin and, sometimes, pepsin, were suspended directly into the acetate or phosphate buffers of varying pH values, and agitated for 24 hours at room temperature. Then, the solutions' enzymatic activities were quantified via peroxidase assay.

### 5.2.3 Myoglobin pH protection

Sodium phosphate monobasic (BioXtra,  $\geq 99\%$ ), sodium phosphate dibasic (BioXtra,  $\geq 99\%$ ), glacial acetic acid (ACS reagent,  $\geq 99.7\%$ ), sodium acetate ( $\geq 99\%$ , anhydrous), and myoglobin from equine heart ( $\geq 90\%$ , essentially salt-free, lyophilized powder) were purchased from Sigma-Aldrich and used without further purification. Mesoporous silica SBA-15 was prepared and characterised as discussed in Chapter 2, and the SBA-15 samples are referred to by their pore diameters.

To further test the protective effects of SBA-15 on immobilised enzymes, myoglobin/SBA-15 composites were prepared and exposed to unfavourable pH conditions. In these experiments, unlike in the pepsin experiments, all buffer solutions had an ionic strength of 100 mM. Consistent ionic strength is important, because enzyme activity is very sensitive to the ionic strength of the solution. Acetate buffers were prepared by mixing a 100 mM solution of acetic acid and a 100 mM solution of sodium acetate to make buffers with final pH values of 3.6, 4.1, 4.6, 5.1, and 5.6. Phosphate buffers were prepared by mixing a 100 mM solution of sodium phosphate monobasic and a 33.3 mM solution of sodium phosphate dibasic to make buffers with final pH values of 5.6, 6.1, 6.6, and 7.6.

Myoglobin/SBA-15 composites were initially prepared with a target loading of 50 mg enzyme per g SBA-15 in phosphate buffer, pH 7.2, with an ionic strength of 100 mM. After the enzyme adsorbed to the SBA-15 over 24 hours, the solutions were centrifuged at 12,000 rpm for 5 minutes, and the supernatants and pellets were separated. The supernatants were saved and later measured with UV-Vis to determine enzyme loading. The pellets were re-suspended to 2 g/L in either acetate or phosphate buffers of varying pH, but all with an ionic strength of 100 mM. After the myoglobin/SBA-15 composites were agitated for 24 hours at room temperature in various buffers, they were centrifuged again. The supernatants were saved and measured with UV-Vis to determine enzyme leaching. The amount of leached myoglobin is taken into account in the specific activity calculations; myoglobin in the supernatant at this step is washed out of the sample before the assay takes place. The pellets were re-suspended in the fresh buffers of the same, varying pH values, and their enzymatic activities were

measured via the peroxidase assay described previously. Each combination of pore size and pH was prepared and measured in triplicate.

These experimental conditions were replicated for 0.1 mg/mL solutions of free myoglobin in the same series of buffers, as controls. In these experiments, lyophilised myoglobin was suspended directly into the acetate or phosphate buffers of varying pH values, and agitated for 24 hours at room temperature. Then, the solutions' enzymatic activities were measured via peroxidase assay.

### 5.3 Results and discussion

#### 5.3.1 Protease protection of immobilised myoglobin

In these experiments, myoglobin immobilised onto SBA-15 samples are exposed to the protease pepsin at a range of pH conditions, and then their peroxidase activities are measured by assay. These data are compared to the activities of myoglobin, free in solution, that are exposed to pepsin at a range of pH conditions. These experiments are performed to probe for possible protective effects of SBA-15 on immobilised enzyme from protease.

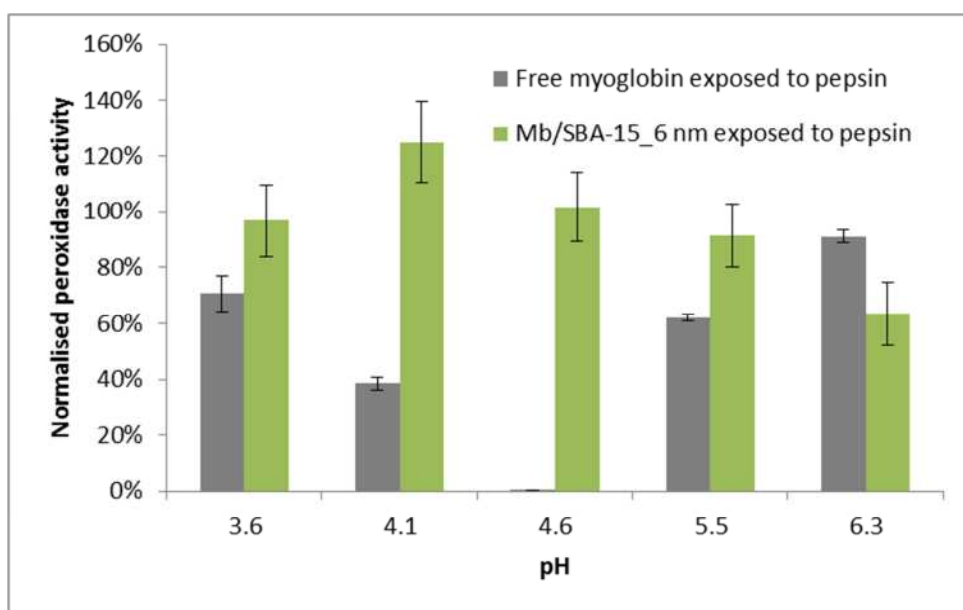


**Figure 22 – Peroxidase activity of free myoglobin and myoglobin immobilised on SBA-15 with a pore diameter of 5.9 nm that have been exposed to pepsin, in solutions with pH values of 3.6 to 6.3. Error bars depict 95% confidence interval.**

Figure 22 displays the peroxidase activity of myoglobin in phosphate or acetate buffer of various pH values that has been exposed to pepsin for 24 hours,

normalised to that of myoglobin in the same buffer which has not been exposed to pepsin. Figure 22 also displays the peroxidase activity of myoglobin immobilised to SBA-15 with a pore diameter of 5.9 nm that has been exposed to pepsin for 24 hours, normalised to that of similarly immobilised myoglobin that have not been exposed to pepsin. Error bars depict the data's 95% confidence interval. Activity is normalised at each pH value because, in this method, the reaction mixtures are not held to a constant ionic strength. Therefore, absolute activity values cannot be meaningfully compared between the different pH values.

Pepsin cleaves amino acid chains optimally between pH 1 and 4; therefore, we would expect exposed myoglobin's relative activity to drop as pH decreases towards these values. This effect on absolute peroxidase activity is obscured by the fact that myoglobin denatures even without the assistance of pepsin at low pH; because the activity of free myoglobin decreases in more acidic conditions, the decrease in activity attributed only to the presence of pepsin is less pronounced. Experiments involving a protease that functions under neutral conditions, trypsin, were also performed, in an attempt to avoid this obscuring effect. However, trypsin was not found to sufficiently proteolyse myoglobin. The data in Figure 22 confirm that the presence of pepsin significantly attenuates the activity of free myoglobin, which serves as our basis of comparison for immobilised myoglobin's protease protection.

SBA-15-immobilised myoglobin that has been exposed to pepsin displays peroxidase specific activity within error of that of immobilised myoglobin that has not been exposed to pepsin at all pH values tested, except for pH 6.3. At all other pH values, confinement to SBA-15 effectively protects myoglobin from being digested by pepsin. This may be because pepsin cannot easily enter SBA-15 pores that have myoglobin loaded within them. The pore diameter is 5.9 nm while myoglobin's diameter is 4.1 nm and pepsin's is 5.1.<sup>138</sup> Though this is a nominally sufficient pore diameter for pepsin to enter, we have seen from Figure 17 in Section 3.3.4 that much less pepsin is able to adsorb onto SBA-15 than myoglobin, and that result is for adsorption onto SBA-15 with a pore size of 8.1 nm. Alternatively, or in conjunction, it's possible that the strong electrostatic attraction between myoglobin and the silica surface at lower pH values prevents

pepsin from accessing and hydrolysing myoglobin's hydrophobic residues. It is possible that these protective effects are not observed at pH 6.3 because this higher pH approaches the pI of myoglobin; close to its pI, more myoglobin will leach off of the SBA-15 and be vulnerable to proteolysis by pepsin, perhaps leading to the lower normalised activity observed.

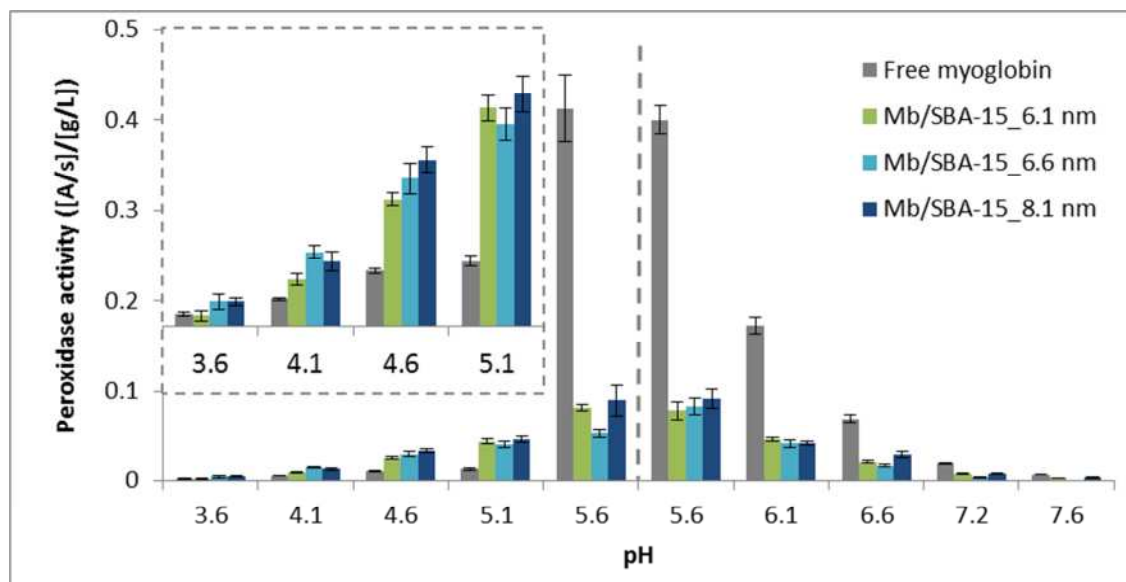
Pepsin has been seen to increase myoglobin's peroxidase activity under certain conditions for a lipid hydroperoxide substrate. Mild proteolysis near pH 4 was hypothesised to liberate smaller, haem-containing fragments from myoglobin that still catalysed the substrate while also being more mobile.<sup>179</sup> Such an effect is not seen in these experiments for free myoglobin, because when exposed to pepsin near pH 4 it has less than 100% activity. It is not clear why high activity for immobilised myoglobin exposed to pepsin, exceeding that of immobilised myoglobin not exposed to pepsin, is observed.

### **5.3.2 pH protection of immobilised myoglobin**

Myoglobin immobilised on SBA-15 of different pore diameters is exposed to a range of pH conditions, and then the samples' peroxidase activities are measured by assay at that pH. This is done to examine the relationship between pH and immobilised enzyme activity, and probe for possible protective effects of SBA-15 on the immobilised enzymes from denaturing pH conditions. As in the pepsin experiments of the previous section, myoglobin loading onto SBA-15 is targeted for 50 mg enzyme per g SBA-15, which results in a wide spacing of myoglobin molecules that are even more isolated when in SBA-15 with larger pores.

For confined samples, myoglobin loading onto SBA-15 is targeted for 50 mg enzyme per g SBA-15. Using the textural parameters of the SBA-15 batches derived from gas physisorption and reported in Section 2.6.2, we can state that this myoglobin loading corresponds to one myoglobin molecule for every 300 nm<sup>2</sup> of SBA-15 surface area for the smallest pore diameter and one for every 400 nm<sup>2</sup> for the largest pore diameter. For reference, one myoglobin molecule has a hydrodynamic packing area of approximately 13 nm<sup>2</sup>. This loading also corresponds to one myoglobin molecule for every 290 nm<sup>3</sup> of pore volume, at the smallest pore size, and one molecule for every 640 nm<sup>3</sup> for the largest pore

size. For comparison, myoglobin's hydrodynamic volume is approximately 36 nm<sup>3</sup>. By either measure, we can see that the myoglobin molecules are spaced quite far from neighbouring molecules, and are more isolated in SBA-15 with larger pores.



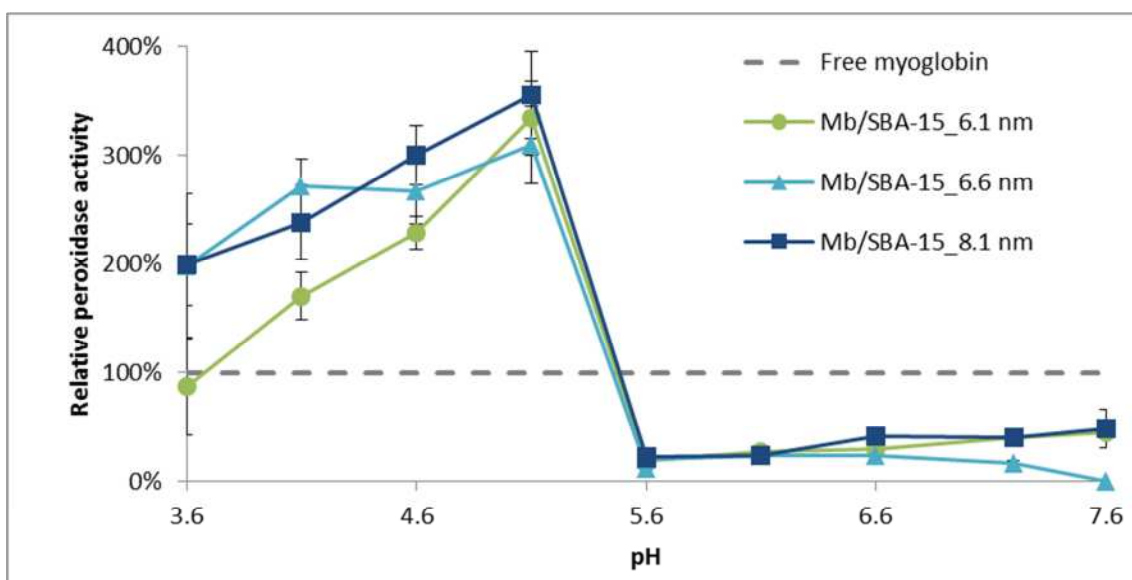
**Figure 23 – Peroxidase activities of free myoglobin and myoglobin immobilised to mesoporous silica SBA-15 (pore diameters of 6.1, 6.6, and 8.1 nm) in solution pH 3.6 to 7.6, 100 mM ionic strength. pH values to the left of the dashed line take place in acetate buffer while those on the right are in phosphate buffer. Inset is magnified x5. Error bars depict 95% confidence interval.**

Figure 23 shows the peroxidase activity of free myoglobin, as well as that of myoglobin immobilised on SBA-15 of different pore diameters. The activity is shown in arbitrary units relating to the rate of the peroxidase reaction (absorbance per second) divided by the concentration of myoglobin in the sample (g/L). Error bars depict the 95% confidence interval of each activity value. Small amounts of myoglobin leaching are observed while the samples are left in the test buffer for 24 hours, which is accounted for in specific activity calculations. At pH 5.6, both phosphate and acetate buffers are used, and the sample's activities are generally found to be within error of one another. This alone is a useful finding, as it suggests that the buffer salt used does not have a significant effect on the enzyme's activity.

As mentioned in Section 1.3.2, myoglobin can function as a peroxidase by virtue of its prosthetic haem group, which several other types of peroxidases

share. The embedding of the haem group in myoglobin is different from those found in native peroxidases, leading to generally lower peroxidase activity.<sup>137</sup> In the ABTS assay, oxygen is bound and released from the haem group, so the positioning of the hydrophobic side chains near the haem, and myoglobin's overall three-dimensional structure, is important for its function. However, a direct link cannot be claimed between native myoglobin structure and optimal peroxidase activity, as a partially unfolded myoglobin may make the haem group more accessible. This is evidenced by the highest peroxidase activity of myoglobin being found at pH 5.6 in Figure 23, not at myoglobin's physiological pH of 7.2. Control experiments using haem groups not bound to myoglobin could perhaps help clarify these results.

This optimal peroxidase activity found at pH 5.6 drops off slowly at more alkaline pH values, but rapidly at more acidic pH values. The quick drop in activity may be attributed to the denaturation of myoglobin due to low pH. We can also see that, for this set of experiments, pH protection does not appear to be affected significantly by the SBA-15's pore size. Immobilisation onto SBA-15 does not improve myoglobin's peroxidase activity at all pH values tested. However, confinement to SBA-15 does shift the effective activity range of myoglobin to more acidic pH values.



**Figure 24 – Normalised peroxidase activities of free myoglobin and myoglobin immobilised to mesoporous silica SBA-15 (pore diameters of 6.1, 6.6, and 8.1 nm) from solution pH 3.6 to 7.6, 100 mM ionic strength. Error bars depict 95% confidence interval.**

Figure 24 depicts the same data, shown normalised to the activity of the free myoglobin at each pH value. The error bars, which depict the 95% confidence interval, show the compounded error of both free and confined samples for each data point. The activity of confined myoglobin surpasses that of free myoglobin at low pH values, with dramatic protection of up to 350%. This indicates that confined myoglobin is protected, to some extent, from denaturing due to the acidic environment. Immobilised myoglobin does not enjoy this protective effect at pH values above 5.1. From this graph we can see that myoglobin immobilised on SBA-15 performs far worse than myoglobin free in aqueous solution and at its optimal pH. The reason for this is uncertain; perhaps confinement prevents accessibility to the haem group or it requisite flexibility. Focusing solely on the acidic pH range where immobilised myoglobin's activity exceeds that of free myoglobin, we can see in Figure 24 that the protective effect appears to diminish as the pH drops. It also clearly shows that the activity of myoglobin immobilised to SBA-15\_6.1 nm is significantly lower than that of the two other immobilised samples at pH values below 4.1.

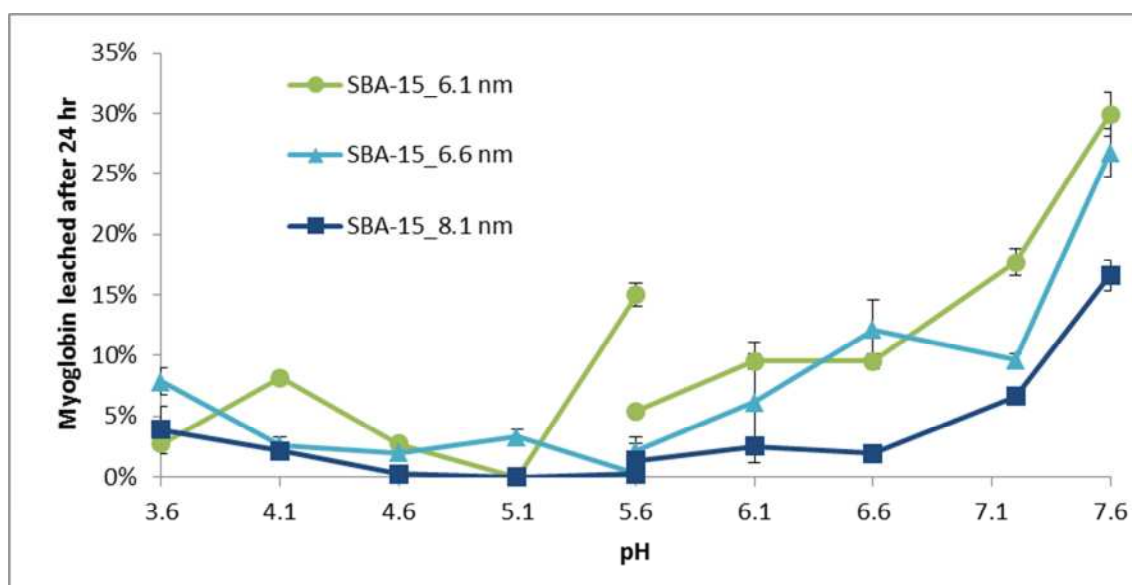


**Figure 25 - Amount of initially-loaded myoglobin leached from mesoporous silica SBA-15 (pore diameters of 6.1, 6.6, and 8.1 nm) after 24 hours in solutions pH 3.6 to 7.6, 100 mM ionic strength. Error bars depict 95% confidence intervals.**

Some myoglobin leaching is observed while the samples are left in the test buffer for 24 hours, which is accounted for in specific activity calculations. Figure 25 depicts the percent of initially-loaded myoglobin that is leached from

the different batches of SBA-15 from each buffer. Myoglobin leaching remains under 15% for almost all SBA-15 samples in most batches. It is unclear why the 6.1 nm SBA-15 experiences an unusually high amount of myoglobin leaching in acetate buffer with a pH of 5.6; the high leaching does match the trends of the other two S or that of the 6.1 nm SBA-15 at other pH values. More leaching is observed from all SBA-15 at the higher pH values of 7.2 and 7.6. This is to be expected, as myoglobin has a net neutral charge near these pH values and is not as strongly attracted to the negatively charged silica surface. These data are also helpful in confirming that the different SBA-15 batches have similar surface charge profiles; if the profiles were different, then their leaching profiles would also differ.

In Figure 25, solutions with pH less than 5.6 are prepared in acetate buffer, and solutions with pH greater than 5.6 are prepared in phosphate buffer. For two of the three SBA-15 batches, the buffer salt used at pH 5.6 does not have a significant influence on the leaching of myoglobin from the material. For the 6.1 nm pore diameter SBA-15, leaching is approximately 10% less in phosphate buffer than in acetate buffer. Despite this difference, the specific activities of these samples are within error of each other when leaching is taken into account.

The results of the experiments concerning the pH protection of immobilised myoglobin, shown in Figure 23, Figure 24, and Figure 25, give insight into the relative importance of different aspects of the immobilisation material. The data indicate that pore diameter does not play a significant role in pH protection, which contradicts the original hypothesis. However, it does indicate that the pH of the solution affects immobilised myoglobin's activity in a more significant way than anticipated, which can be partially explained in the context of the electrostatic attraction between myoglobin and the pore walls of SBA-15.

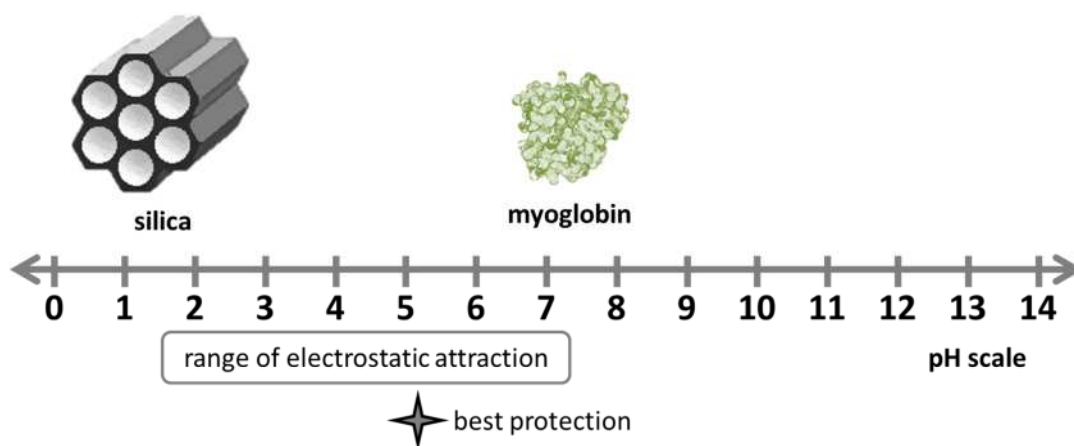


**Figure 26 – Schematic of electrostatic effects between silica and myoglobin**

Silica has its pzc around pH 2.<sup>142</sup> Myoglobin's isoelectric point is at pH 7.2. In any solution between pH 2 and 7.2, silica has a negative net surface charge and myoglobin has a positive net surface charge, and the myoglobin molecules will be electrostatically attracted to the silica surface. This attraction will be strongest at the centre of this pH range. We found that myoglobin immobilised to SBA-15 demonstrates the highest relative activity, or the strongest protective effects, at pH 5.1. This corresponds to the pH at which myoglobin and silica experience the strongest electrostatic attraction. This strong attraction is also evidenced by the low level of myoglobin leaching seen at this pH in Figure 25.

One could interpret the role of electrostatic effects on immobilised enzyme's activity similarly to have certain parallels with the effects of steric confinement: a strongly-attracted enzyme will have more points of contact with the pore, but may have its native structure stretched out, as has been seen on more flat silica surfaces.<sup>75,76</sup> On the other hand, an enzyme with weak or no electrostatic attraction will have fewer stabilising points of contact with the silica wall, but potentially more flexibility. However, such explanations are likely too simplistic, and they don't entirely account for the sudden drop in immobilised myoglobin's relative peroxidase activity above pH 5.1. An additional factor to consider when interpreting these results is the orientation of myoglobin within the pore, particularly whether the active site is accessible to the ABTS substrate molecules.

Myoglobin is immobilised by physical adsorption in these experiments, so a random distribution of orientations may seem like a reasonable assumption to

make. If this were the case, one might assume to see a drop in immobilised enzyme activity, in proportion to the active site's size on the surface of the enzyme and how tightly confined the enzyme is within the pore, even if the enzyme's structure isn't otherwise affected by the physical adsorption or local microenvironment within the pores. However, the assumption that the enzyme would adsorb in completely random orientations onto the pore walls is perhaps not correct. Electrostatic forces have been shown to play an important role in the protein's adsorption, both in literature discussed in Section **Error! Reference source not found.** and in Chapters 3 and 4. This thesis investigates the effects of electrostatic attraction between enzyme and silica on the immobilised enzyme's activity, and the enzyme's orientation during adsorption may be integral to understanding these effects.

Patches of the protein's surface that have more positively-charged residues may preferentially adsorb to the negatively charged silica surface. The more positively-charged regions of the protein's surface will depend on the pH of the solution it is in; if the solution pH falls below 6, for example, histidine residues will gain a positive charge. Negatively charged amino acid residues will lose their electrostatic repulsion from the silica surface at lower pH values as well. The orientation of enzymes adsorbed in SBA-15 pores as a function of solution pH and/or ionic strength is outside of the scope of this thesis, but any possible relationships thereof may contribute substantially to gains or losses of immobilised enzyme activity at different pH values.<sup>77,173</sup> In the instance of myoglobin, for example, the precipitous drop in immobilised myoglobin's relative peroxidase activity may be due to some disruption in charged groups on the protein's surface which lead it to adsorb preferentially in way that blocks its active site. This is not clearly the case, though, because the shift takes place between pH 5.1 and 5.6, which does not correspond to any amino acid's  $pK_a$ .

Experimental methods exist that can clarify changes in immobilised enzyme's secondary structure such as FTIR and CD.<sup>120,121,180</sup> However, none are yet available that can clearly link conformational changes with enzyme activity, or shed light on which orientation the enzyme prefers under given conditions. Computer simulations involving molecular dynamics have indicated that the pH at which a protein is adsorbed onto a flat silica surface affects its final

orientation, as previously described.<sup>181,182</sup> Simulations involving mesoporous silica have also been attempted, which further confirm the role of electrostatic attraction in adsorption.<sup>183</sup> Computational modelling of myoglobin's adsorptive behaviour within silica mesopores would greatly benefit the interpretation of these data.

#### **5.4 Conclusion**

The results of the experiments investigating immobilised myoglobin's protection from pepsin indicate that immobilised enzymes can be protected from proteases. Whether this protection is given by virtue of a size exclusion effect, where the protease cannot enter the pores to digest the immobilised protein, or by the confinement and stabilisation that prevents pepsin from hydrolysing myoglobin's hydrophobic residues, or some combination of both, is unclear. Investigating the effect of SBA-15 pore size on myoglobin's protection from pepsin may clarify how much the size-exclusion effect contributes to myoglobin's protection. Further experiments involving other enzymes being protected from other proteases by SBA-15 would also elucidate this effect, although not all proteases are effective at digesting all enzymes. A good pair of candidate enzymes for future experiments would be lysozyme and trypsin; trypsin can cleave the bonds of lysozyme to render it inactive, and lysozyme's activity can be easily quantified by fluorometric assay, as described in the next chapter.

The results of the experiments concerning pH protection of immobilised myoglobin give insight into which aspects of the immobilisation material are most important for predicting and tuning protective effects. The data indicate that SBA-15's pore diameter does not play as significant a role in pH protection as expected. It is possible that the range of pore diameters investigated in these experiments is too small; the largest pore diameter is only 2 nm larger than the smallest pore diameter, and myoglobin's hydrodynamic diameter is approximately 4.1 nm. If we can produce a larger range of pore diameters, we can probe the effect of pore size on immobilised enzyme further. As smaller pores that are much smaller will not be able to accommodate most enzymes, we must make SBA-15 with larger pores.

In this thesis, the largest pore diameter achieved using conventional synthesis is 8.1 nm, with a hydrothermal ageing step at 100 °C. SBA-15, prepared by conventional synthesis methods, is reported to reach pore diameters of up to 9 nm while retaining monodisperse pore size distributions and pore wall thicknesses with sufficient structural integrity. Other methods require changing the copolymer composition or block sizes, or adding cosolvent organic molecules.<sup>100</sup> Another option for making SBA-15 with larger pore diameters is to do so via microwave synthesis at higher temperatures, as described in Section 2.5.1. Unfortunately, the pore size distribution for the batch of microwave SBA-15 prepared in this thesis is found to be much wider than those made by conventional synthesis, as reported in Section 2.6.2. Wide pore size distributions are undesirable for these experiments, as they would make pore size effects less clear.

While the data from these pH protection experiments with immobilised myoglobin does not demonstrate the importance of SBA-15's pore diameter in the pH stabilisation of the enzyme, it does indicate that the pH of the solution affects immobilised myoglobin's activity significantly. As discussed, catalytic activity assays do not clearly indicate if immobilised myoglobin undergoes any conformational changes, as the data are obfuscated by possible blockage of the enzyme's active site. Computer simulations involving molecular dynamics may indicate that the pH of the solution in which myoglobin is adsorbed onto a silica mesopore affects its orientation. Such information would greatly benefit the interpretation of these data.

These results have been interpreted in the context of the electrostatic attraction between myoglobin and the pore walls of SBA-15, and are the first indication of a general hypothesis in which immobilised enzymes perform catalysis best when in solutions between the isoelectric points of the enzyme and support material. In order to refine this hypothesis, more enzymes with different sizes and isoelectric points should similarly be investigated. In this way, a more generalised and prescriptive hypothesis of the relationship between confinement, electrostatic attraction, and enzyme activity can be developed.

## **6 Glycanase activity of lysozyme immobilised on mesoporous silica SBA-15**

### **6.1 Introduction**

In this thesis, the properties of chaperonin complexes, in relation to their ability to improve the design of enzyme immobilisation systems, are being investigated via mesoporous silica SBA-15 as a simplistic functional analogue. The tunability of SBA-15, and thus its suitability for this investigative purpose, has been demonstrated, and the adsorption of proteins to SBA-15's pores has been observed and explained by geometric models. In the previous chapter, myoglobin immobilised to SBA-15 of different pore sizes and exposed to various attenuating conditions gave our first indications of how the chaperonin-derived properties of steric confinement and electrostatic interaction affect immobilised enzymes' activities. The size of the silica mesopore had no clear effect on the activity of immobilised myoglobin; there could perhaps be no relationship, or it could be that the range of pore sizes tested is too small. The data did inspire the hypothesis that strong electrostatic attraction between enzyme and porous adsorbent leads to higher immobilised enzyme activity. This hypothesis requires testing across many enzymes to discover its validity.

The next enzyme to be tested is lysozyme. As described in Section 1.3.2, lysozyme has an approximate hydrodynamic diameter of 3.9 nm and an isoelectric point at pH 11.3. As such, it is slightly smaller than myoglobin and has a stronger positive net charge in many buffered solutions. Furthermore, lysozyme does not include any prosthetic groups that may complicate the interpretation of its activity. These differences mean that the results of another set of pH protection experiments, this time on lysozyme, can help clarify the relative importance of steric confinement and electrostatic attraction to the improved catalytic activity of immobilised enzymes.

As in the previous chapter with myoglobin, the activity assay used on free or immobilised lysozyme acts as a proxy for understanding the condition of the protein. While useful, the activity assays can only provide limited insight into lysozyme's structure and flexibility. Lysozyme may adsorb to the silica mesopore in such a way that its active site is blocked and inaccessible by substrate molecules. Further, as discussed in Section 5.3.2, its orientation may

be affected by electrostatic forces within the system and change with varying pH.

## 6.2 Materials and methods

### 6.2.1 Lysozyme glycanase assay

Sodium carbonate (ACS reagent, 99.7%), *N,N*-Dimethylformamide (DMF) (ACS reagent,  $\geq 99.8\%$ ), and 4-Methylumbelliferyl  $\beta$ -D-N,N',N'-triacetylchitotrioside hydrate (ACS reagent) were purchased from Sigma-Aldrich. Fluorescence spectroscopy was carried out using the fluorescence mode of a BioTek Synergy H1 Multi-Detection Reader.

Fluorescence spectroscopy is a complementary technique to absorption spectroscopy. It involves using light of a specific wavelength, often in the ultraviolet range, to excite the electrons in certain fluorescent compounds. These compounds will then emit light at another specific wavelength, which is often visible light, and this emission can be quantified. At low concentrations the fluorescence intensity will generally be proportional to the concentration of the fluorophore, as in UV-Vis.

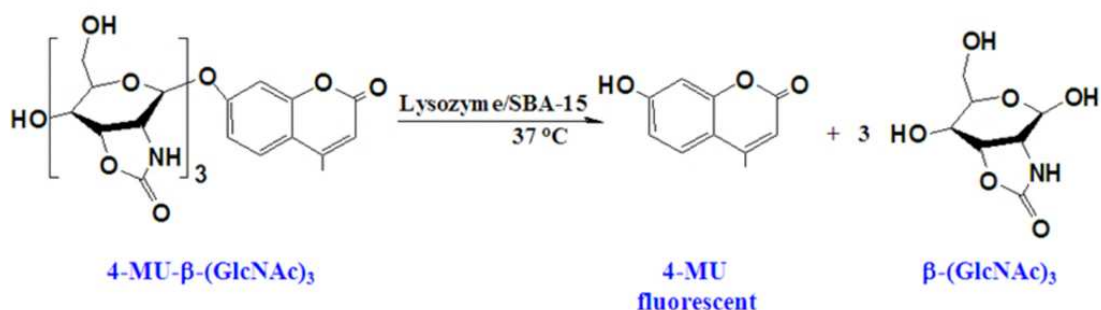


**Figure 27 - Hydrolysis of 4-MU- $\beta$ -(GlcNAc)<sub>3</sub> to a fluorescent product, catalysed by lysozyme**

The glycanase activity of lysozyme was quantified via fluorometric assay; the hydrolysis of the glycan substrate is catalysed with lysozyme as a glycanase.<sup>184</sup> A schematic of this reaction can be seen in Figure 27. As before, the initial, linear rate of reaction was monitored; this corresponds to the maximal catalysed reaction rate.

5 mg of 4-methylumbelliferyl  $\beta$ -D-N,N',N'-triacetylchitotrioside hydrate is dissolved in 250  $\mu$ L deionised water and 250  $\mu$ L DMF to prepare a 10 mg/mL solution. Cleavage of this substrate produces a fluorescent product, 4-methylumbelliferone (4-MU). The released 4-MU can reliably be used as a fluorogenic indicator for lysozyme. The anionic form of methylumbelliferone is responsible for observed fluorescence, and equilibrium does not favour anion formation at acidic pH values. Therefore, the reaction must be stopped and the fluorescent anion formed by the addition of a strong alkaline buffer, 400 mM sodium carbonate.

In these experiments, the 3 mL reaction mixture contained 2 mg of SBA-15 with a target loading of 50 mg lysozyme per g SBA-15 (i.e., approximately 0.1 mg lysozyme) in buffer, and 10  $\mu$ L of stock substrate solution in glass vials. The vials were kept at 37  $^{\circ}$ C, and 150  $\mu$ L aliquots were removed every 10 minutes for 50 minutes. Each aliquot was added to 150  $\mu$ L of stopping buffer in a black, 96-well fluorescence microwell plate. The fluorescence of these wells was measured ( $\lambda_{\text{ex}} = 360$  nm,  $\lambda_{\text{emm}} = 455$  nm) within 5 minutes of mixing. The glycanase activities of lysozyme-containing samples were found by observing the change in fluorescence over time, within the samples' initial linear rate. The activity was normalised to the calculated amount of lysozyme in each sample. Blanks containing no lysozyme were found to have no significant glycanase activity at all pH values tested.

As discussed in Section 5.2.1, a small molecule substrate such as 4-MU- $\beta$ -(GlcNAc)<sub>3</sub> should diffuse through SBA-15 pores of this size within milliseconds, although, admittedly, 4-MU- $\beta$ -(GlcNAc)<sub>3</sub> is a more bulky molecule than ABTS. Again, lysozyme loading onto SBA-15 is very low, and the substrate is likely to be hydrolysed when it encounters an adsorbed lysozyme within the pore, rather than trying to pass around it. For these reasons, this glycanase assay is not expected to have mass transport limitations. Lysozyme uses the negatively-charged aspartic and glutamic acid residues in its active site cleft to hydrolyse 1,4-beta-glycosidic linkages. As mentioned in Section 1.3.2, these residues' positioning within a cleft is crucial to their proper function, because the cleft protects the acid residues from losing their protons. Lysozyme's glycanase

activity can therefore give direct insight into the tertiary structure of free and immobilised lysozyme.

### **6.2.2 Lysozyme pH protection**

Sodium phosphate monobasic (BioXtra,  $\geq 99\%$ ), sodium phosphate dibasic (BioXtra,  $\geq 99\%$ ), glacial acetic acid (ACS reagent,  $\geq 99.7\%$ ), sodium acetate ( $\geq 99\%$ , anhydrous), and lysozyme from chicken egg white (lyophilized powder, protein content  $\geq 90\%$ ,  $\geq 40,000$  units/mg protein) were purchased from Sigma-Aldrich and used without further purification. Mesoporous silica SBA-15 was prepared and characterised as discussed in Chapter 2. In this chapter, SBA-15 samples are referred to by their pore diameters. UV-Vis was carried out using the absorbance mode of a BioTek Synergy H1 Multi-Detection Reader.

To test the protective effects of SBA-15 on immobilised enzyme, lysozyme/SBA-15 composites were prepared and exposed to unfavourable pH conditions. Lysozyme/SBA-15 composites were initially prepared with a target loading of 50 mg enzyme per g SBA-15 in phosphate buffer pH 7.2, with an ionic strength of 100 mM, via the physical adsorption method described in Section 3.2.1. The remaining procedure for investigating the pH protection of immobilised lysozyme is identical to that found in Section 5.2.3 for myoglobin. The solutions' enzymatic activities were quantified via the glycanase assay described in the previous section. As in the previous chapter, each combination of pore size and pH was prepared and measured in triplicate, and activity was compared to that of blank samples.

## **6.3 Results and discussion**

### **6.3.1 pH protection of immobilised lysozyme**

Lysozyme immobilised on SBA-15 of different pore diameters is exposed to a range of pH conditions, and then the samples' glycanase activities are measured by glycanase assay at that pH. This is done to examine the relationship between pH and immobilised enzyme activity, and probe for possible protective effects of SBA-15 on the immobilised enzymes from denaturing pH conditions.

For these experiments, as with the previous myoglobin experiments, lysozyme loading onto SBA-15 is targeted for 50 mg enzyme per g SBA-15. Using the textural parameters of the SBA-15 batches derived from gas physisorption and reported in Section 2.6.2, we can state that this lysozyme loading corresponds to one lysozyme molecule for every 240 nm<sup>2</sup> of SBA-15 surface area for the smallest pore diameter and one for every 330 nm<sup>2</sup> for the largest pore diameter. For reference, one lysozyme molecule has a hydrodynamic packing area of approximately 12 nm<sup>2</sup>. This loading also corresponds to one lysozyme molecule for every 230 nm<sup>3</sup> of pore volume, at the smallest pore size, and one molecule for every 520 nm<sup>3</sup> for the largest pore size. For comparison, lysozyme's hydrodynamic volume is approximately 31 nm<sup>3</sup>. As with myoglobin in the previous chapter, the lysozyme molecules are spaced quite far from neighbouring molecules, and are more isolated in SBA-15 with larger pores.

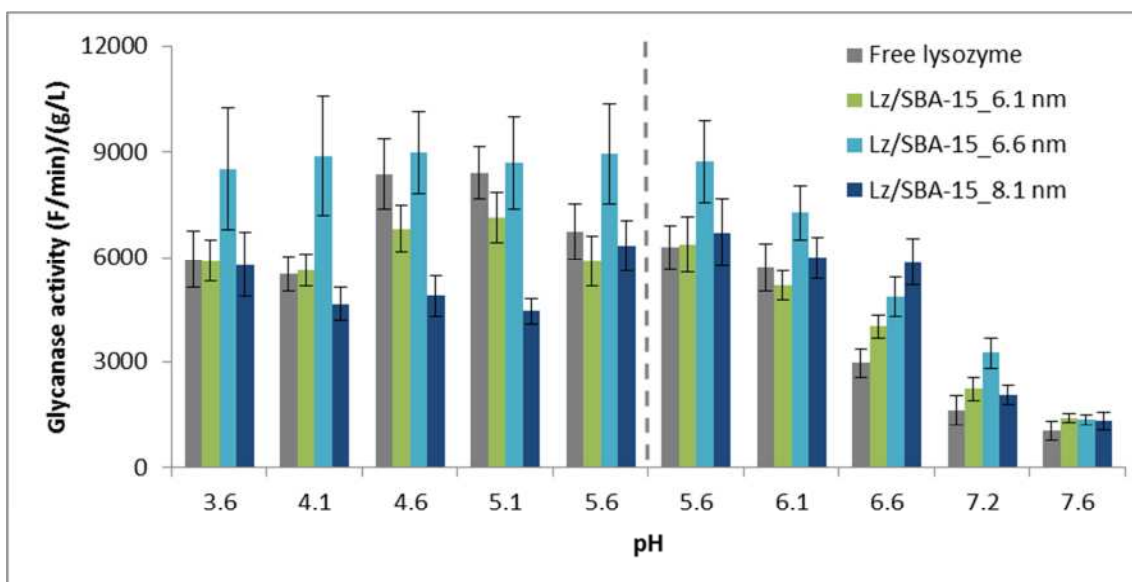
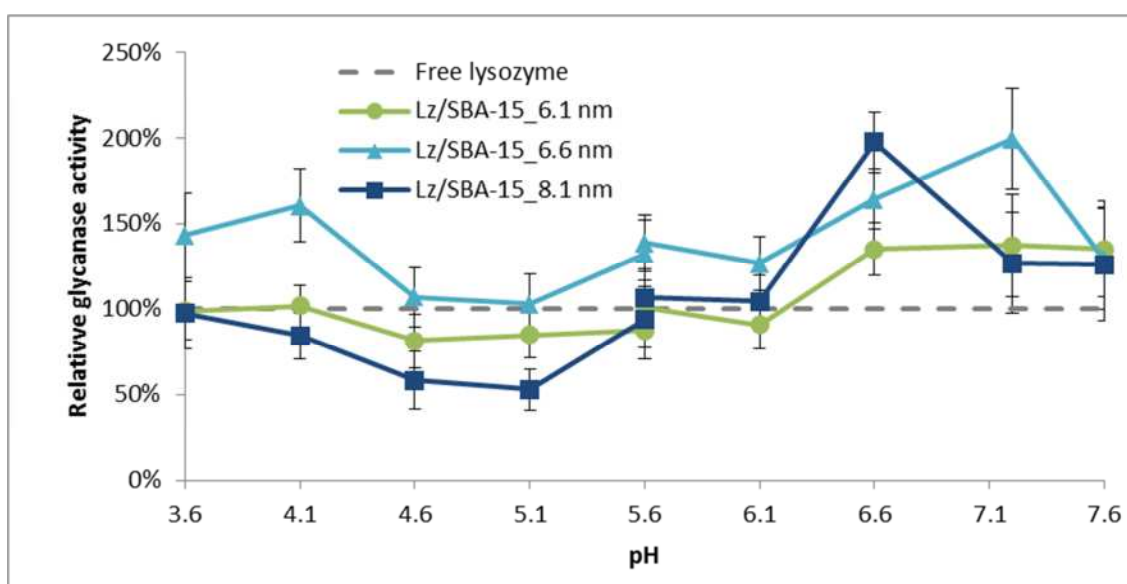


**Figure 28 - Glycanase activities of free lysozyme and lysozyme immobilised to mesoporous silica SBA-15 (pore diameters of 6.1, 6.6, and 8.1 nm) in solutions of pH 3.6 to 7.6, 100 mM ionic strength. pH values to the left of the dashed line take place in acetate buffer while those on the right are in phosphate buffer. Error bars depict 95% confidence intervals.**

Figure 28 shows the glycanase activities of free lysozyme, as well as those of lysozyme immobilised on SBA-15 of different pore diameters, in buffered solutions across a range of pH values. The activities are shown in arbitrary units relating to the rate of the glycanase reaction (fluorescence per minute) divided

by the concentration of lysozyme in the sample (g/L). Some lysozyme leaching is observed while the samples are left in the test buffer for 24 hours, which is accounted for in specific activity calculations. At pH 5.6, both phosphate and acetate buffers are used, and the sample's activities are found to be within error of each other. This was also found in the myoglobin experiments, and is a useful result because it suggests that the buffer salt used does not have a significant effect on lysozyme's activity.

Lysozyme acts as a glycanase on the fluorogenic substrate most effectively between pH 4.6 and 5.1, as can be seen by the free lysozyme bars in Figure 28. Activity decreases at more acidic pH values; this is likely because lysozyme's active site begins to lose protons at glutamic acid's  $pK_a$  of 4.2, and then again at aspartic acid's  $pK_a$  of 3.7. The protons in the active site cleft are crucial to the glycanase function of lysozyme.<sup>184</sup> The reasons for the decrease in glycanase activity of free lysozyme at pH values greater than 5.1 are less clear.



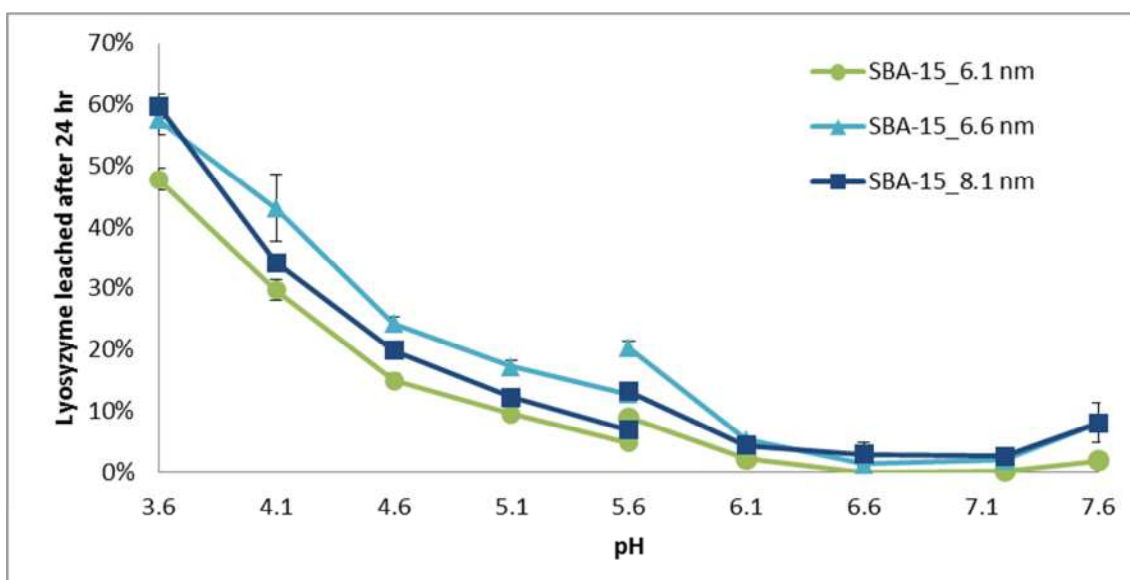
**Figure 29 - Normalised glycanase activities of free lysozyme and lysozyme immobilised to mesoporous silica SBA-15 (pore diameters of 6.1, 6.6, and 8.1 nm) in solutions of pH 3.6 to 7.6, 100 mM ionic strength. Error bars depict 95% confidence intervals.**

Figure 29 depicts the same data, shown normalised to the activities of free lysozyme at each pH. The error bars, which depict the 95% confidence interval, show the compounded error of both free and confined samples for each data

point. At pH values above 6.1, on the more alkaline side of the assay's optimal pH, SBA-15 consistently demonstrates protective effects on lysozyme regardless of pore diameter. The activity of confined lysozyme surpasses that of free lysozyme at these pH values, with activity values of up to 200% of those of free lysozyme at those pH values. This implies that confined lysozyme is protected to some extent. Protective effects are not clearly evident at pH values below 6.6 for two of the three SBA-15 samples.

The pore size of the SBA-15 appears to play a significant role in the extent to which lysozyme's activity is modified. Lysozyme immobilised on SBA-15\_6.6 nm always performs at least as well as, and often better than, free lysozyme. SBA-15\_6.6 nm also shows protective effects against more acidic conditions at pH 3.6 and 4.1. This is a unique result, and may indicate that this particular pore diameter is especially suited to stabilizing and improving the glycanase activity of lysozyme. We see that, in many cases, the activities of lysozyme immobilised on SBA-15\_6.1 nm are within error of those of free lysozyme. This is a modest but positive result, as immobilisation at this pore size does not hinder the enzyme's activity. Lysozyme immobilised to SBA-15\_8.1 nm does not always perform as well as free lysozyme; SBA-15 of the largest pore size attenuates lysozyme's glycanase activity at pH values from 4.1 to 5.1.

Immobilisation onto SBA-15 does not improve lysozyme's glycanase activity at all pH values tested, or with all pore sizes. However, as is the case of myoglobin in the previous chapter, confinement to SBA-15 does widen lysozyme's effective activity range, with substantial protection from unfavorably alkaline conditions of up to 200%.



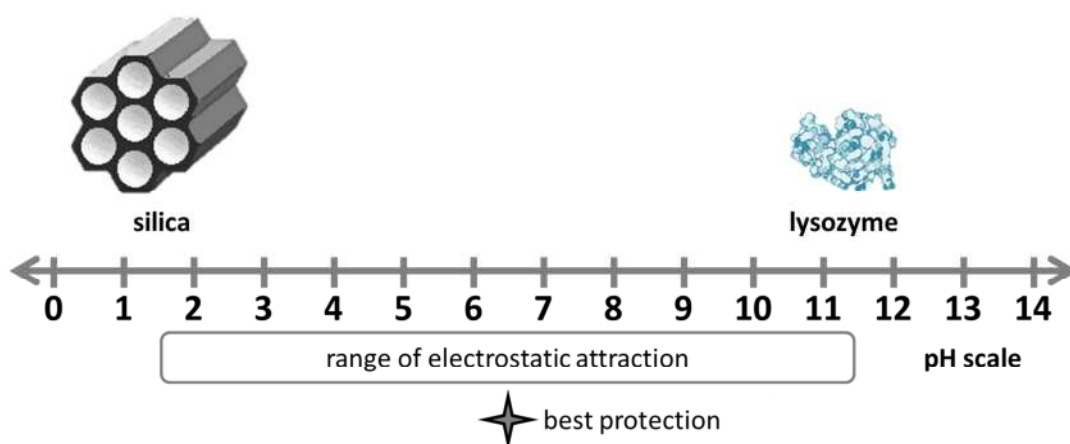
**Figure 30 – Amount of initially-loaded lysozyme leached from mesoporous silica SBA-15 (pore diameters of 6.1, 6.6, and 8.1 nm) after 24 hours in solutions of pH 3.6 to 7.6, 100 mM ionic strength. Error bars depict 95% confidence intervals.**

Figure 30 depicts the percentage of initially loaded lysozyme that leached from the different batches of SBA-15 from each buffer. Lysozyme leaching exceeds that of myoglobin at some pH values, with up to 60% of the initially loaded lysozyme leaching at the low pH value of 3.6. At low pH values, lysozyme will have a strong positive charge while the silica's surface charge will be weakly negative. The increased leaching seen at these pH values may be caused by lower charge density on the silica surface, so close to silica's pzc. As with the myoglobin leaching data, these data are also helpful in confirming that the different SBA-15 batches have similar surface charge profiles.

In Figure 30, solutions with pH less than 5.6 are prepared in acetate buffer and solutions with pH greater than 5.6 are prepared in phosphate buffer. For all SBA-15 samples, lysozyme leaching at pH 5.6 is consistently approximately 5% less in acetate buffer than in phosphate buffer. As discussed in Section 1.2.3, the Hofmeister series ranks ions on their ability to stabilise or destabilise protein structures.<sup>23,63</sup> Phosphate is earlier in the Hofmeister series than acetate, so it should stabilise lysozyme's structure more, decreasing its solubility and strengthening its hydrophobic interactions. With its hydrophobic residues more completely buried, lysozyme in phosphate may more easily adsorb to the hydrophilic surface of the silica, leading to the slightly higher lysozyme loading

in phosphate buffer. Despite these differences in lysozyme loadings, the specific activities of the samples at pH 5.6 are still within error of each other after taking leaching into account.

The results of the pH protection experiments with immobilised lysozyme, shown in Figure 28, Figure 29, and Figure 30, give insight into the relative importance of different aspects of the immobilisation material. The data indicate that the pH of the solution affects immobilised lysozyme's activity significantly, as was seen in the myoglobin pH protection experiments in the previous chapter. As before, the effects of pH can be partially explained in the context of the electrostatic attraction between lysozyme and SBA-15.



**Figure 31 - Schematic of electrostatic effects between silica and lysozyme**

Lysozyme's isoelectric point is at pH 11.3. In any aqueous solution between pH 2 and 11.3, silica will have a negative net surface charge and lysozyme will have a positive net surface charge, and the lysozyme molecules will be electrostatically attracted to the silica surface. We found that lysozyme immobilised to SBA-15 demonstrated the highest relative activity, or the strongest protective effects, at pH 6.6. This comparatively high glycanase activity is found to correspond directly to the pH at which lysozyme and silica experience the strongest electrostatic attraction. Lysozyme's attraction to SBA-15 around pH 6.6 is also illustrated in Figure 30, where lysozyme demonstrates a minimal amount of leaching at these pH values.

An additional factor to consider when interpreting these results is the orientation of lysozyme within the pore, particularly whether the active site is accessible to

the relatively bulky glycanase substrate molecules. As discussed in Section 5.3.2, patches of the protein's surface that have more positively-charged residues may preferentially adsorb to the negatively charged silica surface, and negatively charged amino acid residues will lose their electrostatic repulsion from the silica surface at lower pH values as well. The more positively-charged regions of the protein's surface will depend on the pH of the solution it is in, and any the resultant orientation of the enzyme may contribute substantially to gains or losses of immobilised enzyme activity at different pH values.<sup>77,173</sup>

The relationship between solution pH and immobilised lysozyme's relative activity, seen in Figure 29, is not as dramatic as the one seen with immobilised myoglobin in Figure 24, but immobilised lysozyme seems to undergo a positive shift in activity above pH 6.1. This may correspond to some disruption in charged groups on the protein's surface which lead it to adsorb preferentially in way that blocks its active site. Again, however, this is not clearly the case, because lysozyme has only a single histidine residue that changes its charge at its  $pK_a$  of 6. As before, computer simulations of lysozyme adsorptive behaviour within silica mesopores would greatly benefit the interpretation of these data.

#### **6.4 Conclusion**

In this chapter, lysozyme was immobilised to SBA-15 of different pore sizes, exposed to a range of pH conditions, and tested for its glycanase activity. The purpose of these experiments is to investigate the relative importance of two aspects of enzyme immobilisation, steric confinement and electrostatic attraction, which are inspired by our understanding of chaperonin complexes. These experiments showed that immobilised lysozyme's performance was significantly affected by both parameters: lysozyme's glycanase activity was most enhanced when immobilised to SBA-15\_6.6 nm, which was the intermediate pore size; and immobilised lysozyme's relative activity was highest between pH 6.6 and 7.1, which corresponds to the pH at which lysozyme experiences strong electrostatic attraction to silica. Catalytic activity assays cannot clearly indicate if lysozyme undergoes any conformational changes upon adsorption to SBA-15; as discussed, the lysozyme's active site may or may not be blocked depending on its orientation within the pore, limiting its substrate accessibility. Computer simulations involving molecular dynamics could

potentially indicate whether lysozyme's orientation within the silica mesopore is substantially affected by solution pH, which would assist in the interpretation of these data.

The results of the pH protection experiments on lysozyme, and on myoglobin in the previous chapter, suggest that electrostatic attraction drives the increased enzymatic activity sometimes observed when immobilising enzymes with the physical adsorption method. If electrostatic attraction dominates these protective effects, this information is useful for the design of immobilised enzyme systems; once one knows the isoelectric point of the enzyme that is to be used for catalysis, an immobilisation material can be chosen based on its point of zero charge relative to the optimum pH range of the target reaction. Similarly, when one knows both the enzyme's and immobilisation material's isoelectric points, the pH values that are suitable for the process will also be known. However, more enzymes must be examined to confirm or refute the generality of this hypothesis.

In the pH protection experiments involving immobilised lysozyme, the effect of the pore size of SBA-15 was significant, whereas in the similar experiments of myoglobin in the previous chapter it was not. One explanation may be that the smaller size of lysozyme means that it was more greatly affected by the pore size range tested than myoglobin was. This explanation is unlikely, however, because the ratios between the SBA-15 samples' pore diameters and the sizes of either enzyme overlap, as do their respective ratios for surface area and pore volume. Therefore, it is more likely that steric confinement's role in enzyme protection is either modulated by the level of electrostatic attraction in the system, or dependent on the type of active site of the enzyme, or some combination of both. Again, more enzyme systems must be studied to clarify this effect.

## **7 Hydrolase activity of trypsin immobilised on mesoporous silica SBA-15**

### **7.1 Introduction**

This thesis aims to discover and refine general principles concerning enzyme immobilisation, inspired by chaperonin complexes, which improve their application in industrial biocatalysis. This entails the investigation of two integral chaperonin parameters, steric confinement and electrostatic attraction, on several different model enzymes using mesoporous silica SBA-15 as a tuneable, synthetic chaperonin analogue. In the previous two chapters, the enzymes myoglobin and lysozyme were immobilised to SBA-15 of varying pore sizes and exposed to a range of attenuating conditions. The effects of pore size and pH conditions on the immobilised enzymes' biocatalytic activities are interpreted in the context of these chaperonin parameters. For both immobilised myoglobin and immobilised lysozyme, the enzymes' activities were highest in solutions where the pH was intermediate between the isoelectric points of the enzyme and immobilisation material. In other words, the immobilised enzymes were best protected from denaturing conditions when they were experiencing strong electrostatic attraction to the silica surface. In this chapter, a third enzyme is examined in a similar way: trypsin.

Trypsin is a serine protease that digests other proteins by cleaving their amino acid chains.<sup>17</sup> Trypsin's active site is similar to that of lysozyme's, in that it catalyses hydrolysis, though through different mechanisms. Because trypsin also lacks a prosthetic group, its activity is more directly indicative of its overall, three-dimensional structure. Trypsin also differs from the two previous enzymes in its physiochemical parameters: size and charge. Trypsin's approximate hydrodynamic diameter is 4.6 nm, which is larger than those of the previous two enzymes, myoglobin and lysozyme.<sup>138</sup> Its isoelectric point is around pH 10.3, which is close to that of lysozyme but more basic than that of myoglobin, meaning that trypsin has a net positive charge in most solutions.<sup>141</sup>

Trypsin's differences from the previous two enzymes in size, charge, and catalytic mechanism could help clarify the effects of SBA-15's pore size and surface charge on immobilised enzymes, their relative importance to the enzymes' activity, and if more general trends about enzyme immobilisation

could be inferred for application to a wide range of industrial enzymes. As in the previous chapters with myoglobin and lysozyme, the activity assay used on free or immobilised trypsin is a proxy for understanding the condition of the protein. The assay cannot indicate whether or not trypsin adsorbs to the silica mesopore such that its active site is blocked and inaccessible by substrate molecules. As discussed in Section 5.3.2, trypsin's orientation against the pore wall may be affected by electrostatic forces within the system and change with varying pH.

## 7.2 Materials and methods

### 7.2.1 Trypsin hydrolase assay

Sodium phosphate monobasic (BioXtra,  $\geq 99\%$ ), sodium phosphate dibasic (BioXtra,  $\geq 99\%$ ), glacial acetic acid (ACS reagent,  $\geq 99.7\%$ ), sodium acetate ( $\geq 99\%$ , anhydrous  $N_{\alpha}$ -Benzoyl-L-arginine ethyl ester (BAEE) hydrochloride, and hydrochloric acid (ACS reagent, 37%) were purchased from Sigma-Aldrich. UV-Vis was carried out using the absorbance mode of a BioTek Synergy H1 Multi-Detection Reader.

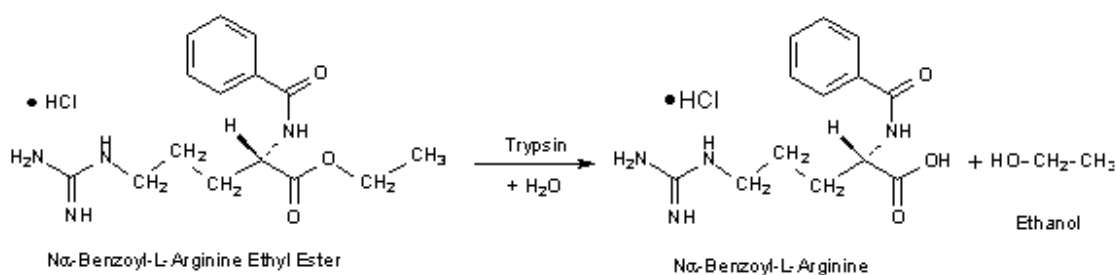


**Figure 32 – Hydrolysis of  $N_{\alpha}$ -Benzoyl-L-arginine ethyl ester, catalysed by trypsin**

Trypsin's hydrolase activity can be quantified by spectrophotometric assay, shown in Figure 32. Trypsin catalyses the hydrolysis of the synthetic substrate, BAEE, to produce  $N_{\alpha}$ -Benzoyl-L-arginine and ethanol.<sup>185</sup>  $N_{\alpha}$ -Benzoyl-L-arginine absorbs light at 253 nm, so the continuous reaction can be observed by UV-Vis. Trypsin functions optimally in this assay between pH 7 and 9. The initial, linear rate of reaction is monitored; this corresponds to the maximal catalysed reaction rate, before enough substrate is consumed to reduce the rate of reaction.

In these experiments, samples containing approximately 0.25 g/L trypsin were diluted 8-fold with 1 mM hydrochloric acid immediately before measurement. 20  $\mu$ L of HCl-diluted trypsin sample was placed in one well of a UV-transparent

microwell plate with 270  $\mu\text{L}$  of buffer. Lastly, 30  $\mu\text{L}$  of 2.5 mM BAEE was added to the well, for a total in-well volume of 320  $\mu\text{L}$ . Absorbance was read immediately at 253 nm for 5 minutes at room temperature. The hydrolase activities of samples were found by observing the change in absorbance at 253 nm over time, within the samples' initial linear rate. The specific activity was calculated by dividing this rate by the amount of trypsin in each sample. Blanks containing no trypsin were found to have some hydrolase activity at low pH; this rate was subtracted from the activity of trypsin samples at that pH.

As discussed in Section 5.2.1, a small molecule substrate such as BAEE should diffuse through SBA-15 pores of this size within milliseconds, so mass transport limitations should not be an issue in this assay. Trypsin's catalytic mechanism is similar to those of other serine proteases: the catalytic triad of histidine, aspartate, and serine form a charge relay that increases the nucleophilicity of the active site serine. Additionally, the serine and a neighbouring glycine residue create an oxyanion hole, which serves to stabilise the developing negative charges of cleaved amides.<sup>140</sup> These residues' positions within the active site cleft are crucial to its proper function. As with lysozyme in the previous chapter, trypsin's hydrolase activity gives qualitative insight into the structures of free or immobilised trypsin.

### **7.2.2 Trypsin pH protection**

Sodium phosphate monobasic (BioXtra,  $\geq 99\%$ ), sodium phosphate dibasic (BioXtra,  $\geq 99\%$ ), glacial acetic acid (ACS reagent,  $\geq 99.7\%$ ), sodium acetate ( $\geq 99\%$ , anhydrous), and trypsin from bovine pancreas (Type XI, lyophilized powder,  $\geq 6,000$  BAEE units/mg protein) were purchased from Sigma-Aldrich and used without further purification. Mesoporous silica SBA-15 was prepared and characterised as discussed in Chapter 2. In this chapter, SBA-15 samples are referred to by their pore diameters. UV-Vis was carried out using the absorbance mode of a BioTek Synergy H1 Multi-Detection Reader.

To test the protective effects of SBA-15 on immobilised enzyme, trypsin/SBA-15 composites were prepared and exposed to unfavourable pH conditions. Trypsin/SBA-15 composites were initially prepared with a target loading of 175 mg enzyme per g SBA-15, and trypsin/MWSBA-15 composites were prepared

with a target loading of 50 mg/g, both in phosphate buffer, pH 7.2, with an ionic strength of 100 mM, via the physical adsorption method described in Section 3.2.1. The remaining procedure for investigating the pH protection of immobilised trypsin is identical to that found in Section 5.2.3. The solutions' enzymatic activities were quantified via the hydrolase assay described in the previous section. As in the previous chapters, each combination of pore size and pH was prepared and measured in triplicate, and activity was compared to those of blank samples.

## **7.3 Results and discussion**

### **7.3.1 Hydrolase activity of immobilised trypsin on SBA-15**

For these experiments, trypsin loading onto SBA-15 is targeted for 175 mg enzyme per g SBA-15, and 50 mg per g microwave-synthesised (MW)SBA-15. Using the textural SBA-15 parameters derived from gas physisorption and reported in Section 2.6.2, we can state that this trypsin loading corresponds to one lysozyme molecule for every 130-150 nm<sup>2</sup> of SBA-15 surface area and one for every 210 nm<sup>2</sup> for MWSBA-15. For reference, one trypsin molecule has a hydrodynamic packing area of approximately 16 nm<sup>2</sup>. This loading also corresponds to one trypsin molecule for every 150-250 nm<sup>3</sup> of pore volume, for conventionally prepared SBA-15, and one molecule for every 780 nm<sup>3</sup> for microwave-synthesised SBA-15. For comparison, trypsin's hydrodynamic volume is approximately 50 nm<sup>3</sup>. These enzyme spacings, as determined by surface area, are similar across SBA-15 batches, but by volume the microwave SBA-15 has much more space between trypsin molecules than the conventional samples have. In general, the trypsin molecules are spaced quite far from neighbouring molecules, and are more isolated in SBA-15 with larger pores.

While the experiments were performed at all pH and buffer conditions as in the myoglobin and lysozyme experiments, the activity of free trypsin was indistinguishable from that of the blanks in all buffers below pH 5.6. Therefore, only results from experiments performed in phosphate buffer are shown in the following figures. The inadequacy of these buffers in the chosen assay are not attributed to the buffer salt, acetate, because experiments performed at pH 5.6 in acetate buffer have activity and leaching within error of those performed in

the phosphate buffer at pH 5.6. It is therefore presumed that this assay will not function meaningfully at pH values lower than 5.6 without modification.

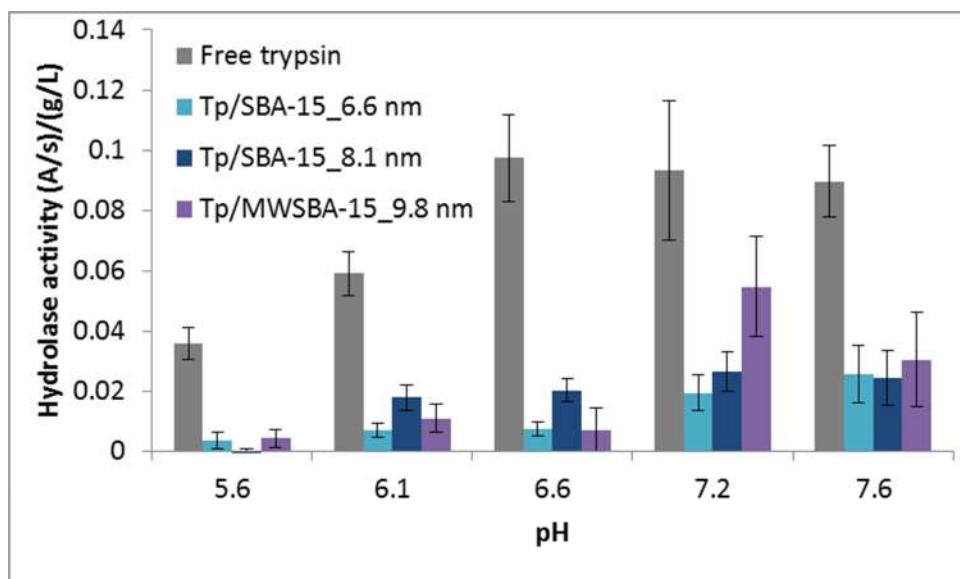


**Figure 33 - Hydrolase activities of free trypsin and of trypsin immobilised to mesoporous silica SBA-15 (pore diameters of 6.6, 8.1, and 9.8 nm) in phosphate buffers, pH 5.6 to 7.6, 100 mM ionic strength. Error bars depict the 95% confidence intervals.**

Figure 33 shows the hydrolase activities of all trypsin samples, free or confined to the three different SBA-15 batches, across five pH values. As in previous chapters, these activities are presented as reaction rate per concentration of enzyme. They take into account the variable amounts of trypsin in each sample due to leaching. At all pH values tested, trypsin immobilised to SBA-15 has a significantly lower hydrolase activity than that of unconfined trypsin.

These data do not show a clear trend of hydrolase activity with the pore size of the SBA-15 on which the trypsin is immobilised; at each pH value, the activities of immobilised trypsin are mostly within error of each other. The exceptions to these observations are that the activity of lysozyme immobilised to SBA-15\_8.1 nm exceeds that of those immobilised to SBA-15\_6.6 nm at pH 6.1 and 6.6. Also, the activity of lysozyme immobilised to MWSBA-15\_9.8 nm exceeds that of those immobilised to SBA-15\_8.1 nm at pH 5.6 and 7.2. While limited, these data would seem to indicate that trypsin performs better when immobilised to SBA-15 of larger pore diameters. However, the fact that many of the other data points are within error of each other fails to support this hypothesis conclusively.

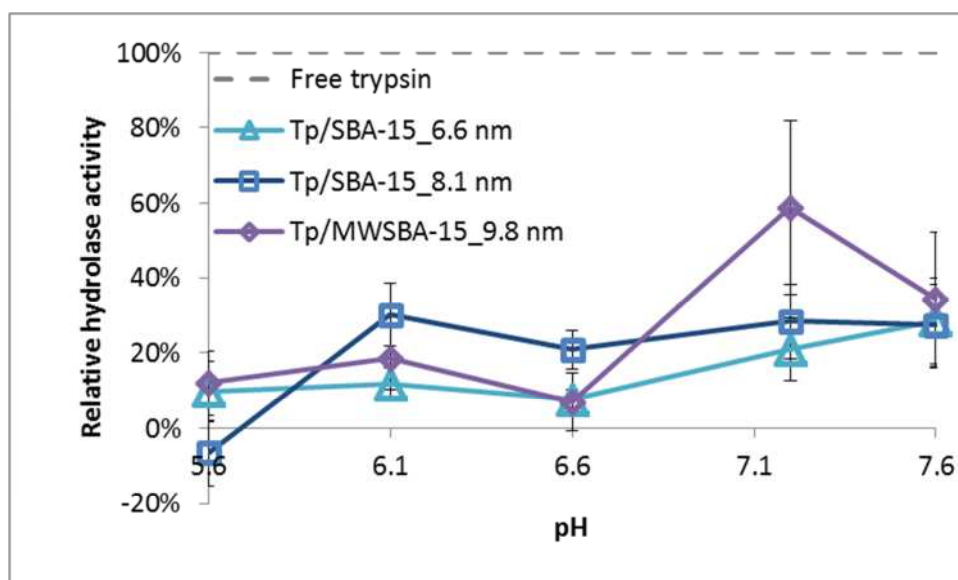


**Figure 34 - Normalised hydrolase activities of free trypsin and of trypsin immobilised to mesoporous silica SBA-15 (pore diameters of 6.6, 8.1, and 9.8 nm) in phosphate buffers, pH 5.6 to 7.6, ionic strength 100 mM. Error bars depict the 95% confidence intervals.**

Figure 34 depicts the same data shown in Figure 33, but normalised such that each activity of immobilised trypsin is shown as a percentage of the activity of non-confined trypsin at that pH. The error bars, which depict the 95% confidence interval, show the compounded error of both free and confined samples for each data point.

As in Figure 33 with pore size, Figure 34 depicts few clear trends between the normalised hydrolase activities of immobilised trypsin and pH, but some slight patterns emerge. Trypsin immobilised to the smallest pore size of SBA-15, which has a 6.6 nm pore diameter, has significantly lower normalised activity at pH 6.6 than at pH 7.2 and 7.6. For the 8.1 nm pore diameter SBA-15, the normalised activity of immobilised trypsin at pH 5.6 is significantly lower than at all of the other, higher pH values tested. And lastly, for the 9.8 nm, microwave-assisted SBA-15, immobilised trypsin tested at pH 7.2 has significantly higher normalised activity than those found at any lower pH value for the same sample. Each of these observations support a hypothesis that immobilised trypsin's activity increases with increasing pH, across the pH values tested, compared to the activities of free trypsin. However, as with pore size, the fact that many of the other data points are within error of each other fails to support

this hypothesis conclusively. More definitively, these data indicate that a more sensitive assay for trypsin activity is required.

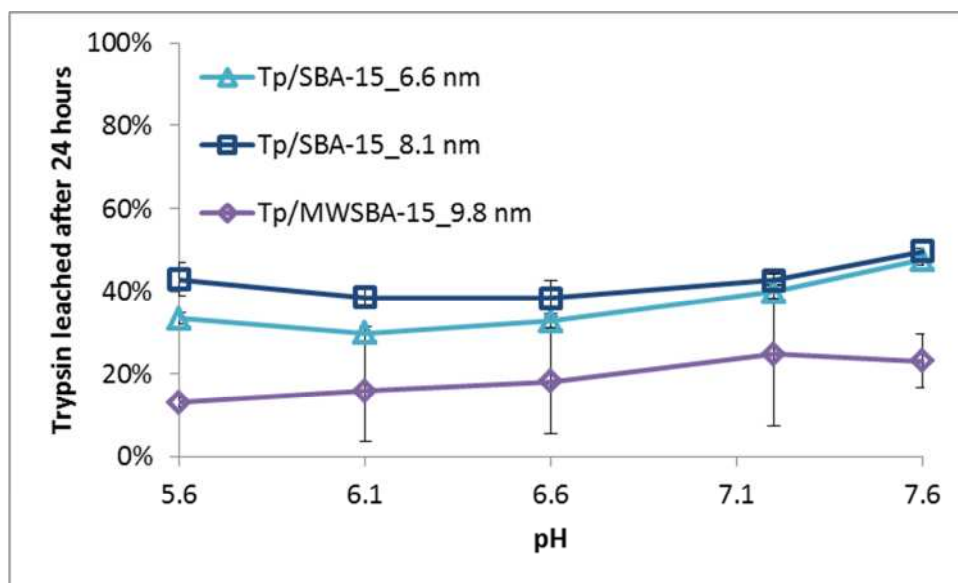


**Figure 35 - Amount of initially-loaded trypsin leached from mesoporous silica SBA-15 (pore diameters of 6.6, 8.1, and 9.8 nm) after 24 hours in phosphate buffers, pH 5.6 to 7.6, ionic strength 100 mM. Error bars depict the 95% confidence intervals.**

Figure 35 shows the amount of trypsin loaded onto the SBA-15 of different pore sizes that has leached off its support after being suspended in the test buffer for 24 hours. As in previous chapters, these data are meant to confirm the pH at which the enzyme is most strongly attracted to the silica surface. In these experiments, the data is less conclusive, but the least amount of trypsin leaching appears to occur between pH 5.6 and 6.6 for the two conventionally-synthesised SBA-15 samples. These data also indicate that the SBA-15 with pore sizes of 6.6 and 8.1 nm have similar leaching trends, and therefore a similar surface charge. SBA-15 with a mean pore diameter of 8.1 nm shows a significantly higher percent of trypsin leached than the SBA-15 with a mean pore diameter 6.6 nm. However, in these experiments, as in previous chapters, the amount of trypsin leached off the support is taken into account when calculating the activity of immobilised trypsin.

The leaching data from the microwave-assisted SBA-15 shown in Figure 35 appear to be much lower than those of the other two materials, but also have large enough error bars to be indistinguishable at many of the pH values tested.

This is because the targeted trypsin loading on the microwave-assisted SBA-15 was much lower, 50 mg/g, compared to the others, which were targeted at 175 mg/g. The amount of trypsin leaching observed is highly dependent on the amount of trypsin initially observed, as can be understood from the protein adsorption isotherms discussed in Chapter 3. This difference in preparation means that the leaching profile from the microwave assisted SBA-15 should not be quantitatively compared to that of the other two materials.

The results of the experiments concerning the pH protection of immobilised trypsin, shown in Figure 33, Figure 34, Figure 35, give little insight into the relative importance of different aspects of the immobilisation material on the immobilised enzyme's catalytic activity. If immobilised trypsin were conforming to the protective theme observed with the previous two enzymes, myoglobin and lysozyme, its normalised activity would be highest at pH values intermediate to the isoelectric points of silica and trypsin. This intermediate point, around pH 6, would be the solution condition under which trypsin has the strongest electrostatic attraction to the silica surface, which is unfortunately neither confirmed nor refuted by the trypsin leaching profile seen in Figure 35. The data in Figure 33 and Figure 34 neither support nor contradict the hypothesis of the necessity of strong electrostatic attraction; they are inconclusive. Furthermore, the SBA-15's pore size showed little consistent effect on immobilised trypsin activity across the ranges tested.

#### **7.4 Conclusion**

In this chapter, trypsin was immobilised to SBA-15 samples with a range of pore sizes, exposed to a range of solution conditions with variable pH but fixed ionic strength, and was tested for its hydrolase activity. These experiments were performed to investigate the relationship between the enzyme's and pore's sizes, i.e., the enzyme's steric confinement, and the enzyme's catalytic activity. They were also performed to examine the effects of the pH of the solution on immobilised trypsin's activity.

The trypsin pH protection experiments did not show SBA-15's pore size to have a discernible effect on immobilised trypsin's activity; almost all data concerning pore size were within error of each other at each pH value. These experiments

also did not clearly determine at which pH value immobilised trypsin had the highest hydrolase activity, compared to that of free trypsin at each pH. Therefore, these experiments do not contribute to supporting or disproving the tentatively proposed mechanism for enhancing enzyme activity from the previous two chapters: that immobilised enzymes perform best in solutions with pH values in-between the isoelectric points of the enzyme and adsorbent, ensuring high electrostatic attraction between the two.

Despite not contributing definitively to these two lines of inquiry, the results from these experiments did show that immobilised trypsin's activity was much lower than that of free trypsin at all pH values between 5.6 and 7.2. These results draw attention to the limitations of any overly-simplistic optimisation of enzyme activity via size and charge: even an enzyme adsorbed to an accommodating pore size, and reacting at a pH conducive to electrostatic attraction, may have poorer activity than the free enzyme, regardless of whether or not these two parameters are optimised. In trypsin's case, the attenuated activity of the enzyme when immobilised likely is due to some specifics of its active site that are not presently accounted for.

At pH values between and including 3.6 and 5.1, neither free nor immobilised trypsin had appreciable activity over a blank baseline using the current assay method. Therefore, the range of pH values tested in these experiments was restricted, making it more difficult to compare immobilised trypsin's activities under different levels of internal electrostatic attraction. Even at the higher pH values, from pH 5.6 to 7.2, the activity assay was often not sufficient to differentiate activity values of the immobilised samples at different pore sizes and pH values. The hydrolase assay used in these experiments needs to be further developed to be able to utilise these type of experiments more effectively using trypsin. Perhaps an entirely different assay must be used; silica absorbs UV light to some extent and may be interfering with the assay, which produces a UV-adsorbing product.

## 8 Summary and recommendations

### 8.1 Summary

The specific aim of this thesis is to demonstrate the use of mesoporous silica SBA-15 to investigate two chaperonin-inspired parameters, steric confinement and electrostatic attraction. By probing the effects of pore diameter and surface charge of the SBA-15 materials on their ability protect cargo proteins from denaturation, this thesis develops SBA-15 as an enzyme immobilisation material. More importantly, these experiments help to achieve a better understanding of the fundamentals behind enzyme immobilisation in general, and make future efforts in this field more straightforward.

As reported in Chapter 2, batches of SBA-15 have been synthesised by acidic sol-gel method to have different pore diameters. Scanning electron microscopy has shown the samples have regular external morphologies: rod-like with lengths of one micron. Nitrogen gas physisorption, corroborated by transmission electron microscopy, has shown that the SBA-15 has straight, cylindrical pores of monodisperse diameters. These pore diameters increase with increasing temperature during the hydrothermal condensation step of synthesis. Nitrogen physisorption has also indicated that the SBA-15 have high surface area and pore volume. Small-angle x-ray scattering shows that the pores are well-ordered in a 2D hexagonal array. The high degree of control demonstrated over SBA-15's morphology indicates its suitability as a simplistic chaperonin analogue for studying the roles of steric confinement and electrostatic attraction in enzyme immobilisation.

In Chapter 3, the synthesised SBA-15 is shown to adsorb and immobilise several model proteins, myoglobin, lysozyme, trypsin, and pepsin, in accordance with the Langmuir model of physical adsorption. The maximum amount of protein that can be adsorbed onto SBA-15 increases with increasing pore size. Chapter 4 reported how myoglobin adsorption kinetics is influenced by SBA-15's pore diameter. Myoglobin adsorption kinetics is compared with that of lysozyme under the same solution conditions, and electrostatic attraction is not found to affect protein diffusivity within the pores. Together, Chapters 3 and

4 demonstrate the important role of steric confinement in protein adsorption to porous silica.

In Chapters 5 and 6, immobilising the enzymes myoglobin and lysozyme to SBA-15 is shown to increase their biocatalytic activities under some solution conditions, compared to the activities of the same enzymes free in the same solutions. For both enzymes, the protective effects were strongest in pH values where the enzyme is strongly electrostatically attracted to the silica surface. The different buffer salts used, acetate and phosphate, were not found to significantly affect enzyme leaching or activity. Immobilised myoglobin is also found to be protected from digestion by the protease pepsin. For the enzyme trypsin, discussed in Chapter 7, the relationship between electrostatic attraction and improved activity was inconclusive. Pore size was shown to significantly affect the activity of only the smallest enzyme, lysozyme. These chapters demonstrate that electrostatic attraction between an enzyme and the silica pore has a greater influence on the immobilised enzyme's activity than pore size, in the ranges of parameters tested.

In summary, this thesis would recommend the following prioritisations for enzyme immobilisation onto porous materials by physical adsorption: strong electrostatic attraction between enzyme and host material, followed by pore size just exceeding the diameter of the enzyme. As this thesis has demonstrated, however, the effectiveness of this approach cannot be guaranteed. In the experiments presented, pore size was found to have a greater effect on protein adsorption, i.e. biocatalyst preparation, than on its use in catalysis. Hopefully, this information can help direct future screenings of enzyme immobilisation materials for biochemical reactors, making the process more efficient. These insights help us to understand which microenvironments are best for protecting and enhancing enzyme activity under unfavourable conditions, but there are many questions that remain unanswered.

## **8.2 Further studies**

### **8.2.1 Continuations of presented studies**

There are several extensions to the experiments presented in this thesis that would more clearly answer outstanding inquiries, which were discussed in their respective chapters' conclusions.

The experiments reported in Chapter 3 did not indicate that electrostatic attraction affects equilibrium protein adsorption onto SBA-15. However, electrostatic interactions are shown to play a role in equilibrium protein adsorption in other literature.<sup>113,118,121</sup> By performing similar adsorption experiments to those reported in Chapter 3 in solutions with different pH values, the importance of electrostatic attraction to the adsorption of these proteins at equilibrium could be clarified. In Chapter 4, the observations presented contradict the hypothesis that electrostatic attraction increases a protein's diffusivity in a pore. However, this refutation is severely limited by how few systems on which the hypothesis has been tested. By varying the pH and ionic strength of the adsorption kinetics experiments on myoglobin and lysozyme, and by performing similar experiments on other proteins, this claim could be strengthened.

The experiments involving pepsin protection of immobilised myoglobin in Chapter 5 did not indicate whether this protection is given by virtue of a size exclusion effect, or by the confinement and stabilisation of myoglobin. Investigating the effect of SBA-15 pore size on myoglobin's protection from pepsin may clarify how much the size-exclusion effect contributes to myoglobin's protection. Further experiments involving other enzymes protected from other proteases by SBA-15, such as of lysozyme being protected from proteolysis by trypsin, would also elucidate this effect. Also in Chapter 5, the pH protection experiments of immobilised myoglobin indicate that SBA-15's pore diameter did not play as significant a role in pH protection. It is possible that the range of pore diameters investigated in these experiments was too small; a larger range of pore diameters could probe the effect of pore size on immobilised enzyme further.

In the context of the research question of this thesis, the pH protection experiments involving trypsin presented in Chapter 7 was largely inconclusive. At low pH values, neither free nor immobilised trypsin had appreciable activity over a blank baseline using the current assay method, which restricted comparison of immobilised trypsin's activities under different levels of electrostatic attraction. Even at higher pH values, the trypsin activity assay was not sufficient to differentiate activity values of the immobilised samples at different pore sizes and pH values. The hydrolase assay used in these experiments should be further developed.

These extensions of these sets of experiments would clarify several questions posed in this thesis concerning the relative importance of steric confinement and electrostatic attraction to the adsorption of enzymes to mesoporous silica and their subsequent activity. There are also larger studies which would further explore the general premise of chaperonins as inspiration for the design of enzyme immobilisation systems, which will be introduced in the following sections.

### **8.2.2 Thermal stability of proteins immobilised to mesoporous silica SBA-15**

This thesis has demonstrated how SBA-15 can protect immobilised enzymes from unfavourable pH and the presence of protease. A more common issue in industrial biocatalysis is the need to protect enzymes from high temperatures. In fact, measuring an enzyme's thermal stability is an integral part of assessing its performance. This measurement is often carried out using differential scanning calorimetry (DSC).

DSC measures the amount of heat required to increase a sample's temperature as a function of the sample's temperature. Samples with fixed heat capacities would be expected to have a linear correlation between heat flow and temperature. However, when a material undergoes a phase transition, its heat capacity will change significantly, raising or lowering depending on if the transition is endothermic or exothermic. For samples containing protein, thermal denaturation can be seen as an endothermic peak on a DSC curve, and the temperature at which this occurs is the protein's melting point,  $T_m$ .<sup>186</sup> By

comparing the melting points of free enzymes and those immobilised to SBA-15, we can learn more about how the material affects enzyme stability. The accuracy of this technique should not be affected by the presence of silica in the sample, as the melting point of protein will be far less than the glass transition temperature of silica.

### **8.2.3 Co-immobilisation of enzymes to mesoporous silica SBA-15 for tandem reactions**

A future research direction is to investigate the effectiveness of co-immobilised enzymes, also known as tandem reactors, on SBA-15. Tandem reactors contain two or more enzymes immobilised on the same material which catalyse cascade reactions, where the product released from one enzyme is the substrate for another enzyme. The advantage of tandem reactors is that the substrate can reach the second enzyme quickly, avoiding diffusion limitations within the porous support.<sup>30</sup> Many candidate enzymes exist for use in tandem reactors: alcohol dehydrogenases can be paired with ketoreductases to produce enantiomerically-enriched alcohols; transaminases and amino acid dehydrogenases can couple to produce optically active amino acids; and aldolases and hydroxynitrile lyases can work together for carbon-carbon bond formation.<sup>187,188</sup>

A prime candidate enzyme cascade for these experiments is the pairing of transketolase and transaminase to produce chiral amino alcohols from non-chiral substrates. Transketolase catalyses asymmetric carbon-carbon bond formation and transaminase catalyses amine group additions. This cascade is useful to the pharmaceutical industry, as it can produce a single diastereomer of 2-amino-1,3,4-butanetriol (ABT) which is used to build protease inhibitors.<sup>189,190</sup> To create a tandem reactor in SBA-15, the parameters identified in this thesis must be integrated into experiments. SBA-15 with adequate pore diameter to accommodate each of the enzymes will need to be synthesised. Then, it must be determined if the cascade reaction takes place adequately in a pH intermediate to the isoelectric points of the enzymes and the silica.

#### **8.2.4 Chaperonin-inspired refolding of denatured enzymes**

The inspiration for this thesis is the GroEL/ES chaperonin complex, which helps newly synthesised proteins fold into their correct three-dimensional structures. It is an interesting research question to consider if our inorganic chaperonin analogue, SBA-15, is capable of such behaviour in vitro. Like chaperonins, SBA-15 supplies precise steric confinement to immobilised enzymes, as well as an electrostatically-favourable and hydrophilic microenvironment.

To investigate this idea, enzymes such as myoglobin, lysozyme, and trypsin could be denatured by high temperature or acid. Then, SBA-15 would be introduced to the solution. The amount of unfolded enzyme adsorbed to SBA-15 would be quantified, and the immobilised enzymes' activities tested. These enzyme activities would be compared to those of still-unfolded enzyme, as controls.

It is unlikely that adsorbing unfolded enzyme to SBA-15 would completely recover their activity. This is especially true in the case of myoglobin, which will often lose its haem prosthetic group upon unfolding. However, if even some activity is regained, it would be a completely novel finding. Further, if any such effect is affected by the SBA-15 pore size, or by the solution pH at which the unfolded enzymes is adsorbed, it would help to clarify the relative importance of SBA-15's controllable pore size and negatively-charged surface to its effectiveness as an immobilisation material.

## References

1. Pellis, A., Cantone, S., Ebert, C. & Gardossi, L. Evolving biocatalysis to meet bioeconomy challenges and opportunities. *N. Biotechnol.* **40**, 154–169 (2018).
2. Nestl, B. M., Nebel, B. A. & Hauer, B. Recent progress in industrial biocatalysis. *Curr. Opin. Chem. Biol.* **15**, 187–193 (2011).
3. Choi, J.-M. M., Han, S.-S. S. & Kim, H.-S. S. Industrial applications of enzyme biocatalysis: Current status and future aspects. *Biotechnol. Adv.* **33**, 1443–1454 (2015).
4. Panke, S. & Wubbolts, M. Advances in biocatalytic synthesis of pharmaceutical intermediates. *Curr. Opin. Chem. Biol.* **9**, 188–194 (2005).
5. Nestl, B. M., Hammer, S. C., Nebel, B. A. & Hauer, B. New generation of biocatalysts for organic synthesis. *Angew. Chemie - Int. Ed.* **53**, 3070–3095 (2014).
6. Bommarius, A. S., Schwarm, M. & Drauz, K. Biocatalysis to amino acid-based chiral pharmaceuticals - Examples and perspectives. *J. Mol. Catal. - B Enzym.* **5**, 1–11 (1998).
7. Pollard, D. J. & Woodley, J. M. Biocatalysis for pharmaceutical intermediates: the future is now. *Trends Biotechnol.* **25**, 66–73 (2007).
8. Huisman, G. W. & Collier, S. J. On the development of new biocatalytic processes for practical pharmaceutical synthesis. *Curr. Opin. Chem. Biol.* **17**, 284–292 (2013).
9. Patel, R. N. Biocatalytic synthesis of intermediates for the synthesis of chiral drug substances. *Curr. Opin. Biotechnol.* **12**, 587–604 (2001).
10. Patel, R. N. Microbial/enzymatic synthesis of chiral intermediates for pharmaceuticals. *Enzyme Microb. Technol.* **31**, 804–826 (2002).
11. Patel, R. N. Synthesis of chiral pharmaceutical intermediates by biocatalysis. *Coord. Chem. Rev.* **252**, 659–701 (2008).

12. Anastas, P. T. & Warner, J. C. *Green Chemistry: Theory and Practice*. (Oxford University Press, 1998).
13. Tao, J. & Xu, J. H. Biocatalysis in development of green pharmaceutical processes. *Curr. Opin. Chem. Biol.* **13**, 43–50 (2009).
14. Woodley, J. M. New opportunities for biocatalysis: making pharmaceutical processes greener. *Trends Biotechnol.* **26**, 321–327 (2008).
15. Wohlgemuth, R. Asymmetric biocatalysis with microbial enzymes and cells. *Curr. Opin. Microbiol.* **13**, 283–292 (2010).
16. Wohlgemuth, R. Biocatalysis-key to sustainable industrial chemistry. *Curr. Opin. Biotechnol.* **21**, 713–724 (2010).
17. Pratt, C. W., Voet, D. & Voet, J. G. *Fundamentals of Biochemistry*. (Wiley, 1998).
18. Anfinsen, C. B. Principles that Govern the Folding of Protein Chains. *Science (80-. )*. **181**, 223–230 (1973).
19. Koshland, D. E. The Key–Lock Theory and the Induced Fit Theory. *Angew. Chemie Int. Ed. English* **33**, 2375–2378 (1995).
20. Fischer, E. Einfluss der Configuration auf die Wirkung der Enzyme. *Ber Dtsch Chem Ges* **27**, 2984–2993 (1894).
21. Koshland, D. E. Application of a Theory of Enzyme Specificity to Protein Synthesis. *Proc. Natl. Acad. Sci.* **44**, 98–104 (1958).
22. Pace, C. N. Measuring and increasing protein stability. *Trends Biochem. Sci.* **8**, 93–98 (1990).
23. Hofmeister, F. Zur Lehre von der Wirkung der Salze. *Arch. Exp. Pathol. Pharmacol.* **24**, 247–260 (1888).
24. Sarmiento, F., Peralta, R. & Blamey, J. M. Cold and Hot Extremozymes: Industrial Relevance and Current Trends. *Front. Bioeng. Biotechnol.* **3**, (2015).

25. Brady, D. & Jordaan, J. Advances in enzyme immobilisation. *Biotechnol. Lett.* **31**, 1639–1650 (2009).
26. Hanefeld, U., Gardossi, L. & Magner, E. Understanding enzyme immobilisation. *Chem. Soc. Rev.* **38**, 453–468 (2009).
27. Sheldon, R. A. & Van Pelt, S. Enzyme immobilisation in biocatalysis: why, what and how. *Chem. Soc. Rev.* **42**, 6223–6235 (2013).
28. Hanefeld, U., Cao, L. & Magner, E. Enzyme immobilisation: fundamentals and application. *Chem. Soc. Rev.* **42**, 6211 (2013).
29. Liese, A. & Hilterhaus, L. Evaluation of immobilized enzymes for industrial applications. *Chem. Soc. Rev.* **42**, 6236–49 (2013).
30. Tran, D. N. & Balkus, K. J. Perspective of recent progress in immobilization of enzymes. *ACS Catal.* **1**, 956–968 (2011).
31. Hartmann, M. & Jung, D. Biocatalysis with enzymes immobilized on mesoporous hosts: the status quo and future trends. *J. Mater. Chem.* **20**, 844 (2010).
32. Mohamad, N. R., Marzuki, N. H. C., Buang, N. A., Huyop, F. & Wahab, R. A. An overview of technologies for immobilization of enzymes and surface analysis techniques for immobilized enzymes. *Biotechnol. Biotechnol. Equip.* **29**, 205–220 (2015).
33. Sheldon, R. A. Enzyme immobilization: The quest for optimum performance. *Adv. Synth. Catal.* **349**, 1289–1307 (2007).
34. Tischer, W. & Kasche, V. Immobilized enzymes: Crystals or carriers? *Trends Biotechnol.* **17**, 326–335 (1999).
35. Cao, L., van Langen, L. & Sheldon, R. A. Immobilised enzymes: Carrier-bound or carrier-free? *Curr. Opin. Biotechnol.* **14**, 387–394 (2003).
36. Woodley, J. M. Protein engineering of enzymes for process applications. *Curr. Opin. Chem. Biol.* **17**, 310–316 (2013).

37. Denard, C. A., Ren, H. & Zhao, H. Improving and repurposing biocatalysts via directed evolution. *Curr. Opin. Chem. Biol.* **25**, 55–64 (2015).
38. Porter, J. L., Rusli, R. A. & Ollis, D. L. Directed Evolution of Enzymes for Industrial Biocatalysis. *ChemBioChem* **17**, 197–203 (2016).
39. Wang, M., Si, T. & Zhao, H. Biocatalyst development by directed evolution. *Bioresour. Technol.* **115**, 117–125 (2012).
40. Bryjak, J. & Kolarz, B. N. Immobilisation of trypsin on acrylic copolymers. *Process Biochem.* **33**, 409–417 (1998).
41. Katchalski-Katzir, E. & Kraemer, D. M. Eupergit® C, a carrier for immobilization of enzymes of industrial potential. *J. Mol. Catal. - B Enzym.* **10**, 157–176 (2000).
42. Homaei, A. A., Sariri, R., Vianello, F. & Stevanato, R. Enzyme immobilization: An update. *J. Chem. Biol.* **6**, 185–205 (2013).
43. Klouda, L. & Mikos, A. G. Thermoresponsive hydrogels in biomedical applications -a review. *European J. Pharm. Biopharm.* **68**, 34–45 (2008).
44. Klis, M., Karbarz, M., Stojek, Z., Rogalski, J. & Bilewicz, R. Thermoresponsive Poly ( N -isopropylacrylamide ) Gel for Immobilization of Laccase on Indium Tin Oxide Electrodes. *J. Phys. Chem. B* **113**, 6062–6067 (2009).
45. Krajewska, B. Application of chitin- and chitosan-based materials for enzyme immobilizations: A review. *Enzyme Microb. Technol.* **35**, 126–139 (2004).
46. Mateo, C., Palomo, J. M., Fuentes, M., Betancor, L., Grazu, V., López-Gallego, F., Pessela, B. C. C., Hidalgo, A., Fernández-Lorente, G., Fernández-Lafuente, R. & Guisán, J. M. Glyoxyl agarose: A fully inert and hydrophilic support for immobilization and high stabilization of proteins. *Enzyme Microb. Technol.* **39**, 274–280 (2006).
47. Wu, S. C. & Lia, Y. K. Application of bacterial cellulose pellets in enzyme immobilization. *J. Mol. Catal. B Enzym.* **54**, 103–108 (2008).

48. de Alteriis, E., Parascandola, P., Pecorella, M. A. & Scardi, V. Effect of gelatin-immobilization on the catalytic activity of enzymes and microbial cells. *Biotechnol. Tech.* **2**, 205–210 (1988).
49. Corma, A., Fornés, V., Jordá, J. L., Rey, F., Fernandez-Lafuente, R., Guisan, J. M. & Mateo, C. Electrostatic and covalent immobilisation of enzymes on ITQ-6 delaminated zeolitic materials. *Chem. Commun.* 419–420 (2001). doi:10.1039/b009232k
50. Gonçalves, A. P. V., Lopes, J. M., Lemos, F., Ramôa Ribeiro, F., Prazeres, D. M. F., Cabrai, J. M. S. & Aires-Barros, M. R. Zeolites as supports for enzymatic hydrolysis reactions. Comparative study of several zeolites. *J. Mol. Catal. B Enzym.* **1**, 53–60 (1996).
51. Serralha, F. N., Lopes, J. M., Lemos, F., Prazeres, D. M. F., Aires-Barros, M. R., Cabral, J. M. S. & Ramôa Ribeiro, F. Zeolites as supports for an enzymatic alcoholysis reaction. *J. Mol. Catal. - B Enzym.* **4**, 303–311 (1998).
52. Kovalenko, G. A., Komova, O. V., Simakov, A. V., Khomov, V. V. & Rudina, N. A. Macrostructured carbonized ceramics as adsorbents for immobilization of glucoamylase. *J. Mol. Catal. A Chem.* **182**, 73–80 (2002).
53. Meunier, S. M. & Legge, R. L. Evaluation of diatomaceous earth as a support for sol-gel immobilized lipase for transesterification. *J. Mol. Catal. B Enzym.* **62**, 53–57 (2010).
54. Feng, W. & Ji, P. Enzymes immobilized on carbon nanotubes. *Biotechnol. Adv.* **29**, 889–895 (2011).
55. Rouquerol, J., Avnir, D., Fairbridge, C. W. W., Everett, D. H. H., Haynes, J. H. M., Pernicone, N., Ramsay, J. D. F. D. F., Sing, K. S. W. S. W. & Unger, K. K. K. Recommendations for the characterization of porous solids. *Pure Appl. Chem.* **66**, 1739–1758 (1994).
56. Diaz, J. F., Balkus Jr., K. J. & Jr, K. J. B. Enzyme immobilization in MCM-4 1 molecular sieve. *J. Mol. Catal. B Enzym.* **77**, 115–126 (1996).

57. Blanco, R. M., Terreros, P., Fernández-Pérez, M., Otero, C. & Díaz-González, G. Functionalization of mesoporous silica for lipase immobilization: Characterization of the support and the catalysts. *J. Mol. Catal. B Enzym.* **30**, 83–93 (2004).
58. Qhobosheane, M., Santra, S., Zhang, P. & Tan, W. Biochemically functionalized silica nanoparticles. *Analyst* **126**, 1274–1278 (2001).
59. Mateo, C., Palomo, J. M., Fernandez-Lorente, G., Guisan, J. M. & Fernandez-Lafuente, R. Improvement of enzyme activity, stability and selectivity via immobilization techniques. *Enzyme Microb. Technol.* **40**, 1451–1463 (2007).
60. Rodrigues, R. C., Ortiz, C., Berenguer-Murcia, Á., Torres, R. & Fernández-Lafuente, R. Modifying enzyme activity and selectivity by immobilization. *Chem. Soc. Rev.* **42**, 6290–6307 (2013).
61. Cantone, S., Ferrario, V., Corici, L., Ebert, C., Fattor, D., Spizzo, P. & Gardossi, L. Efficient immobilisation of industrial biocatalysts: criteria and constraints for the selection of organic polymeric carriers and immobilisation methods. *Chem. Soc. Rev.* **42**, 6262–76 (2013).
62. Cao, L. *Carrier-bound Immobilized Enzymes: Principles, Application and Design*. (Wiley-VCH, 2006).
63. Rabe, M., Verdes, D. & Seeger, S. Understanding protein adsorption phenomena at solid surfaces. *Adv. Colloid Interface Sci.* **162**, 87–106 (2011).
64. Hook, F., Rodahl, M., Kasemo, B. & Brzezinski, P. Structural changes in hemoglobin during adsorption to solid surfaces: Effects of pH, ionic strength, and ligand binding. *Proc. Natl. Acad. Sci. U. S. A.* **95**, 12271–12276 (1998).
65. Demanèche, S., Chapel, J. P., Monrozier, L. J. & Quiquampoix, H. Dissimilar pH-dependent adsorption features of bovine serum albumin and  $\alpha$ -chymotrypsin on mica probed by AFM. *Colloids Surfaces B Biointerfaces* **70**, 226–231 (2009).

66. Dér, A., Kelemen, L., Fábrián, L., Taneva, S. G., Fodor, E., Páli, T., Cupane, A., Cacace, M. G. & Ramsden, J. J. Interfacial Water Structure Controls Protein Conformation. *J. Phys. Chem. B* **111**, 5344–5350 (2007).
67. Andrade, J. D., Hlady, V. & Wei, A. P. Adsorption of complex proteins at interfaces. *Pure Appl. Chem.* **64**, 1777–1781 (1992).
68. Norde, W. My voyage of discovery to proteins in flatland ...and beyond. *Colloids Surfaces B Biointerfaces* **61**, 1–9 (2008).
69. Asthagiri, D. & Lenhoff, A. M. Influence of Structural Details in Modeling Electrostatically Driven Protein Adsorption. *Langmuir* **13**, 6761–6768 (1997).
70. De Vos, W. M., Leermakers, F. A. M., De Keizer, A., Stuart, M. A. C. & Kleijn, J. M. Field theoretical analysis of driving forces for the uptake of proteins by like-charged polyelectrolyte brushes: Effects of charge regulation and patchiness. *Langmuir* **26**, 249–259 (2010).
71. Sethuraman, A. & Belfort, G. Protein structural perturbation and aggregation on homogeneous surfaces. *Biophys. J.* **88**, 1322–1333 (2005).
72. Santore, M. M. & Wertz, C. F. Protein spreading kinetics at liquid-solid interfaces via an adsorption probe method. *Langmuir* **21**, 10172–10178 (2005).
73. Marsh, R. J., Jones, R. A. L. & Sferrazza, M. Heat-treatment and displacement of adsorbed lysozyme layers. *J. Colloid Interface Sci.* **37**, 789–792 (2004).
74. Zoungrana, T., Findenegg, G. H. & Norde, W. Structure, stability, and activity of adsorbed enzymes. *J. Colloid Interface Sci.* **190**, 437–448 (1997).
75. Vertegel, A. A., Siegel, R. W. & Dordick, J. S. Silica nanoparticle size influences the structure and enzymatic activity of adsorbed lysozyme. *Langmuir* **20**, 6800–6807 (2004).

76. Lord, M. S., Foss, M. & Besenbacher, F. Influence of nanoscale surface topography on protein adsorption and cellular response. *Nano Today* **5**, 66–78 (2010).
77. Sang, L.-C. & Coppens, M.-O. Effects of surface curvature and surface chemistry on the structure and activity of proteins adsorbed in nanopores. *Phys. Chem. Chem. Phys.* **13**, 6689 (2011).
78. Hladílková, J., Callisen, T. H. & Lund, M. Lateral Protein-Protein Interactions at Hydrophobic and Charged Surfaces as a Function of pH and Salt Concentration. *J. Phys. Chem. B* **120**, 3303–3310 (2016).
79. Ramsden, J. J. Puzzles and paradoxes in protein adsorption. *Chem. Soc. Rev.* **24**, 73 (1995).
80. Langmuir, I. The adsorption of gases on plane surfaces of glass, mica and platinum. *J. Am. Chem. Soc.* **40**, 1361–1403 (1918).
81. Schaaf, P. & Talbot, J. Surface exclusion effects in adsorption processes. *J. Chem. Phys.* **91**, 4401–4409 (1989).
82. Adamczyk, Z. & Weroński, P. Random sequential adsorption of spheroidal particles: Kinetics and jamming limit. *J. Chem. Phys.* **105**, 5562–5573 (1996).
83. Koutsopoulos, S., Patzschy, K., Bosker, W. T. E. & Norde, W. Adsorption of trypsin on hydrophilic and hydrophobic surfaces. *Langmuir* **23**, 2000–2006 (2007).
84. Kondo, A. & Mihara, J. Comparison of Adsorption and Conformation of Hemoglobin and Myoglobin on Various Inorganic Ultrafine Particles. *J. Colloid Interface Sci.* **177**, 214–221 (1996).
85. Lundqvist, M., Sethson, I. & Jonsson, B. H. Protein adsorption onto silica nanoparticles: Conformational changes depend on the particles' curvature and the protein stability. *Langmuir* **20**, 10639–10647 (2004).

86. Bharti, B., Meissner, J. & Findenegg, G. H. Aggregation of silica nanoparticles directed by adsorption of lysozyme. *Langmuir* **27**, 9823–9833 (2011).
87. Levinthal, C. Are there pathways to protein folding? *J. Chim. Phys.* **65**, 44–45 (1968).
88. Saibil, H. Chaperone machines for protein folding, unfolding and disaggregation. *Nat. Rev. Mol. Cell Biol.* **14**, 630–642 (2013).
89. Braig, K., Otwinowski, Z., Hegde, R., Boisvert, D. C., Joachimiak, A., Horwich, A. L. & Sigler, P. B. The crystal structure of the bacterial chaperonin GroEL at 2.8 Å. *Nature* **371**, 578–586 (1994).
90. Hartl, F. U., Bracher, A. & Hayer-Hartl, M. Molecular chaperones in protein folding and proteostasis. *Nature* **475**, 324–332 (2011).
91. Hayer-Hartl, M., Bracher, A. & Hartl, F. U. The GroEL-GroES Chaperonin Machine: A Nano-Cage for Protein Folding. *Trends Biochem. Sci.* **41**, 62–76 (2016).
92. Martin, J., Mayhew, M., Langer, T. & Hartl, F. U. The reaction cycle of GroEL and GroES in chaperonin-assisted protein folding. *Nature* **366**, 228–233 (1993).
93. Martin, J., Langer, T., Boteva, R., Schramel, A., Horwich, A. L. & Hartl, F.-U. U. Chaperonin-mediated protein folding at the surface of groEL through a 'molten globule'-like intermediate. *Nature* **352**, 36–42 (1991).
94. Mayhew, M., da Silva, A. C. R. A. C. R., Martin, J. J., Erdjument-Bromage, H., Tempst, P. & Hartl, F. U. Protein folding in the central cavity of the GroEL-GroES chaperonin complex. *Nature* **379**, 420–426 (1996).
95. Sigler, P. B., Xu, Z., Rye, H. S., Burston, S. G., Fenton, W. A. & Horwich, A. L. Structure and Function in GroEL-Mediated Protein Folding. *Annu. Rev. Biochem.* **67**, 581–608 (1998).

96. Marchenkov, V. V. & Semisotnov, G. V. GroEL-assisted protein folding: Does it occur within the chaperonin inner cavity? *Int. J. Mol. Sci.* **10**, 2066–2083 (2009).
97. Clare, D. K., Vasishtan, D., Stagg, S., Quispe, J., Farr, G. W., Topf, M., Horwich, A. L. & Saibil, H. R. ATP-triggered conformational changes delineate substrate-binding and -folding mechanics of the GroEL chaperonin. *Cell* **149**, 113–123 (2012).
98. Saibil, H. R., Fenton, W. A., Clare, D. K. & Horwich, A. L. Structure and allostery of the chaperonin GroEL. *J. Mol. Biol.* **425**, 1476–1487 (2013).
99. Thommes, M., Kaneko, K., Neimark, A. V., Olivier, J. P., Rodriguez-Reinoso, F., Rouquerol, J. & Sing, K. S. W. W. Physisorption of gases, with special reference to the evaluation of surface area and pore size distribution (IUPAC Technical Report). *Pure Appl. Chem.* **87**, 1051–1069 (2015).
100. Zhao, D., Feng, J., Huo, Q., Melosh, N., Fredrickson, G., Chmelka, B. & Stucky, G. Triblock Copolymer Syntheses of Mesoporous Silica with Periodic 50 to 300 Angstrom Pores. *Science (80-. )*. **279**, 548–552 (1998).
101. Persello, J. & Papirer, E. *Adsorption on Silica Surfaces*. (CRC Press, 2000).
102. Hartmann, M. Ordered mesoporous materials for bioadsorption and biocatalysis. *Chem. Mater.* **17**, 4577–4593 (2005).
103. Hudson, S. P., Cooney, J. C., Magner, E., White, S., Goradia, D., Essa, H., Liu, B., Qiao, L., Liu, Y., Cooney, J. C., Hodnett, B. K. & Magner, E. Proteins in mesoporous silicates. *Angew. Chemie Int. Ed.* **47**, 49–60 (2008).
104. Magner, E. Immobilisation of enzymes on mesoporous silicate materials. *Chem. Soc. Rev.* **42**, 6213–22 (2013).
105. Hartmann, M. & Kostrov, X. Immobilization of enzymes on porous silicas-- benefits and challenges. *Chem. Soc. Rev.* **42**, 6277–89 (2013).

106. Zhou, Z. & Hartmann, M. Progress in enzyme immobilization in ordered mesoporous materials and related applications. *Chem. Soc. Rev.* **42**, 3894 (2013).
107. Deere, J., Magner, E., Wall, J. G. & Hodnett, B. K. Adsorption and activity of cytochrome c on mesoporous silicates. *Chem. Commun.* 465–465 (2001). doi:10.1039/b009478l
108. Deere, J., Magner, E., Wall, J. G. & Hodnett, B. K. Adsorption and activity of proteins onto mesoporous silica. *Catal. Letters* **85**, 19–23 (2003).
109. Katiyar, A., Yadav, S., Smirniotis, P. G. & Pinto, N. G. Synthesis of ordered large pore SBA-15 spherical particles for adsorption of biomolecules. *J. Chromatogr. A* **1122**, 13–20 (2006).
110. Yiu, H. H. P., Wright, P. A. & Botting, N. P. Enzyme immobilization using siliceous mesoporous molecular sieves. *Microporous Mesoporous Mater.* **44–45**, 763–768 (2001).
111. Goradia, D., Cooney, J., Hodnett, B. K. & Magner, E. The adsorption characteristics, activity and stability of trypsin onto mesoporous silicates. *J. Mol. Catal. B Enzym.* **32**, 231–239 (2005).
112. Miyahara, M., Vinu, A., Hossain, K. Z., Nakanishi, T. & Ariga, K. Adsorption study of heme proteins on SBA-15 mesoporous silica with pore-filling models. *Thin Solid Films* **499**, 13–18 (2006).
113. Miyahara, M., Vinu, A. & Ariga, K. Adsorption myoglobin over mesoporous silica molecular sieves: Pore size effect and pore-filling model. *Mater. Sci. Eng. C* **27**, 232–236 (2007).
114. Sang, L.-C., Vinu, A. & Coppens, M.-O. General description of the adsorption of proteins at their iso-electric point in nanoporous materials. *Langmuir* **27**, 13828–13837 (2011).
115. Deere, J., Magner, E., Wall, J. G. & Hodnett, B. K. Mechanistic and structural features of protein adsorption onto mesoporous silicates. *J. Phys. Chem. B* **106**, 7340–7347 (2002).

116. Hudson, S., Magner, E., Cooney, J. & Hodnett, B. K. Methodology for the immobilization of enzymes onto mesoporous materials. *J. Phys. Chem. B* **109**, 19496–19506 (2005).
117. Katiyar, A., Ji, L., Smirniotis, P. & Pinto, N. G. Protein adsorption on the mesoporous molecular sieve silicate SBA-15: Effects of pH and pore size. *J. Chromatogr. A* **1069**, 119–126 (2005).
118. Essa, H., Magner, E., Cooney, J. & Hodnett, B. K. Influence of pH and ionic strength on the adsorption, leaching and activity of myoglobin immobilized onto ordered mesoporous silicates. *J. Mol. Catal. B Enzym.* **49**, 61–68 (2007).
119. Vinu, A., Murugaesan, V., Tangermann, O., Hartmann, M., Murugesan, V., Tangermann, O. & Hartmann, M. Adsorption of cytochrome c on mesoporous molecular sieves: Influence of pH, pore diameter, and aluminum incorporation. *Chem. Mater.* **16**, 3056–3065 (2004).
120. Vinu, A., Murugesan, V. & Hartmann, M. Adsorption of Lysozyme over Mesoporous Molecular Sieves MCM-41 and SBA-15: Influence of pH and Aluminum Incorporation. *J. Phys. Chem. B* **108**, 7323–7330 (2004).
121. Sang, L. Systematic Study of Proteins Confined in Nanoporous SBA-15 with a Controlled Pore Size. (2010).
122. Steri, D., Monduzzi, M. & Salis, A. Ionic strength affects lysozyme adsorption and release from SBA-15 mesoporous silica. *Microporous Mesoporous Mater.* **170**, 164–172 (2013).
123. Bhattacharyya, M. S., Hiwale, P., Piras, M., Medda, L., Steri, D., Piludu, M., Salis, A. & Monduzzi, M. Lysozyme adsorption and release from ordered mesoporous materials. *J. Phys. Chem. C* **114**, 19928–19934 (2010).
124. Goradia, D., Cooney, J., Hodnett, B. K. & Magner, E. Characteristics of a mesoporous silicate immobilized trypsin bioreactor in organic media. *Biotechnol. Prog.* **22**, 1125–1131 (2006).

125. Jung, D., Streb, C. & Hartmann, M. Oxidation of indole using chloroperoxidase and glucose oxidase immobilized on SBA-15 as tandem biocatalyst. *Microporous Mesoporous Mater.* **113**, 523–529 (2008).
126. Jung, D. & Hartmann, M. Oxidation of indole with CPO and GOx immobilized on mesoporous molecular sieves. *Catal. Today* **157**, 378–383 (2010).
127. Yiu, H. H. P. P., Wright, P. A. & Botting, N. P. Enzyme immobilisation using SBA-15 mesoporous molecular sieves with functionalised surfaces. *J. Mol. Catal. - B Enzym.* **15**, 81–92 (2001).
128. Jung, D., Streb, C. & Hartmann, M. Covalent anchoring of chloroperoxidase and glucose oxidase on the mesoporous Molecular Sieve SBA-15. *Int. J. Mol. Sci.* **11**, 762–778 (2010).
129. Zhou, Z., Inayat, A., Schwieger, W. & Hartmann, M. Improved activity and stability of lipase immobilized in cage-like large pore mesoporous organosilicas. *Microporous Mesoporous Mater.* **154**, 133–141 (2012).
130. Ikemoto, H., Chi, Q. & Ulstrup, J. Stability and catalytic kinetics of horseradish peroxidase confined in nanoporous SBA-15. *J. Phys. Chem. C* **114**, 16174–16180 (2010).
131. Itoh, T., Ishii, R., Ebina, T., Hanaoka, T., Fukushima, Y. & Mizukami, F. Encapsulation of myoglobin with a mesoporous silicate results in new capabilities. *Bioconjug. Chem.* **17**, 236–240 (2006).
132. Hudson, S., Cooney, J., Hodnett, B. K. & Magner, E. Chloroperoxidase on periodic mesoporous organosilanes: Immobilization and reuse. *Chem. Mater.* **19**, 2049–2055 (2007).
133. Kendrew, J., Dickerson, R. E., Strandberg, B. E., Hart, R. G., Davies, D. R., Phillips, D. C. & Shore, V. C. Structure of Myoglobin: A Three-Dimensional Fourier Synthesis at 2 Å Resolution. *Nature* **185**, 422–427 (1960).

134. Sielecki, A. R., Fedorov, A. A., Boodhoo, A., Andreeva, N. S. & James, M. N. G. Molecular and crystal structures of monoclinic porcine pepsin refined at 1.8Å resolution. *J. Mol. Biol.* **214**, 143–170 (1990).
135. Blake, C. C. F., Johnson, L. N., Mair, G. A., North, A. C. T., Phillips, D. C. & Sarma, V. R. Crystallographic studies of the activity of hen egg-white lysozyme. *Proc. R. Soc. Lond. B. Biol. Sci.* **167**, 378–388 (1967).
136. Liebschner, D., Dauter, M., Brzuszkiewicz, A. & Dauter, Z. On the reproducibility of protein crystal structures: Five atomic resolution structures of trypsin. *Acta Crystallogr. Sect. D Biol. Crystallogr.* **69**, 1447–1462 (2013).
137. Carlsen, C. U., Skovgaard, I. M. & Skibsted, L. H. Pseudoperoxidase activity of myoglobin: Kinetics and mechanism of the peroxidase cycle of myoglobin with H<sub>2</sub>O<sub>2</sub> and 2,2-azino-bis(3-ethylbenzthiazoline-6-sulfonate) as substrates. *J. Agric. Food Chem.* **51**, 5815–5823 (2003).
138. Wilkins, D. K., Grimshaw, S. B., Receveur, V., Dobson, C. M., Jones, J. A. & Smith, L. J. Hydrodynamic radii of native and denatured proteins measured by pulse field gradient NMR techniques. *Biochemistry* **38**, 16424–16431 (1999).
139. Sharon, N. The chemical structure of lysozyme substrates and their cleavage by the enzyme\*! *Biol. Sci.* **167**, 402–415 (1967).
140. Polgár, L. The catalytic triad of serine peptidases. *Cell. Mol. Life Sci.* **62**, 2161–2172 (2005).
141. Walsh, K. A. Trypsinogens and trypsins of various species. *Methods Enzymol.* **19**, 41–63 (1970).
142. Iler, R. K. *Chemistry of Silica - Solubility, Polymerization, Colloid and Surface Properties and Biochemistry.* (John Wiley & Sons, 1979).

143. Alexandridis, P., Holzwarth, J. F. & Hatton, T. A. Micellization of Poly(ethylene oxide)-Poly(propylene oxide)-Poly(ethylene oxide) Triblock Copolymers in Aqueous Solutions: Thermodynamics of Copolymer Association. *Macromolecules* **27**, 2414–2425 (1994).
144. Ruthstein, S., Schmidt, J., Kesselman, E., Talmon, Y. & Goldfarb, D. Resolving intermediate solution structures during the formation of mesoporous SBA-15. *J. Am. Chem. Soc.* **128**, 3366–3374 (2006).
145. Zana, R. Micellization of amphiphiles: Selected aspects. *Colloids Surfaces A Physicochem. Eng. Asp.* **123–124**, 27–35 (1997).
146. Sayari, A., Han, B. H. & Yang, Y. Simple synthesis route to monodispersed SBA-15 silica rods. *J. Am. Chem. Soc.* **126**, 14348–14349 (2004).
147. Zhao, D., Sun, J., Li, Q., Stucky, G. D. & Barbara, S. Morphological Control of Highly Ordered Mesoporous Silica SBA-15. *Chem. Mater.* **12**, 275–279 (2000).
148. Galarneau, A., Cambon, H., Di Renzo, F. & Fajula, F. True microporosity and surface area of mesoporous SBA-15 silicas as a function of synthesis temperature. *Langmuir* **17**, 8328–8335 (2001).
149. Brunauer, S., Emmett, P. H. & Teller, E. Adsorption of Gases in Multimolecular Layers. *J. Am. Chem. Soc.* **60**, 309–319 (1938).
150. Barrett, E. P., Joyner, L. G. & Halenda, P. P. The Determination of Pore Volume and Area Distributions in Porous Substances. I. Computations from Nitrogen Isotherms. *J. Am. Chem. Soc.* **73**, 373–380 (1951).
151. Luisa Ojeda, M., Marcos Esparza, J., Campero, A., Cordero, S., Kornhauser, I. & Rojas, F. On comparing BJH and NLDFT pore-size distributions determined from N<sub>2</sub> sorption on SBA-15 substrata. *Phys. Chem. Chem. Phys.* **5**, 1859 (2003).

152. Ravikovitch, P. I., Haller, G. L. & Neimark, A. V. Density functional theory model for calculating pore size distributions: pore structure of nanoporous catalysts. *Adv. Colloid Interface Sci.* **76**, 203–226 (1998).
153. Ravikovitch, P. I. & Neimark, A. V. Characterization of micro- and mesoporosity in SBA-15 materials from adsorption data by the NLDFT method. *J. Phys. Chem. B* **105**, 6817–6823 (2001).
154. Landers, J., Gor, G. Y. & Neimark, A. V. Density functional theory methods for characterization of porous materials. *Colloids Surfaces A Physicochem. Eng. Asp.* **437**, 3–32 (2013).
155. Weidenthaler, C. Pitfalls in the characterization of nanoporous and nanosized materials. *Nanoscale* **3**, 792–810 (2011).
156. Meynen, V., Cool, P. & Vansant, E. F. Verified syntheses of mesoporous materials. *Microporous Mesoporous Mater.* **125**, 170–223 (2009).
157. Kruk, M., Jaroniec, M., Ko, C. H. & Ryoo, R. Characterization of the porous structure of SBA-15. *Chem. Mater.* **12**, 1961–1968 (2000).
158. Sang, L.-C., Vinu, A. & Coppens, M.-O. Ordered mesoporous carbon with tunable, unusually large pore size and well-controlled particle morphology. *J. Mater. Chem.* **21**, 7410 (2011).
159. Sayari, A. & Yang, Y. SBA-15 templated mesoporous carbon: New insights into the SBA-15 pore structure. *Chem. Mater.* **17**, 6108–6113 (2005).
160. Henry, W. Experiments on the quantity of gases absorbed by water, at different temperatures, and under different pressures. *Phil. Trans. R. Soc. Lond.* **93**, 29–274 (1803).
161. Freundlich, H. Über die Adsorption in Lösungen. *Zeitschrift für Phys. Chemie - Stöchiometrie und Verwandtschaftslehre* **57**, 385–470 (1907).
162. Devineau, S., Zanotti, J. M., Loupiac, C., Zargarian, L. L., Neiers, F., Pin, S. & Renault, J. P. Myoglobin on silica: A case study of the impact of adsorption on protein structure and dynamics. *Langmuir* **29**, 1–2 (2013).

163. Dubinin, M. M. Generalization Of The Theory Of Volume Filling Of Micropores To Nonhomogeneous Microporous Structures. *Carbon N. Y.* **23**, 373–380 (1985).
164. Nguyen, C. & Do, D. D. The Dubinin-Radushkevich equation and the underlying microscopic adsorption description. *Carbon N. Y.* **39**, 1327–1336 (2001).
165. Suen, S. Y. A comparison of isotherm and kinetic models for binary-solute adsorption to affinity membranes. *J. Chem. Technol. Biotechnol.* **65**, 249–257 (1996).
166. Sadana, A. Protein Adsorption and Inactivation on Surfaces. Influence of Heterogeneities. *Chem. Rev.* **92**, 1799–1818 (1992).
167. Rudzinski, W. & Plazinski, W. Theoretical description of the kinetics of solute adsorption at heterogeneous solid/solution interfaces. *Appl. Surf. Sci.* **253**, 5827–5840 (2007).
168. Qiu, H., Lv, L., Pan, B., Zhang, Q., Zhang, W. & Zhang, Q. Critical review in adsorption kinetic models. *J. Zhejiang Univ. A* **10**, 716–724 (2009).
169. Young, M. E., Carroad, P. A. & Bell, R. L. Estimation of Diffusion Coefficients of Proteins. *Biothechnology Bioeng.* **XXII**, 947–955 (1980).
170. Chen, W.-D., Dong, X.-Y. & Sun, Y. Analysis of diffusion models for protein adsorption to porous anion-exchange adsorbent. *J. Chromatogr. A* **962**, 29–40 (2002).
171. Chen, W. D., Dong, X. Y., Bai, S. & Sun, Y. Dependence of pore diffusivity of protein on adsorption density in anion-exchange adsorbent. *Biochem. Eng. J.* **14**, 45–50 (2003).
172. Einstein, A. Über die von der molekularkinetischen Theorie der Wärme geforderte Bewegung von in ruhenden Flüssigkeiten suspendierten Teilchen. *Ann. Phys.* **322**, 549–560 (1905).

173. Carlsson, N., Gustafsson, H., Thörn, C., Olsson, L., Holmberg, K. & Åkerman, B. Enzymes immobilized in mesoporous silica: A physical-chemical perspective. *Adv. Colloid Interface Sci.* **205**, 339–360 (2014).
174. Childs, B. R. E. & Bardsley, W. G. The Steady-State Kinetics of Peroxidase with 2,2'-Azino-di-(3-ethylbenzthiazoline- 6-sulphonic acid) as Chromogen. *Biochem. J.* **145**, 93–103 (1975).
175. Chantong, A. & Massoth, F. E. Restrictive diffusion in aluminas. *AIChE J.* **29**, 725–731 (1983).
176. Satterfield, C. N., Colton, C. K. & Pitcher, W. H. Restricted diffusion in liquids within fine pores. *AIChE J.* **19**, 628–635 (1973).
177. Wang, Y., Zhao, Q., Han, N., Bai, L., Li, J., Liu, J., Che, E., Hu, L., Zhang, Q., Jiang, T. & Wang, S. Mesoporous silica nanoparticles in drug delivery and biomedical applications. *Nanomedicine Nanotechnology, Biol. Med.* **11**, 313–327 (2015).
178. Siefker, J., Karande, P. & Coppens, M.-O. Packaging biological cargoes in mesoporous materials: opportunities for drug delivery. *Expert Opin. Drug Deliv.* **11**, 1781–1793 (2014).
179. Carlsen, C. U. & Skibsted, L. H. Myoglobin Species with Enhanced Prooxidative Activity Is Formed during Mild Proteolysis by Pepsin. *J. Agric. Food Chem.* **52**, 1675–1681 (2004).
180. Chen, B., Lei, C., Shin, Y. & Liu, J. Probing mechanisms for enzymatic activity enhancement of organophosphorus hydrolase in functionalized mesoporous silica. *Biochem. Biophys. Res. Commun.* **390**, 1177–1181 (2009).
181. Giussani, L., Tabacchi, G., Gianotti, E., Coluccia, S. & Fois, E. Disentangling protein-silica interactions. *Philos. Trans. R. Soc. A Math. Phys. Eng. Sci.* **370**, 1463–1477 (2012).

182. Tosaka, R., Yamamoto, H., Ohdomari, I. & Watanabe, T. Adsorption mechanism of ribosomal protein L2 onto a silica surface: A molecular dynamics simulation study. *Langmuir* **26**, 9950–9955 (2010).
183. Gomes, D. E. B., Lins, R. D., Pascutti, P. G., Lei, C. & Soares, T. A. The role of nonbonded interactions in the conformational dynamics of organophosphorous hydrolase adsorbed onto functionalized mesoporous silica surfaces. *J. Phys. Chem. B* **114**, 531–540 (2010).
184. Yang, Y. & Hamaguchi, K. Hydrolysis of 4-methylumbelliferyl N-acetylchitotrioside catalyzed by hen and turkey lysozymes. pH dependence of the kinetics constants. *J. Biochem.* **87**, 1003–1014 (1980).
185. Bergmeyer, H. U. *Methods of Enzymatic Analysis*. (Academic Press, Inc., 1974).
186. Larsericsdotter, H., Oscarsson, S. & Buijs, J. Thermodynamic analysis of lysozyme adsorbed to silica. *J. Colloid Interface Sci.* **276**, 261–268 (2004).
187. Ricca, E., Brucher, B. & Schrittwieser, J. H. Multi-enzymatic cascade reactions: Overview and perspectives. *Adv. Synth. Catal.* **353**, 2239–2262 (2011).
188. Oroz-Guinea, I. & García-Junceda, E. Enzyme catalysed tandem reactions. *Curr. Opin. Chem. Biol.* **17**, 236–249 (2013).
189. Rios-Solis, L., Halim, M., Cázares, A., Morris, P., Ward, J. M., Hailes, H. C., Dalby, P. A., Baganz, F. & Lye, G. J. A toolbox approach for the rapid evaluation of multi-step enzymatic syntheses comprising a ‘mix and match’ E. coli expression system with microscale experimentation. *Biocatal. Biotransformation* **29**, 192–203 (2011).

190. Smith, M. E. B. B., Chen, B. H., Hibbert, E. G., Kaulmann, U., Smithies, K., Galman, J. L., Baganz, F., Dalby, P. A., Hailes, H. C., Lye, G. J., Ward, J. M., Woodley, J. M. & Micheletti, M. A Multidisciplinary Approach Toward the Rapid and Preparative-Scale Biocatalytic Synthesis of Chiral Amino Alcohols: A Concise Transketolase-/ $\omega$ -Transaminase-Mediated Synthesis of (2S,3S)-2-Aminopentane-1,3-diol. *Org. Process Res. Dev.* **14**, 99–107 (2010).